222
49

Long-term Creep Modeling of Wood using Time Temperature Superposition Principle

by

Sandhya Samarasinghe Gamalath

Dissertation submitted to the Faculty of the

Virginia Polytechnic Institute and State University

in partial fulfillment of the requirements for the degree of

Doctor of Philosophy

in

Wood Science and Forest Products

APPROVED:

J. R. Loferski, Co-chairperson

S. M. Holzer, Co-Chairperson

D. A. Dillard

T. E. McLain

F. E. Woeste

January 24, 1991

Blacksburg, Virginia

Long-term Creep Modeling of Wood using Time Temperature Superposition Principle

by

Sandhya Samarasinghe Gamalath

J. R. Loferski, Co-chairperson

S. M. Holzer, Co-Chairperson

Wood Science and Forest Products

(ABSTRACT)

Long-term creep and recovery models (master curves) were developed from short-term data using the time temperature superposition principle (TTSP) for kiln-dried southern pine loaded in compression parallel-to-grain and exposed to constant environmental conditions (≃70°F, ≃9%EMC). Short-term accelerated creep (17 hour) and recovery (35 hour) data were collected for each specimen at a range of temperature (70°F-150°F) and constant moisture condition of 9%. The compressive strain was measured using bonded electrical resistance strain gages. For each specimen, the compliance curves for all the temperature levels were plotted against log-time on the same plot. The curve segments at successively higher temperature levels were shifted along the log-time axis with respect to the curve section at 70°F to construct a master curve for each specimen. The extrapolation of the developed master curves ranged from 0.23 to 6.4 years.

The requirement that the shift factors below glass transition temperature follow Arrhenius formulation was satisfied by the empirical shift factors. The activation energy for creep and recovery of kiln-dried southern pine derived from the slope of the plot of horizontal shift factor and the inverse of the absolute temperature was 28 KCal/mole. Creep and recovery master curves were represented by power functions and the nonlinear regression analysis was used to estimate the model parameters. Linear regression models were developed to predict one parameter in creep and recovery models from Young's modulus. The other model parameter showed weak correlations with material properties; therefore, an average value was recommended.

The validity of the master curves for predicting creep of wood exposed to normal interior environmental conditions in buildings was tested by conducting long-term (10 month) creep tests in a heated/cooled laboratory environment. The fluctuating test environmental conditions caused

geometry changes in the surface of the wood specimens in addition to mechanosorptive creep leading to fluctuating long-term data. Therefore, a good agreement between the master curves and long-term data was not found.

Creep behavior of shallow southern pine arches was studied to demonstrate the application of the finite element method, incorporating the long-term curves based on TTSP, to predict creep in wood structures. Creep tests were conducted at various load levels applied at ambient environmental conditions for two months. One arch failed (i.e., snapped-through) nine days after the tests began indicating that creep can indeed cause instability failure in shallow structures. It was found that the supports in the arch test fixture deflected elastically; therefore, the arches were modeled as three pin structures with base pin joints supported by zero-length linear elastic springs. However, the elastic analysis results revealed the presence of other factors affecting the experimental response which complicated the modeling procedure. The creep analysis was performed using a finite element model incorporating the developed creep master curves; however, due to the complexity in the creep experimental apparatus, the numerical predictions were not validated experimentally.

Acknowledgements

I express my sincere gratitude to my advisor, Dr. J.R. Loferski for his continual support and guidance throughout my studies at Virginia Tech. I am grateful to Professor S.M. Holzer, my co-chairperson, for his friendship, personal concern, moral support, and continual assistance in finite element analysis. I thank Dr. D.A. Dillard for his expert advice in creep modeling. My gratitude is extended to Professor T.E. McLain for his valuable advice and to Dr. F.E. Woeste for participating in the dissertation committee. I am indebted to Professor G. Ifju, Head of the department, for going through numerous difficulties in providing me the opportunity to pursue my degree. My gratitude is for him for his moral and financial support provided throughout this study.

I thank J.W. Akers for his willing participation in my experiments and, above all, for his friendship and kindness. My appreciation is for Harold Vandivort for diligently preparing my experimental apparatus and for Kenneth Albert for all his assistance.

I thank Curt Mackes for his valuable assistance in finite element analysis during the last part of this study. My love is extended to Ilona Koloszar-Peszlen for being a true friend in my need and for her continual assistance in conducting experiments. I thank Jan Wiedenbeck, my office partner, for her friendship and personal concern. My love and appreciation are for my husband, Kulasiri, for encouraging me to pursue this degree and for his love and moral support. Finally, I am forever grateful to my parents who always did the best for me.

Table of Contents

Chapter 1 ..... **1**

Introduction 1

1.1 Objectives 3

1.2 Overview 4

Chapter 2 ..... **5**

Literature Review 5

2.1 Design guides on creep 7

2.2 Factors influencing creep of wood 7

2.2.1 Stress level and load duration 8

2.2.2 Constant temperature 8

2.2.3 Variable temperature 9

2.2.4 Constant moisture content 12

2.2.5 Variable moisture content 12

2.3 Linear viscoelastic characterization of wood 13

2.4 Creep models 15

2.4.1. Creep models for wood under constant Environmental conditions 18

2.4.2 Creep Models for Transient Environment 22
2.5 Time Temperature Superposition Principle (TTSP) 24
2.6 Creep Analysis by the Finite Element Method 30
2.6.1 Creep Analysis 31
2.7 Viscoelastic Stability 34

Chapter 3 ..... **38**
Development of Long-term Creep and Recovery models for wood 38
3.1 Short-term Accelerated Compression Creep Tests 39
3.1.1 Test Material 39
3.1.2 Moisture Content 39
3.1.3 Specimen Preparation 39
3.1.4 Number of Specimens 40
3.1.5 Mechanical and Physical Properties of the Test Material 40
3.1.6 Load Level 42
3.1.7 Temperature and Relative Humidity Conditions 43
3.1.8 Test Duration 45
3.1.9 Strain Measurement with Bonded Strain Gages 47
3.1.10. Measuring Compressive Strains with Strain Gages 48
3.1.11 Data Acquisition 53
3.1.12 Accelerated Compression Test Apparatus 53
3.1.13 Accelerated Test Procedure 56
3.2 Development of Long-term Creep and Recovery Curves (master curves) 58
3.2.1 Accelerated Test Results 59
3.2.2 Master Curve Formation Procedure 61
3.2.3. Mathematical Representation of Master Curves 73
3.2.4. Predicting Model Parameters from Wood Properties 75

Chapter 4 ..... **80**

Testing Validity of Developed Long-term Creep Models 80

4.1 Long-term Compression Creep Tests 80

4.1.1 Long-term Creep Test Apparatus 81

4.1.2 Test Procedure 83

4.2 Long-term Creep Test Results and Validity of Master Curves 85

4.2.1 Long-term Creep Test Observations 85

4.2.2 Comparison of master curves with long-term creep experimental data 89

Chapter 5 ..... **96**

Creep Behavior of Shallow Wood Arches 96

5.1 Creep Tests on Shallow Wood Arches 97

5.1.1 Preparation of Arch Members 97

5.1.2 Material Properties of Arch Members 99

5.1.3 Load Level 99

5.1.4 Arch Test Fixture 99

5.1.5 Elastic Buckling Load of Arches 102

5.1.6 Creep Test Procedure 106

5.2 Experimental Creep Response and Finite Element Analysis 106

5.2.1 Experimental Observations 106

4.3.2 Finite Element Analysis 110

Elastic Analysis of Arches 113

Chapter 6 ..... **116**

Summary, Conclusions, and Recommendations 116

Summary 116

Conclusions 118

Recommendations 120

Literature Cited **122**

Appendix A. **127**

Accelerated Data and Master Curves (Cont'd) 127

Appendix B. **144**

Effect of Variable Thermal Expansion and Shrinkage of Wood on Strain Gage Measurements 144

Effect of Variability of Thermal Expansion Coefficients 144

Effect of Variability of Shrinkage Coefficients 147

Vita **151**

List of Illustrations

Figure 2.1. Creep behavior of wood 6
Figure 2.2. Representation of creep by mechanical models 21
Figure 2.3. Application of TTSP to a polymer 25
Figure 2.4. Illustration of snap-through buckling 35
Figure 3.1. Glass transition temperature of kiln-dried southern pine 44
Figure 3.2. Creep strain measurement 50
Figure 3.3. Schematic diagram of accelerated test fixture 54
Figure 3.4. Short-term accelerated test arrangement 55
Figure 3.5. Short-term accelerated data for specimen No. 2 62
Figure 3.6. Master curves and shift factor data for specimen No. 2 63
Figure 3.7. Short-term accelerated data for specimen No. 4 64
Figure 3.8. Master curves and shift factor data for specimen No. 4 65
Figure 3.9. Short-term accelerated data for specimen No. 9 66
Figure 3.10. Master curves and shift factor data for specimen No. 9 67
Figure 3.11. Relationship between power model parameters and Young's modulus 78
Figure 4.1. Long-term creep test arrangement 82
Figure 4.2. Effect of environmental conditions on long-term data 86
Figure 4.3. Predicted vs. experimental creep compliance 91
Figure 4.4. Predicted vs. experimental creep compliance 92
Figure 4.5. Predicted vs. experimental creep compliance 93
Figure 4.6. Predicted vs. experimental creep compliance 94

Figure 5.1. Geometry of the shallow arch 98
Figure 5.2. Arch test fixture 101
Figure 5.3. Arch creep test arrangement 107
Figure 5.4. Arch creep test data 109
Figure 5.5. Model of the experimental arches 111
Figure A.1. Short-term accelerated data for specimen No. 1 128
Figure A.2. Master curves and shift factor data for specimen No. 1 129
Figure A.3. Short-term accelerated data for specimen No. 3 130
Figure A.4. Master curves and shift factor data for specimen No. 3 131
Figure A.5. Short-term accelerated data for specimen No. 5 132
Figure A.6. Master curves and shift factor data for specimen No. 5 133
Figure A.7. Short-term accelerated data for specimen No. 6 134
Figure A.8. Master curves and shift factor data for specimen No. 6 135
Figure A.9. Short-term accelerated data for specimen No. 7 136
Figure A.10. Master curves and shift factor data for specimen No. 7 137
Figure A.11. Short-term accelerated data for specimen No. 8 138
Figure A.12. Master curves and shift factor data for specimen No. 8 139
Figure A.13. Short-term accelerated data for specimen No. 10 140
Figure A.14. Master curves and shift factor data for specimen No. 10 141
Figure A.15. Short-term accelerated data for specimen No. 11 142
Figure A.16. Master curve and shift factor data for specimen No. 11 143

List of Tables

Table 3.1. Material properties of accelerated test specimens 41

Table 3.2. Temperature and relative humidity to maintain 9% EMC in accelerated test environment 46

Table 3.3. Horizontal and vertical shift factors for master curve No. 2 68

Table 3.4. Extrapolation time and maximum relative compliance from master curves 70

Table 3.5. Activation energy for creep and recovery 72

Table 3.6. Power function parameters for creep and recovery master curves 76

Table 5.1. Moisture content, specific gravity, and Young's modulus of arch members 100

Table 5.2. Theoretical and experimental short-term buckling load of arches and creep load levels 104

Table 5.3. Effect of support deflection on short-term buckling load of arches 105

Chapter 1

Introduction

Wood has become a competitive construction material due to technological advances in the development of engineered wood products. For instance, wood space trusses and frames, including domes, have entered the market which had been dominated by metallic structures (Holzer et al., 1989). The efficient and economical use of wood in structures demands optimum structural design with adequate levels of safety. Guaranteeing the safety of these innovative wood structures requires knowledge of their long-term behavior. The goal of this research is to develop methods to predict long-term creep response of wood structures. This study is the first part of a research project designed to predict creep effects in wood space structures, including shallow single layer glulam domes.

Wood members undergo time dependent deformation under sustained load: this is called creep. By contrast, relaxation is the reduction of the force required to maintain a prescribed deformation imposed on a member. Creep of wood has been observed for centuries and a wealth of experimental data are available on various aspects of creep behavior. However, due to the lack of long-term creep models, there are no generally accepted methods to investigate creep effects on the safety and serviceability of wood structures.

Excessive creep deflections can induce system instability and loss of load carrying capacity in structures. For instance, creep can magnify deflection in columns, shallow arches, and shells due to geometric nonlinearity (Holzer et al., 1988). The geometric nonlinearity known as the P- Δ effect (Bathe, 1982) causes the coupling of the axial and bending actions leading to reduced strength and stiffness and possibly structural instability. Initial curvature and/or load eccentricity in columns, compression panels, and shallow arches gives rise to an initial lateral deflection which in turn causes a moment and thereby a flexural stress. Over time, creep increases the lateral deflection which further magnifies the flexural stress. Flexural stress in turn increases lateral deflection. This feed back loop process can continue until it may result in the collapse of the structure.

The effects of creep can be particularly significant on the performance of shallow single layer dome structures, such as glulam lattice domes and arches, because the geometric nonlinearity can lead to global snap-through buckling: This may be a predominant failure mode in these structures (1). Snap-through buckling results in a drastic reversal in the geometric shape of a structure due to structural instability. This phenomenon in a shallow arch was demonstrated by Hayman (1981). He conducted creep tests on shallow concrete arches at load levels of 85%, 65%, 35%, and 16.5% of the short-term elastic buckling load of arches. Creep caused a sudden collapse in the first three arches after a period of time. Only the fourth arch did not snap-through during the ten month test period. An overview of Hayman's theoretical study on elastic and creep behavior of shallow arches is presented in Chapter 2.

The effect of geometric nonlinearity magnified by creep is a complex phenomenon and requires a rational approach to investigate it. Since the availability of high speed digital computers, sophisticated numerical analysis techniques have been developed for obtaining solutions to complex creep problems in metallic and concrete structures (Bathe, 1982, Kraus, 1980, CEMS, 1978). Also, acceleration characterization techniques, such as Time Temperature Superposition Principle (TTSP), are highly developed for polymers to extend the short-term test measurement to longer periods (Aklonis and MacKnight, 1983, Rosen, 1971, Ferry, 1980). In this study, the time temperature superposition principle and the finite element method are used to develop a methodology to predict creep effects in wood structures.

1.1 Objectives

The goal of this study is to develop a method to predict long-term creep effects in wood structures. The specific objectives are:

1. To test the applicability of the TTSP to wood exposed to constant environmental conditions. If successful, the TTSP will be used to develop long-term creep and recovery models for kiln-dried southern pine loaded in compression parallel-to-grain using short-term experimental data.

2. To test the validity of the developed creep models for predicting long-term creep response of wood exposed to conditioned environments as found in buildings. This will be accomplished by conducting long-term compression creep experiments in a normal heated/cooled interior laboratory environment.

3. To demonstrate the application of the developed creep models and the finite element method (FEM) to predict creep effects in wood structures. Shallow wood arches are selected as example structures.

The above three objectives were accomplished by conducting three types of tests:

- Short-term compression creep and recovery tests (17 hour and 35 hour) were conducted at temperature levels ranging from 70°F to 150 °F (i.e., accelerated creep tests) to develop long-term response curves representing the time dependent behavior of wood under constant equilibrium moisture content (EMC) conditions.

- Long-term (10 month) compression creep tests were conducted in normal heated/cooled interior laboratory environmental conditions on specimens matched with the accelerated creep test specimens.

- Creep tests were conducted on shallow three-pin wood arches subjected to various load levels to demonstrate the significance of creep effects in the design and analysis of shallow structures.

1.2 Overview

This dissertation contains six chapters. In Chapter 2, a review of literature on creep behavior, factors influencing creep, and creep models for wood is presented. In addition, viscoelastic behavior of wood is characterized, the time temperature superposition principle is illustrated, and a finite element formulation of creep analysis is presented.

In Chapter 3, the information relevant to the formation of long-term creep and recovery models based on TTSP is presented. The materials and experimental procedures used for short-term accelerated compression experiments are discussed in section 3.1. Also included is a detailed discussion on measuring compressive strains in wood with bonded electrical resistance strain gages. In section 3.2, long-term creep and recovery master curves are developed from accelerated compression data and the master curves are represented by a power function. Finally, regression relationships are developed to predict the mathematical creep model parameters from Young's modulus of wood.

Chapter 4 presents the long-term creep experimental procedure (section 4.1) and the comparison of the creep response predicted by the developed long-term creep models with the long-term experimental data (section 4.2).

In Chapter 5, the experimental details of the creep tests on shallow wood arches are discussed (section 5.1), the finite element analysis of creep in shallow arches is presented, and the complexity in the creep experimental apparatus is discussed.

Chapter 6 contains summary and conclusions of this study and recommendations for future research.

Chapter 2

Literature Review

Creep is defined as the time- dependent deformation of materials under sustained load. Although almost every material exhibits creep, it is not always significant at room temperature. However, creep in wood under normal service conditions can be practically important as evidenced by the sagging of wooden beams.

Three stages of creep can be observed as shown in Figure 2.1. The application of a load at time t_0 causes an instantaneous elastic deflection and soon the material enters the primary creep region, from t_0 to t_1. This region is characterized by an increase in deflection at a decreasing rate. The material may then enter the secondary creep region where deflection increases at a constant rate (from t_1 to t_2). If the load is large enough, the material may experience tertiary creep (from t_2 to t_3) where strain increases at an increasing rate causing failure if the load is maintained. At a given time, the total deformation consists of three components: initial elastic, delayed elastic, and permanent deformations (Bodig and Jayne, 1982).

If the load is removed at time t, recovery is observed. The initial deflection is instantly recovered and the delayed elastic deflection is recovered with time.

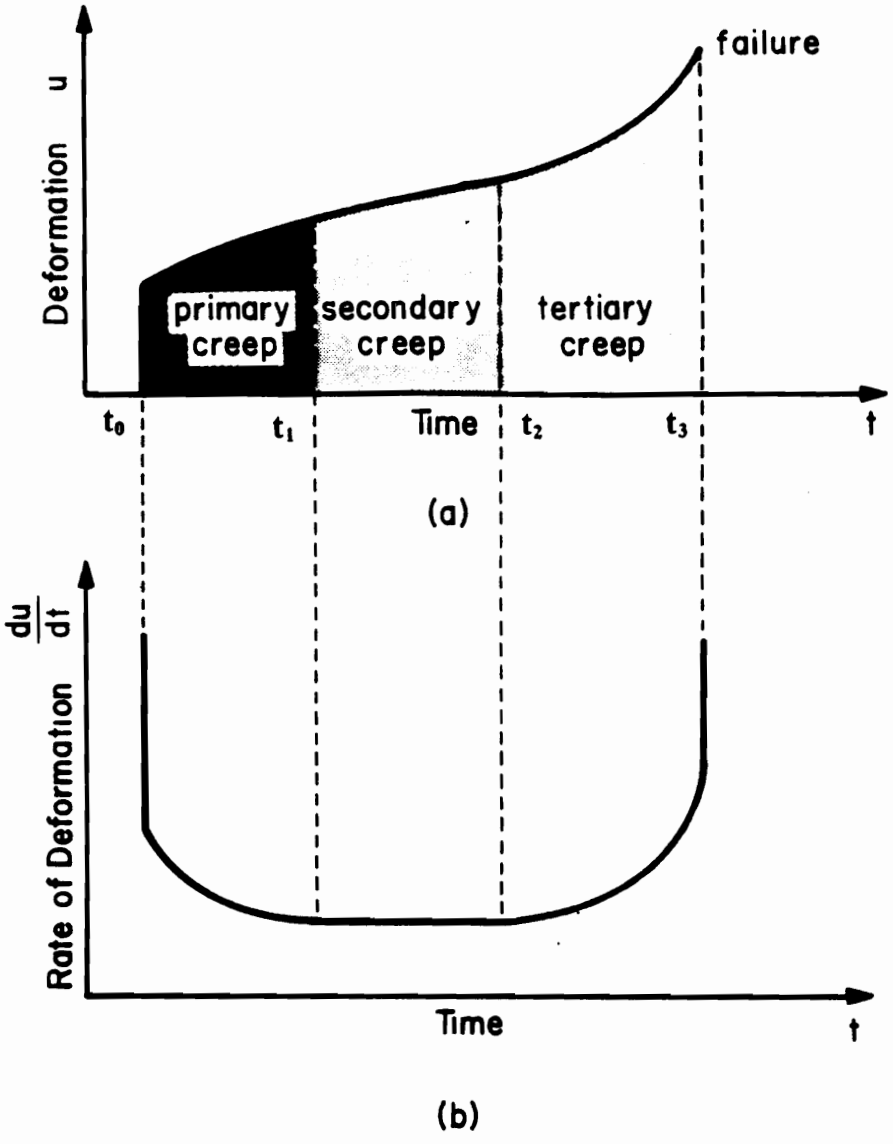

Figure 2.1. Creep behavior of wood: (a) Stages of creep (b) creep rate (Source: Bodig and Jayne (1982)

2.1 Design guides on creep

Creep of wood members is addressed in Appendix F of the National Design Specification (NDS, 1986). It states that the customary practice has been to use a deflection factor of 1.5 for glued laminated timber or seasoned sawn lumber, or 2 for unseasoned sawn lumber, when calculating deflection due to long-term loading. In simply supported beams, creep occurs under constant or variable dead loads. Therefore, a deflection factor can account for creep deformation. However, in space structures, geometric nonlinearity can magnify stresses leading to elastic instability, snap-through buckling, and structural collapse (Holzer et al., 1988). Therefore, a deflection factor may not be sufficient to compensate for the loss of load carrying capacity induced by geometric nonlinearity.

The NDS (1986) and the Timber Construction Manual (AITC, 1985) recognize that creep rates are greater for members drying under load or exposed to varying temperature and relative humidity conditions than for members in a stable environment and at constant moisture content. It is questionable, however, whether the "rule of thumb" factor of 1.5 used in glulam design is valid for fluctuations in moisture content and temperature over the design life. Moreover, the use of a single factor can lead to conservative designs or unsafe structures. In summary, design guides do not provide a satisfactory method to investigate long-term creep effects on the safety and serviceability of wood structures.

2.2 Factors influencing creep of wood

Creep of wood is influenced by stress level and load duration, temperature, moisture content, species, and grain direction (Bodig and Jayne, 1982). Moreover, Schniewind (1968) states that the creep behavior of wood under variable temperature and moisture content is markedly different from the behavior under constant temperature and moisture content and the two conditions need to be

treated separately. Accordingly, the following review summarizes the effects of these variables separately.

2.2.1 Stress level and load duration

Higher stress levels produce greater creep. The relative creep (ratio of creep deflection to initial deflection) is constant for stresses up to a certain level beyond which the relative creep increases with increasing stress level (Miller and George, 1974). The region where the relative creep is constant is characterized by linear viscoelastic behavior. In this region, the stress-strain relationship for a given load duration is linear. Load duration is the time period during which load is sustained on a member. If the stress level is relatively small, creep can remain in the primary region for long periods of time. Depending on the stress level and load duration, creep may enter the secondary and tertiary regions and accelerate failure (Bodig and Jayne, 1982). Failure can be either creep induced structural instability or excessive creep deflections of individual members leading to a loss of load carrying capacity.

2.2.2 Constant temperature

The time dependent behavior of wood is closely associated with temperature because heat induces changes in wood properties (Schaffer, 1972). For example, Bach and Pentoney (1968) found that Young's modulus of wood decreased with increasing temperature. Schaffer (1972) reports that in dry wood hemicelluloses and lignin begin to soften at 60°C and 120°C, respectively. Softening of lignin is associated with a transition from glassy to rubbery behavior of wood and the temperature characterizing the transition is known as glass transition temperature, T_g. The T_g is critical to the viscoelastic characterization of wood. For example, the deformation of wood near T_g rapidly increases compared to the rate of deflection at lower temperatures (Schaffer, 1972).

Arima (1967) states that increasing temperature accelerates the creep rate and increases the deformation reached at failure. He conducted 50 minute creep tests in compression perpendicular to the grain of small specimens of Hinoki at constant temperatures of 20, 40, 50, 60, and 75 °C. His results reveal that the relationship between creep deflection and time becomes increasingly nonlinear with increasing temperature. Bach and Pentoney (1968) tested small specimens of hard maple in tension along the grain at temperatures 30, 50, and 70°C for 1000 minutes. They found that tensile creep parallel to the grain was proportional to the square of the temperature. Kingston et al. (1961,1972) report from bending and compression tests of hoop pine that doubling the temperature in the range of 20 to 50°C, while maintaining a constant stress level, doubled the relative creep.

Davidson (1962) studied the influence of temperature on the creep and recovery of six small bending specimens of several species, including eastern white pine, subjected to 10 hour creep and 100 minute recovery at 20, 30, 40, 50, and 60°C. In all cases, an increase in temperature resulted in recovery curves with increasing slopes. This effect was rather small in the range from 20 to 50°C; however, a large change occurred between 50 and 60°C. Davidson (1962) thought that in the range of 50 to 60°C some of the hydrogen bonds in the wood cellulose were broken resulting in more rapid deformation.

2.2.3 Variable temperature

Behavior of wood under variable temperature follows a complex pattern (Arima, 1972, Urakami and Nakato, 1966). Arima (1972) investigated the influence of constant, increasing, and decreasing temperature on the transverse compressive creep in radial direction of small specimens (25x15x15mm) of Hinoki (Chamaccyparis obtusa ENDL.) in water saturated conditions for 50 minutes. He found that up to 50°C, creep under increasing temperature is slightly greater than that at the constant temperature at the highest level. However, above 60°C, creep at increasing tem-

perature is considerably higher. This indicates a transition in wood substance between 50°C and 60°C.

Davidson (1962) observed a similar transition between 50°C and 60°C while studying the effects of temperature on the bending creep of small specimens of eastern white pine (Pinus Strobus L.), western red cedar (Thuja plicata Donn.), and sugar maple (Acer saccharum Marsh). Davidson (1962) found a marked increase in the internal friction ($\tan\delta$) at 60°C compared to that at 50°C. Schaffer (1972) attributed this transition between 50-60 °C to softening of hemicellulose in wood fiber-matrix network. A similar transition was also observed by Urakami and Nakato (1966). They conducted torsional creep tests on small specimens of Hinoki under water saturated conditions at temperatures ranging from 20-80°C with 10°C increments. They found that the shear strain at a given time decreased abruptly in the range of 50- 60°C.

Patterson (1972) reports on an investigation carried out by Kitahara and Yukawa (1964) on the effect of transient and constant temperature on bending creep of Hinoki wood under saturated conditions. The specimens were supported at quarter span points and the loads were applied at the ends. A dial gage measured the mid-span deflection for 120 minutes. After a creep test has begun, the water temperature was raised from either 20, 30, or 40 to 50°C. in three different patterns: (i) rapid change of temperature, (ii) slow change of temperature, (iii) change of temperature with the time of low temperature long. They also studied the effect of decreasing temperature on the creep deformation of wood. They found that a temperature rise either from 20, 30, or 40, to 50°C resulted in greater creep deflections compared to that at 50°C. Larger temperature difference during a creep test resulted in larger creep deflections. Rate of change of temperature also affected the rate of creep and the magnitude of the final creep deflection. For example, the magnitude of the creep deflection after 120 minutes was greater under slow change of temperature than that under rapid change of temperature.

Schniewind (1967) focused on the creep rupture life of Douglas-fir under cyclic environmental conditions. Small Dougls-fir beams were subjected to constant loads under 5 cyclically varying humidity and temperature conditions and time to failure was recorded. Two of the conditions were: (1) both temperature and humidity were cycled so that the maximum temperature coincided with

minimum relative humidity, (2) the temperature was cycled and the humidity was varied so that the equilibrium moisture content (EMC) remained constant. The former was thought to represent a somewhat extreme form of actual conditions where temperature and humidity both vary on a daily basis and the latter was supposed to show the effects of temperature change alone. In the first test, temperature was cycled sinusoidally from 60- 90°F and humidity from 35- 87% and the beams were loaded at 70% of the maximum bending strength. He found that the average range of moisture content in his 6 specimens during the test was 2% and the average time to failure was 8,170 minutes, which was very short compared to tests at constant conditions where the specimens carried the load for 100,000 minutes.

Schniewind (1967) conducted his second test under temperature varying sinusoidally from 60 to 90°F and the humidity was adjusted to maintain a nominal equilibrium moisture content. The load level was 70% of the maximum bending strength. Average life time of his four specimens was 26,190 minutes which is 220% higher than when the humidity was cycled. Based on the results of these two tests, Schniewind (1967) indicated that within the temperature range tested the temperature is of minor importance in the determination of creep rupture life but influences the life to failure indirectly by affecting the extent of moisture content change. He established a relationship between the range in average moisture content in his specimens and average life to failure and showed that the logarithm of time to failure and the logarithm of range of moisture content are approximately linearly related. Schniewind (1967) concluded that the cyclic environmental changes shorten the creep rupture life of Douglas-fir considerably, and the extent of this reduction mainly depends on the range of extreme values of integral moisture content attained by the specimen during cycling. He states that in large beams "only the surface moisture content changes due to the daily variations in temperature and humidity". Therefore, the "integral moisture change in large beams may be negligibly small" and thus results in "only minor reduction in creep- rupture life".

2.2.4 Constant moisture content

Moisture in wood acts as a plasticizer leading to increased creep deflections with increasing moisture content (Schniewind, 1968, Bodig and Jayne, 1982). Bach and Pentoney (1968) noted from 1000 minute tensile creep tests on hard maple conducted at 4%, 8%, and 12% moisture contents that creep was proportional to the square of the moisture content. Youngs (1957) carried out tension and compression tests perpendicular to the grain of red oak at green, 18%, 12%, and 6% moisture contents. He also concluded that creep increased curvilinearly with increasing moisture content. Moreover, the moisture adsorbed below fiber saturation point has a greater effect on creep than on the initial deflection (Bodig and Jayne, 1982).

2.2.5 Variable moisture content

In loaded wood members, variable moisture conditions causes an effect called mechano-sorptive creep (Grossman, 1976). For example, the relative creep of a small loaded beam allowed to dry can be at least twice that under constant moisture content. Szabo and Ifju (1969) state that when dry specimens are loaded and placed in high relative humidity conditions, adsorption occurs and creep takes place which gradually levels off as sorption is completed. Redrying of specimens under load will further increase creep. In subsequent sorption cycles partial recovery is induced by further adsorptions and creep by desorptions. Szabo and Ifju (1969) also report that the beams loaded green and kept green, and loaded dry and kept dry, during a creep test had the same relative creep. Schniewind (1967) state that under variable environmental conditions, it is the integral change of moisture content within a wood member that most affects its creep rupture life.

Creep under variable moisture conditions is called mechano-sorptive (M-S) creep. Studies on M-S creep have been done on small clear specimens. However, it is important to know if this behavior is significant in structural wood members. Schniewind (1967) suggests that since in large beams, moisture interacts only with the surface layers of beams resulting in a negligible integral

change in moisture content, mechano-sorptive creep in large beams may be insignificant. A survey conducted by Forest Products Lab (Hann et al., 1970) on the moisture content change in laminated timbers revealed that in interior normal exposure there was very little geographical or seasonal variation in the moisture content. In the protected exposure moisture range was narrow. In unprotected exposure, however, the moisture content was extremely variable. Holzer et al. (1988) state that the "slow rate of moisture migration in large structural members reduces at least the rate of mechano-sorptive creep deflection". Bodig and Jayne (1982) state that larger structural members are less sensitive to moisture cycling than small specimens but the effect of variable moisture content can be significant and should be incorporated into design of wood members exposed to moisture cycling.

2.3 Linear viscoelastic characterization of wood

The viscoelastic behavior of a material can be characterized as either linear or nonlinear. For a linear viscoelastic material, elastic effects are Hookian and the viscous effects are Newtonian (Aklonis and MacKnight, 1983). Therefore, for a given load duration, the stress strain relationship is linear. The Boltzman superposition principle states that if a material is linearly viscoelastic, stresses applied at different times act independently and the resultant strains add linearly. "This principle is one of the simplest but most powerful principles in polymer science" (Aklonis and MacKnight, 1983). For example, suppose a stress σ_0 is applied to a linear viscoelastic material at time t = 0. Then time dependent strain $\gamma(t)$ is given by

$$\gamma(t) = \sigma_0 \; D(t) \qquad [2.1]$$

where

D(t) = creep compliance.

If a stress σ_1 is applied not at time t = 0 but at time t = τ, then equation [2.1] becomes

$$\gamma(t) = \sigma_1 \; D(t - \tau) \qquad [2.2]$$

If the two stress increments σ_0 and σ_1 are applied at times t = 0 and τ, respectively, the resultant strain according to the Boltzman superposition principle is given by

$$\gamma(t) = \sigma_0 \; D(t) + \sigma_1 \; D(t - \tau) \qquad [2.3]$$

For several stress increments $\sigma_1,\sigma_2,...,\sigma_n$ applied at times $\tau_1,\tau_2,....,\tau_n$, the strain is

$$\gamma(t) = \sum_{i=1}^{n} \sigma_i \; D(t - \tau_i) \qquad [2.4]$$

For a continuous stress application $\sigma(t)$

$$\gamma(t) = \int \frac{\partial \sigma(\tau)}{\partial \tau} \; D(t - \tau) \; d\tau \qquad [2.5]$$

where

t = fixed time of the observation of the strain

τ = integration variable

Thus, the linear viscoelastic characterization simplifies the analysis of the response of a structure subjected to arbitrary loading or strain histories. It is of practical importance if wood is linearly viscoelastic at design stress levels (Schniewind, 1968, Miller and George, 1974). The following investigators studied the conditions under which wood can be considered as a linear viscoelastic material.

Bach and Pentoney (1968) studied the creep of maple in tension parallel to the grain and showed that deformation- stress relationship is essentially linearly elastic when stress, moisture content, and temperature are sufficiently low. The behavior was linearly viscoelastic at intermediate values of these variables but essentially nonlinear at higher levels. Grossman and Kingston (1963)

observed the linear viscoelastic behavior for creep of hoop pine in tension parallel to the grain even at a stress level of 75% of the static strength and at 50 °C. They state that it is taken for granted that for wood the superposition principle holds for stresses and strains lower than those for which it was confirmed, and it is likely to hold for shorter test duration and for lower temperatures. The linear behavior was also observed by King (1961) for creep in tension parallel to grain for a variety of species at stress levels ranging from 36 to 84 percent of the short-term ultimate strength.

2.4 Creep models

In experimental studies of the viscoelastic behavior of materials, the relationship between material parameters and time is established. For example, in creep studies, creep strain or creep compliance are expressed as functions of time. In the past, creep behavior of wood was modeled by either fitting a mathematical function to experimental data (empirical models) or by constructing mechanical models consisting of springs and dash pots to simulate the time dependent behavior (Pentoney and Davidson, 1962). In this section, formulation of two basic types of general creep models and their applicability in numerical analysis of creep is first discussed. Then, the creep models developed for wood are reviewed.

To model creep, creep strain is required in the following form (Kraus, 1980):

$$\varepsilon^c = F(\sigma, T, t) \qquad [2.6]$$

where

ε^c = creep strain

F = a function of the stress σ, temperature T, and time t.

Customarily, it is assumed that the effects are separable leading to

$$\varepsilon^c = f_i(T)\ g_i(\sigma)\ h_i(t) \qquad [2.7]$$

where

f, g, h = functions of temperature, stress, and time, respectively.

In statically indeterminate structures, such as space frames, creep can cause long-term stress redistributions even under constant load (Holzer et al., 1988). This requires variable stress creep laws for the analysis of such structures. There are two choices for such a formulation by assuming either one of the following (Kraus, 1980):

1. The response of the material depends on the present state explicitly, or

2. The material remembers its past explicitly and responds to the present in such a way that reflects its past history.

The first approach yields the equation of state or rate-type formulation while the second gives rise to the memory theory or integral-type formulation. The equation of state approach is used in most of the creep problems due to the following reasons as discussed by Kraus (1980):

1. It has been extensively applied and much experience has been gained with it.

2. It is simple to apply and understand.

3. It is easy to incorporate into existing computer programs.

4. It requires a minimum of experimental data: only single step creep tests at various stresses and temperatures.

In the equation of state approach, an expression of the following form, known as the Bailey-Nortan law, is assumed at the outset:

$$\varepsilon^c = A\ \sigma^m\ t^n \qquad [2.8]$$

where A, m, and n are constants that are functions of temperature.

The value of m is equal to or greater than one and n is a fraction. This law models primary and secondary creep only.

For a variable stress problem strain rate is required. Differentiating Eq.[2.8] with respect to time one obtains

$$\dot{\varepsilon}^c = A\,\sigma^m\ n\ t^{n-1} \qquad [2.9]$$

This is called the time-hardening formulation which states that in a variable stress situation creep strain rate is a function of stress, time, and through the constants, temperature. Note that in differentiating Eq.2.8, the time derivative of stress was ignored although a variable stress creep law was desired. This is a shortcoming of the equation of state approach which limits it to step changes of stresses of long duration. However, this approach has been successfully applied (Kraus, 1980).

Another formulation, known as strain hardening formulation, can be obtained by eliminating time from Eq.2.9, which states that in variable stress situations the creep strain rate depends on the stress, strain, and temperature. Equation 2.8 is first solved for time to give

$$t = \left(\frac{\varepsilon^c}{A\ \sigma^m}\right)^{1/n} \qquad [2.10]$$

Substituting t into Eq.2.9 yields

$$\dot{\varepsilon}^c = A^{1/n}\ n\ \sigma^{m/n}\ (\varepsilon^c)^{(n-1)/n} \qquad [2.11]$$

Kraus (1980) states that the experimental results from variable stress creep tests show that the strain-hardening formulation produces more accurate results than the time-hardening formulation. Therefore, the strain-hardening model is favored in numerical analysis of creep problems. However, it is worth noting that both strain- and time- hardening models are applicable as long as stress reversals do not occur. If stress reversals occur, auxiliary models must be employed in conjunction with the hardening model.

The memory approach is based on the Boltzman superposition principle and seems to be the only valid representation of creep. However, the limited experience and the need to store the

complete stress history in the memory approach makes the equation of state approach more suitable on practical grounds (Kraus, 1980). The integral-type creep law (memory approach) defines the creep strain as a function of the entire stress history (σ_τ) in the following manner:

$$\varepsilon_{cr}(t) = \int D(t-\tau) \frac{d\,\sigma(\tau)}{d\,\tau} d\,\tau \qquad [2.12]$$

where

D = creep compliance function

t = time

τ = integration variable

For wood, creep models similar to Equation [2.8] and other empirical models are more common than mechanical models because of the complexity associated with the mechanical modeling procedure. The following is a limited review of creep models of wood under constant and transient temperature. More details details are contained an exhaustive review by Schniewind (1968).

2.4.1. Creep models for wood under constant Environmental conditions

Empirical creep models

Bending: Clauser (1959) developed an empirical power model in the form of Equation 2.13, based on 10 year beam bending tests on Douglas-fir (Pseudotsuga menzesii). Hoyle et al. (1985) investigated the primary creep in full size Douglas-fir beams. The creep model they developed also took the form of Equation [2.13] and was based on creep in flexure over 400 hours at four stress levels, 12% moisture content, and 70°F. The objective of Gressel's (1984) work was to evaluate commonly used creep equations on the basis of long-term creep experiments. He carried out 10 year beam bending tests at 12% moisture content and 20°C on timber and wood composite specimens composed of spruce, pine, and beech. The data were fitted to two empirical creep equations and two mechanical models existing in the literature to evaluate the ability of these models to predict

10 year creep behavior. He found that the model in the form of Equation 2.13 was the best for extrapolation to 10 years.

$$\varepsilon(t) = \varepsilon_0 + a\ t^n \qquad [2.13]$$

where

a, n, and ε_0 are constants.

Tension and Compression: Youngs (1957) developed power models similar to Eq. 2.13 for tensile and compressive creep perpendicular to the grain of red oak (Quercus rubra). His experiments were carried out for 70 hours at 80, 130, and 180°F and green, 18%, and 12% moisture contents. King Jr. (1961) formulated an empirical model similar to Equation 2.14, based on 30 minute tensile tests on Douglas-fir and several other species at room temperature and at 12% moisture content. Bach and Pentoney (1968) developed empirical creep compliance functions in the form of Equation [2.15]. They conducted tensile tests on hard maple specimens at 30, 50, and 70°C and 4%, 8%, and 12% moisture contents. They applied several stress levels ranging from 20-80% of the short-term strength. Schniewind and Barrett (1972) fitted data from tensile creep tests on small Douglas-fir specimens to Eq. 2.16. All tests were conducted at 75°F and 50% relative humidity.

$$\varepsilon(t) = \varepsilon_0 + b\ \log(t + 1) \qquad [2.14]$$

$$J(t) = A + A_1\ \log(t + 1) + A_2\ \log(t + 1) \qquad [2.15]$$

$$J(t) = J_0 + m\ t^n \qquad [2.16]$$

where

$\varepsilon(t)$ = creep strain at time t

J(t) = creep compliance at time t

ε_0, b, A, A_1, A_2, m, n, J_0 are empirical constants

Shear: Schniewind and Barrett (1972) developed a power model for shear creep compliance in the form of Eq. 2.16. The environmental conditions for the shear tests were similar to those for the creep tests in tension and compression.

Mechanical Models:

Empirical creep models do not provide qualitative information on creep phenomena. In contrast, mechanical models describe various types of time dependent behavior and they also yield a mathematical representation (Pentoney and Davidson, 1962).

The basic components of a mechanical creep model are a spring, dash pot, and Kelvin element as shown in Figure 2.2(a). The free spring with stiffness E_0 represents the instantaneous deformation and the free dash pot with viscosity η_0 models the permanent deformation, or flow of the material. The parameters E_1 and η_1 are the stiffness and viscosity associated with the spring and dash pot of the Kelvin element which represents the recoverable time dependent deformation. Associated with a Kelvin element is the retardation time (τ), which determines the speed of the element extension and is expressed by $\frac{E_1}{\eta_1}$. Thus, the Kelvin element determines duration to which the model predictions are applicable.

The disadvantage of the mechanical models is that a model with one Kelvin element does not produce a response comparable to the actual response of a material. To obtain quantitative agreement between the model and the real material, the model must be extended with a series of Kelvin elements to form a generalized Kelvin model as shown in Figure 2.2(b). The strain in the generalized Kelvin model is expressed as:

$$\varepsilon(t) = \sigma\left[\frac{1}{E_0} + \sum_{i=1}^{n} \frac{1}{E_i}\left(1 - e^{\frac{-t}{\tau_i}}\right) + t/\eta\right] \qquad [2.17]$$

where

E_0 = stiffness of the free spring

E_i = stiffness of the spring in the ith Kelvin element

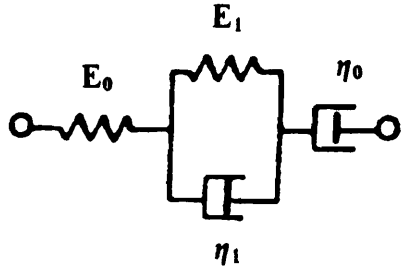

(a)

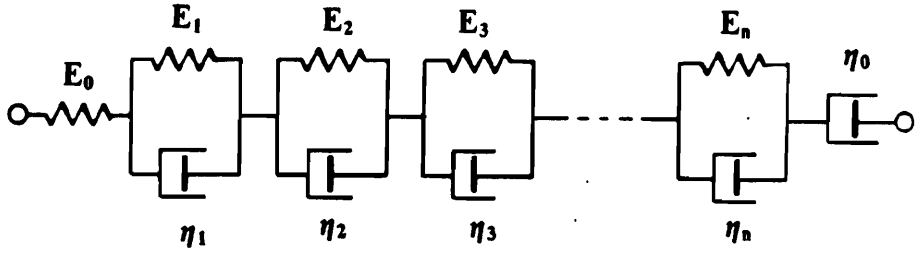

(b)

Figure 2.2. Representation of creep by mechanical models: (a) single Kelvin element,free spring, and dash pot (b) generalized Kelvin element

$\tau_i = \frac{E_i}{\eta_i}$ = retardation time of the ith Kelvin element

η_i = viscosity of the dash pot in the ith Kelvin element

η_0 = viscosity of the free dash pot

σ = applied stress

Davidson (1962) developed a mechanical model for wood with a free spring and 40 Kelvin elements. He showed the similarity in behavior between the model and the real material using experimental creep and recovery data obtained from beam creep tests of several species at different temperatures and moisture contents.

2.4.2 Creep Models for Transient Environment

The response of a loaded material under moisture change consists of two simultaneously occurring processes: viscoelastic creep, and mechano-sorptive creep (Leicester, 1971). It is impossible to separate these processes because moisture change is present throughout the response. Therefore, attempts have been made to incorporate both phenomena into time dependent models.

Leicester (1971) used an elastic spring and mechano-sorptive (M-S) element in series in his model to simulate the behavior of wood under changing moisture content. He tested the model against creep data collected from small eucalyptus (Eucalyptus oblique) beams loaded at 15% of the static ultimate load and dried from approximately 65% to 12% moisture content over 400 hours. Leicester (1971) found that his model accounted for 85% of the total deformation. This model could only describe a single sorption process because of the absence of a recoverable M-S element.

Schaffer (1972) introduced a mathematical model to explain the change of creep response with changing moisture content by considering the effect of moisture diffusion within the loaded specimen. The model predicts an acceleration in creep rate at a point in a wood specimen in proportion to the increase or decrease in moisture content until a steady moisture content is attained.

The previous discussion shows that empirical models have been widely used and mechanical models have been occasionally developed to model creep behavior of wood. However, neither model is appropriate to predict long-term response over the design life of a structure because empirical models need long-periods of time and mechanical models require many model elements to represent the long-term material response. Acceleration characterization techniques, such as time temperature superposition principle, are widely employed to predict the long-term response of polymers from experimentally observed short-term data (Aklonis and MacKnight, 1983). The next section presents a detailed discussion of the time temperature superposition principle.

2.5 Time Temperature Superposition Principle (TTSP)

The time temperature superposition principle is widely used to extend the range of measurements when viscoelastic parameters are studied in polymers as functions of time at different temperatures (Aklonis and MacKnight, 1983). The basis of this principle is that time and temperature have equivalent effects on the performance of a material. For example, a property measured over a short time at a higher temperature is equivalent to the property measured for a long time at a lower temperature. The application of TTSP to a polymer is graphically illustrated in Figure 2.3 for relaxation modulus of a polymer. Short-term response curves (Figure 2.3(a)) are obtained at different temperatures and these curve segments are then shifted along the log(time) axis to construct a master curve (Figure 2.3(b)), applicable for a reference temperature (T_{ref}) and very long or very short time period (Povolo and Fontelos, 1987). The master curve is then represented by a suitable mathematical function which defines the desired long-term response, i.e. constitutive creep law. The shift factor for a curve segment is designated by a_T. The log a_T is the segment's horizontal displacement needed to form the master curve. This is the factor by which the time scale is altered due to the difference in temperature, and is related to the temperature as shown in Figure 2.3(c) (Povolo and Fontelos, 1987).

The TTSP is based on the relation (Aklonis MacKnight, 1983)

$$D_{cr}(t_0, T_0) = D_{cr}(t_1, T_1) = D_{cr}\left(\frac{t_0}{a_T}, T_1\right) \qquad [2.18]$$

where

$D_{cr}(t_0, T_0)$ = creep compliance at T_0 and time t_0

T_0 = reference temperature

$D_{cr}(t_1, T_1)$ = creep compliance at temperature T_1 and time t_1

The relationship in Eq.2.18 can be expressed for any viscoelastic property. The time parameters t and t_1 are related by the shift factor, a_T, and is defined by the relation (Aklonis and MacKnight, 1983):

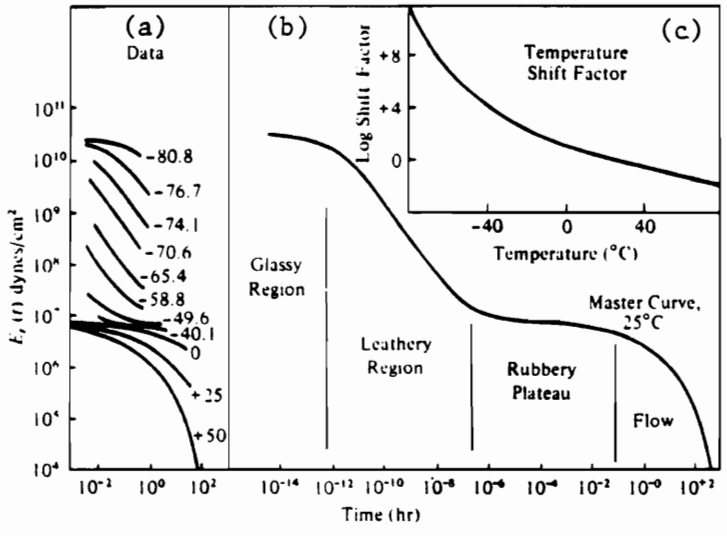

Figure 2.3. Application of TTSP to a polymer: (a) short-term experimental curves (b) Master curve based on TTSP (c) relationship between the shift factor and the absolute temperature (Source: Rosen, 1971)

$$t_1 = \frac{t_0}{a_T} \qquad [2.19]$$

For ambient temperatures below the glass transition temperature, (Tg), the shift factors are related to the ambient temperature by an apparent activation energy, Delta E, as follows (Schaffer, 1972):

$$\Delta E = \frac{R \; d(\ln a_T)}{d(\frac{1}{T})} \qquad [2.20]$$

where

R = gas constant

If $\ln a_T$ is directly proportional to $\frac{1}{T}$, Eq.2.20 is simplified to an Arrhenius type equation (Aklonis and MacKnight, 1983) as follows:

$$\Delta E = \frac{2.303 \; R \log a_T}{\{\frac{1}{T} - \frac{1}{T_g}\}} \qquad [2.21]$$

If the ambient temperature is at or above Tg, then the shift factor is related to the ambient temperature by an empirical equation known as William- Landel- Ferry (WLF) equation. The WLF expression is given by

$$\log a_T = \frac{-C1 \, (T - T_g)}{C2 + T - T_g)} \qquad [2.22]$$

where

C1 and C2 are material parameters known as "universal" WLF constants

Tg is the reference temperature = glass transition temperature

For a reference temperature above Tg, the relationship between $\log a_T$ and the temperature is as shown in Figure 2.3(c).

As shown in Figure 2.3, a polymer can show a range of response regions. In the glassy region, the thermal energy is insufficient to break the potential energy barriers for the movement of seg-

ments of polymer molecules. With increasing temperature, the motion of the molecules becomes greater, and eventually, the thermal energy surmounts the potential energy barriers for segmental movement. In this leathery region, the polymer is at a glass transition temperature range , where short-range diffusional motion of molecules begins and the "brittle glass becomes a resilient leather" (Aklonis and MacKnight, 1983). In the rubbery region, short-range diffusional molecular motion becomes faster and the segments of polymer chains reorient relative to one another. In the flow region, the polymer segments undergo large scale translational motion and the molecules move relative one another.

The response of wood structural members in "normal" environments remains in the glassy region of the polymer response shown in Figure 2.3(b). Therefore, the sift factor-temperature relationship must be based on Arrhenius formulation (Eq.2.21). However, in order for the TTSP to hold, several criteria must be satisfied (Ferry, 1980):

1. The material must be thermorheologically simple, i.e., the shape of the response curves at different temperature levels is the same except that curves are shifted along the time axis.

2. There must be no chemical changes in the material.

3. There must be no failure mechanisms and damage accumulations within the material.

4. The shift factors must be the same for all the viscoelastic functions and they must be consistent with the experience.

5. Adjacent curves must be exactly matched.

Central to the TTSP is the thermorheologically simple material behavior. An important question is whether and under what conditions wood is a thermorheologically simple material. Schaffer (1972) confirms from strain- time data at several temperature levels that over narrow temperature ranges wood responds as a thermorheologically simple material. The application of the time temperature superposition principle to wood is a controversial issue. Schaffer (1972) re-

ports that Yamada et al. (1961) observed a good compliance with TTSP for the normal to grain relaxation modulus of wet beech wood over temperature range of 6 - 73°C. They found that the shift factor is apparently linearly related to the reciprocal of the absolute temperature, satisfying the Arrhenius formulation (Eq.2.21).

Salmen (1984) successfully applied the TTSP to the dynamic mechanical behavior perpendicular to the grain of small bending specimens of water saturated Norway spruce (Picea abies). The properties measured were storage modulus (E′) and the loss modulus (E″). These properties are related to a complex dynamic modulus (E*) which is by definition

$$|E^*| = \frac{\sigma_0}{\varepsilon_0} \qquad [2.23]$$

where

σ_0 and ε_0 = stress and the strain amplitude, respectively, and

$$|E^*| = (E'^2 + E''^2)^{1/2} \qquad [2.24]$$

Forced sinusoidal vibrations in the frequency range of 0.05 to 20 Hz were applied using a servohydraulic universal testing machine and E′ and E″ were measured at temperatures between 20°C and 140°C. Then E′ and E″ were plotted against log of frequency at different temperatures similar to those shown in Figure 2.3(a) and the curves were horizontally translated to form a master curve at a reference temperature of 112.3°C. Both E′ and E″ gave smooth master curves. Between 72°C and 130°C the shift factor followed the WLF equation indicating that the T_g of water saturated wood at low frequencies is near 72°C. Thus, the water saturated wood followed the WLF behavior up to T_g + 55°C. Below 72°C, the shift factor followed an Arrhenius type of behavior. Using the the master curve, they also established the relationship between the logE′ and temperature at different frequencies.

Kelly et al. (1986) applied the TTSP to sitka spruce (Pices sitchensis Bong.Carr.) plasticized with ethyl formamide. The sample used was a 3 mm thick and 6 mm wide dual cantilever beam tested at low frequencies within a temperature range of -150°C to 150°C. on a dynamic mechanical

thermal analyzer (DMTA). They obtained a smooth master curve of logE′ against frequency at 60°C. The shift factor plot at this reference temperature showed that the major portion of the plot (-30 to 56 °C) fits the WLF equation represented in Figure 3(c) and Eq.[2.22]. The values of the constants obtained from this portion of the plot (C_1 = 17.7 and C_2 = 52.1) compared well with the "universal" WLF constants (C_1 = 17.44 and C_2 = 52.1). The shift factor below -30°C deviated from WLF behavior and followed a linear path. This temperature, -30°C, approximately represented the T_g of ethyl-formamide- plasticized wood. Therefore, they found that wood plasticized with ethyl formamide shows the WLF behavior upto T_g + 85 °C.

Ganowicz (1988) mathematically modeled the creep behavior of wooden beams of Baltic redwood (Pinus sylvestric L.) under non-isothermal environmental conditions at temperatures ranging from 21°C to 35°.C. His model is based on the assumption that wood is a thermorheologically simple material. Experimental creep compliance obtained from 1400 hour bending tests, and the compliance predicted from the model were found to be in good agreement.

Less conclusive support for TTSP for wood was given by Davidson (1962). He found from the recovery curves of bending tests that temperature slightly affected the slope of the curves up to 50°C and the influence was significant between 50 to 60°C. Therefore, he suspected that the temperature affected the shape of the response curve. He concluded that wood may not be a thermorheologically simple material and, therefore, TTSP must be used with caution.

2.6 Creep Analysis by the Finite Element Method

Creep is a materially nonlinear problem, therefore, equilibrium equation in creep is nonlinear (Kraus, 1980). Moreover, in a structure creep can magnify geometrically nonlinear behavior if the displacements or strains become large. As a result, creep problems cannot be solved exactly and numerical solution methods must be used. The Finite Difference Method (FDM) and the Finite Element Method (FEM) are two most widely used techniques to solve complex creep problems in engineering structures (Bernasconi and Piatti, 1978). However, the FEM has gained wide popularity in structural analysis due to its ability to deal with complex geometries and arbitrary distribution of material properties (Kraus, 1980).

In nonlinear analysis, the nonlinear equilibrium equations are formulated and solved incrementally. The basic problem in nonlinear analysis is to find the equilibrium state of a body corresponding to external loads. Assuming that the applied loads can be described as a function of time, the equilibrium conditions of a body consisting of a system of finite elements can be expressed as

$$ {}^{t}R - {}^{t}F = 0 \qquad [2.25] $$

where

${}^{t}R$ = vector of externally applied nodal loads at time t

${}^{t}F$ = vector of internal nodal forces at time t

In Eq.2.25, time t takes any value between 0 and the maximum time of interest. In static analysis, t is only a convenient variable used to describe load intensities and deformations of a body. However, in creep analysis, t is the actual time.

In nonlinear analysis, Equation 2.25 is formulated incrementally using the principle of virtual work and the resultant system finite element equation is (Bathe, 1982)

$$ {}^{t}_{t}K\ \Delta U = {}^{t+\Delta t}R - {}^{t}_{t}F \qquad [2.26] $$

where

${}^{t}K$ = tangent stiffness matrix at time t

Equation 2.26 is the incremental linearized finite element equation for a system of finite elements. This equation is solved step by step for unknown displacements using iterative solution procedures, such as Newton Raphson or Modified Riks Wempner method (Bathe, 1982)

2.6.1 Creep Analysis

The creep analysis based on the finite element method requires the constitutive creep law in rate form. Creep strain rate can be expressed as a function of time (time hardening models) or as a function of creep strain (strain hardening models) as discussed in section 2.4. The following finite element formulation is based on the Bailey-Norton time hardening creep model for primary and secondary creep under constant loading and isothermal conditions as reported by Ahmed (1988).

For constant loading and isothermal conditions, the rate form of the Bailey-Norton relationship was expressed in Eqn. 2.9 as

$$\dot{\varepsilon}_c = A\,\sigma^n\,t^p \qquad [2.27]$$

where

$\dot{\varepsilon}_c$ = creep strain rate

t = time

σ = stress

A,n,p = constants

For the purpose of iteration, Eq. 2.26 can be written for time $t + \Delta t$ as

$${}^{t+\Delta t}K^{(i-1)}\,\Delta U^{(i)} = {}^{t+\Delta t}R - {}^{t+\Delta t}F^{(i-1)} \qquad [2.28]$$

where;

i = iteration counter = 1,2,3,...,n

The initial conditions are

$${}^{t+\Delta t}K^{(0)} = {}^{t}K$$

$${}^{t+\Delta t}F^{(0)} = {}^{t}F$$

The internal force vector can be expressed as

$$ {}^{t+\Delta t}F^{(i-1)} = \int_{{}^{t+\Delta t}V^{(i-1)}} {}^{t+\Delta t}B_L^T(i-1)\ {}^{t+\Delta t}\tau(i-1)\ {}^{t+\Delta t}dV^{(i-1)} \qquad [2.29] $$

where

B_L = linear strain-displacement matrix

τ = Cauchy stress matrix

V = volume of the body

The most common creep analysis is based on the initial strain method. This method treats creep problems analogous to thermal stress problems. Specifically, the method converts creep effects into equivalent nodal forces. Assuming that the total strain (e) at a given time can be decomposed into elastic (e_0) and creep strain (e_c) components, the constitutive law can be written as

$$ {}^{t+\Delta t}\tau^{(i-1)} = C({}^{t+\Delta t}e^{(i-1)} - {}^{t+\Delta t}_{(k)}e_c) \qquad [2.30] $$

where

C = constitutive matrix

${}^{t+\Delta t}_{(k)}e_c$ = creep strain at time $t + \Delta t$ obtained from Eq. 2.80 by applying the Alpha method with the iteration (k) as discussed next.

Alpha Method

The Alpha method is a one parameter integration scheme for ordinary differential equations (Ahmed, 1988). In the Alpha method, the parameter α approximates a weighted average of the time derivative of a dependent variable at two consecutive time steps by the linear interpolation of the variables at these two times steps using the relation

$$\alpha\ {}^{t+\Delta t}\dot{e}_c + (1-\alpha)\ {}^{t}\dot{e}_c = \frac{{}^{t+\Delta t}e_c + {}^{t}e_c}{\Delta t} \qquad [2.31]$$

where

${}^{t}\dot{e}_c$, ${}^{t+\Delta t}\dot{e}_c$ = creep strain rate at times t and t + Δt, respectively

${}^{t}e_c$, ${}^{t+\Delta t}e_c$ = creep strain at times t and t + Δt, respectively

Δt = time step between two consecutive time points

From Eq.2.31 one obtains

$${}^{t+\Delta t}_{(k)}e_c = {}^{t}e_c + \Delta t[(1-\alpha)\ {}^{t}\dot{e}_c + \alpha\ {}^{t+\Delta t}_{(k-1)}\dot{e}_c] \qquad [2.32]$$

where

k = an iteration counter = 1,2,3.,....,n

for the i-th iteration

${}^{t+\Delta t}_{(0)}\dot{e}_c = {}^{t}\dot{e}_c$

The iteration of Eq. 2.32 continues until

$$\left|{}^{t+\Delta t}_{(k)}e_c - {}^{t+\Delta t}_{(k-1)}e_c\right| \le \beta \qquad [2.33]$$

where

β = specified tolerance

Equations 2.28 through 2.30 and 2.32 yield the following form of the equilibrium equation in creep analysis

$${}^{t+\Delta t}K^{(i-1)}\ \Delta U(i) = {}^{t+\Delta t}R - \int_{{}^{t+\Delta t}V^{(i-1)}} {}^{t+\Delta t}B_L^{T\ (i-1)}\ [{}^{t+\Delta t}e^{(i-1)} - {}^{t+\Delta t}_{(k)}e_c]\ {}^{t+\Delta t}dV^{(i-1)} \qquad [2.34]$$

Equation 2.34 is solved using an iterative solution procedure to obtain an incremental solution for the ith iteration. At the ith iteration,

$$^{t+\Delta t}U = {}^{t+\Delta t}U^{(i-1)} + \Delta U^{(i)}$$

The iteration is continued until a convergence criterion is met. At the convergence $\Delta U^{(i)}$ approaches zero and the equilibrium is satisfied. Upon convergence, a new trial value for creep strain rate $\dot{e}_c$ is obtained from Eq. 2.27 and this value is substituted into Eq.2.32 to calculate the new creep strain value. The new creep strain is compared with the previous trial value. If the condition given in eqn. 2.33 is satisfied, the solution moves to a new time step, otherwise the iteration procedure is repeated within the same time step until the creep strain is converged. In this manner, the equilibrium path is traced for the total time of interest (Ahmed, 1988).

In creep analysis, even a reasonably small time step can result in large creep strains and stresses and consequently, a large number of iterations is required to obtain the displacements and stresses. The Alpha method is effective in creep analysis because it subdivides the time increment Δt into smaller time steps and calculates the creep response by successive substitutions. It uses one time step size for the calculation of nodal displacements and a smaller time step to calculate stresses and strains.

2.7 Viscoelastic Stability

Instability of the equilibrium can lead to the collapse of elastic structures at a "modest" stress level: Viscoelastic structures exhibit similar "but more complex" behavior (Flugge, 1975). Viscoelastic instability can cause snap-through buckling in structures, such as, shallow arches and domes. This phenomenon was graphically and mathematically illustrated by Hayman (1981) for a shallow three-hinged concrete arch as shown in Figure 2.4.

The three-pin arch shown in Figure 2.4(a) supports a central load P. The arch consists of thick bars (BC and CD) of cross sectional area A and the bars are assumed not to buckle. Before loading, they are inclined to the horizontal at a small angle α. After loading the deformation is measured

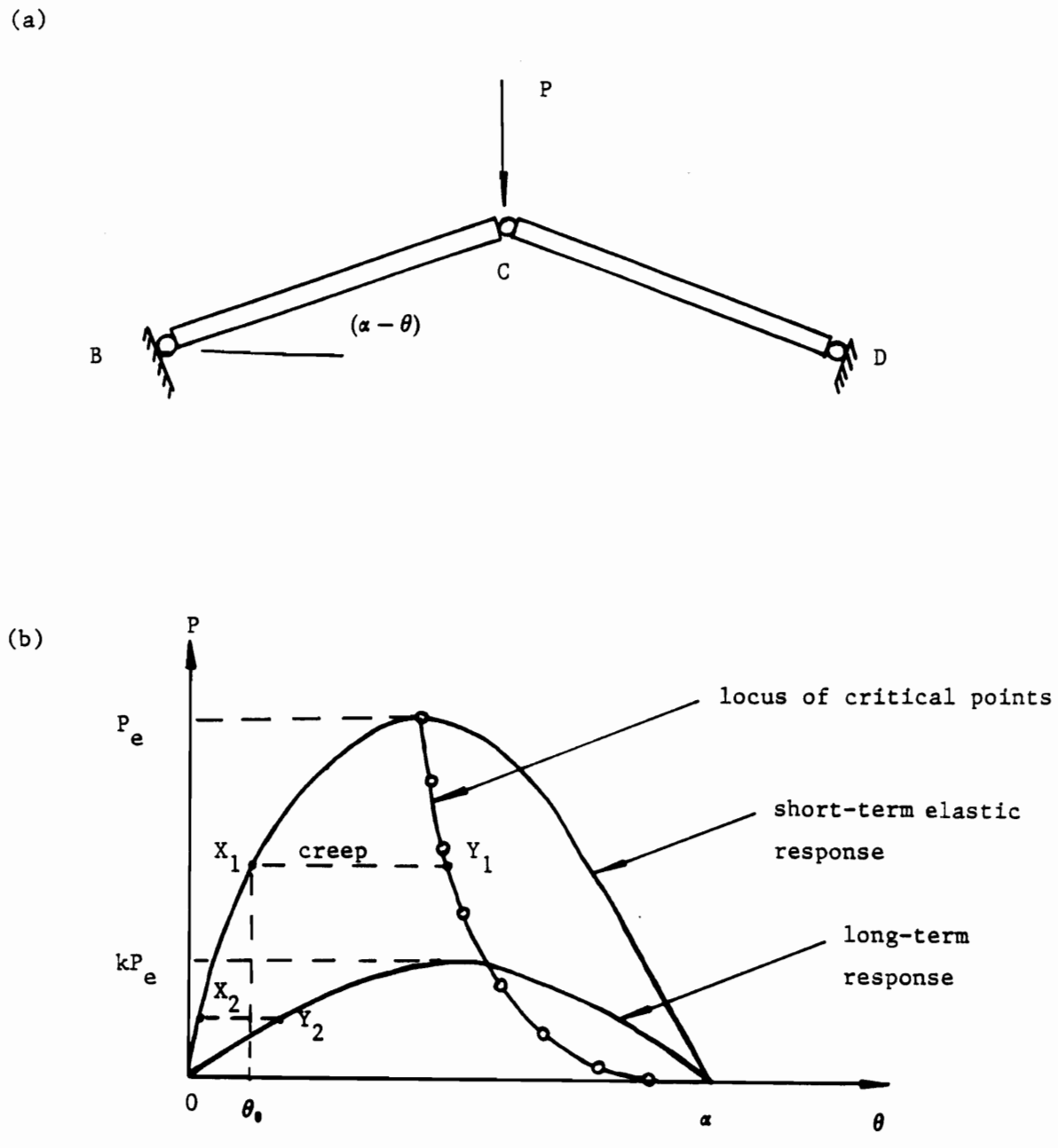

Figure 2.4. Illustration of snap-through buckling: (a) three-pin arch (b) its response (Source: Hayman (1981))

by the decrease (θ) in this angle. The elastic response as shown in Figure 2.4(b) is given by (Hayman, 1981)

$$P = A\ E\ (\alpha - \theta)\ [\alpha^2 - (\alpha - \theta)^2] \qquad [2.35]$$

where

E = Young's modulus of the bars

Snap-through buckling to an inverted position occurs if P is increased to the critical load for the system given by (Hayman, 1981)

$$P_e = \frac{2\ A\ E\ \alpha^3}{3\ \sqrt{3}} \qquad [2.36]$$

where

P_e = critical load for the system

If a load $P < P_e$ is applied, the deflection increases instantly to $\theta = \theta_0$ as given by Eq.2.35. Sustained load produces an increasing compressive creep strain causing the arch to be shallower. Figure 2.4(b) shows two distinct types of possible creep behavior. If $P > k\,P_e$, where $k\,P_e$ is the long-term elastic critical load of the arch, collapse occurs at the critical point locus expressed by (Hayman, 1981)

$$P = 2\,A\,E\,(\alpha - \theta)^3 \qquad [2.37]$$

If $P < k\,P_e$, the arch gradually subsides to a shallower configuration given by long-term response curve which takes the following form (Hayman, 1981):

$$P = k\,A\,E\,(\alpha - \theta)\ [\alpha^2 - (\alpha - \theta)^2] \qquad [2.38]$$

where

kE = long-term modulus of bars which replaces E in Eq.2.35

The arch does not reach the critical point locus and therefore does not fail.

Stability of an equilibrium state of a structure can be examined by using the tangent stiffness matrix formulated at each point in the equilibrium path. In this method, the eigenvalues and the eigenvectors are computed and the equilibrium is stable if all the eigenvalues of the tangent stiffness matrix at that point are positive, which implies that the stiffness matrix must be positive definite. If at least one eigenvalue is zero, the equilibrium is critical and the buckling mode is described by the corresponding eigenvector. If eigenvalues are negative, equilibrium is unstable.

Chapter 3

Development of Long-term Creep and Recovery models for wood

In this Chapter, long-term creep and recovery models are developed from experimental short-term accelerated compression data using the time temperature superposition principle. In section 3.1, a discussion of the test specimens and test conditions are presented and a description of the short-term accelerated test procedure is given. Also included are the material properties of the test specimens (section 3.1.2) and a detailed discussion on measuring compressive strains in wood with bonded electrical resistance strain gages. Creep and recovery master curves are developed from the accelerated compression data in section 3.2. The accelerated test results are presented in section 3.2.1., and the master curve formation is illustrated and shift factor data are presented in section 3.2.2.. Power functions are developed using regression analysis techniques to represent the master curves (section 3.2.3.), and linear regression relationships are developed to predict creep model parameters from the Young's modulus of wood (section 3.2.4.).

3.1 Short-term Accelerated Compression Creep Tests

3.1.1 Test Material

All the specimens in this study were prepared from kiln dried, dense select structural, 2″x4″x14′ southern pine (Pinus spp.) boards obtained from a lumber company in Salem, Virginia.

3.1.2 Moisture Content

Since the desired long-term creep prediction was for interior normal exposure conditions in buildings, the southern pine boards were conditioned in the laboratory at 70°F temperature and 50% relative humidity for six months until the moisture content of the boards reached approximately 9%. After equilibrating, the specimens were coated with a moisture protective coating ″Daran wrap″ to minimize moisture change during creep tests.

3.1.3 Specimen Preparation

The accelerated and long-term creep tests (Chapter 4) were conducted on end-matched wood specimens. Therefore, the specimen preparation for both tests are discussed here. To prepare a matched pair of accelerated and long-term test specimens, a clear, straight-grained, 1″x1″x20″ block was cut from the conditioned southern pine boards. A 4″ long piece was cut from one end for use in static compression tests to determine Young's modulus and the compressive strength of the test material. From the remaining piece, four 3″ long specimens with a cross section of 1/2″x1/2″ were prepared. The first two specimens were used as matched accelerated and long-term creep test specimens (active specimens), and the remaining two specimens were used as stress-free specimens (compensating or dummy specimens) to minimize temperature induced effects in the Wheatstone

bridge circuit used for measuring strains. More details on temperature compensation and strain measurements are discussed else where in this chapter. The remaining sample was used to determine the moisture content and the specific gravity of the test material.

3.1.4 Number of Specimens

A total of twenty accelerated test specimens, twenty static compression test specimens, and twenty moisture content test specimens were prepared. Seventeen specimens were used in accelerated creep tests; however, due to some experimental difficulties encountered in preliminary creep experiments, these tests could be completed only on eleven specimens.

3.1.5 Mechanical and Physical Properties of the Test Material

Moisture Content and Specific Gravity

The moisture content and the specific gravity of the test specimens could not be measured directly from the creep test specimens due to the bonded strain gages used to measure strains and the moisture protective coating applied over the gages and the specimen. Therefore, these properties (dry basis) were determined from the tests on the twenty representative moisture content specimens. The mean and the standard deviation for the moisture content were 9.34% and 0.55%, respectively, and these parameters for specific gravity were 0.678 and 0.034, respectively. The moisture content and the specific gravity corresponding to the eleven accelerated creep test specimens are presented in Table 3.1.

Modulus of Elasticity and Ultimate Compressive Stress

Knowing the ultimate stress of the test material, the creep stress level could be presented as a percentage of the ultimate stress. The ultimate compressive stress of the test specimens were obtained from static compression tests conducted on the twenty prepared 1"x1"x4" specimens end matched with the creep test specimens. The specimens were prepared so that the ends were square

Table 3.1. Material properties of accelerated creep test specimens

Specimen No.	Moisture content (%)	Specific gravity	Young's modulus (10^6psi)	Max. Comp. stress (psi)
1	10.26	0.727	2.961	11149
2	8.87	0.695	2.911	10823
3	9.35	0.719	2.811	10340
4	9.65	0.621	2.766	10741
5	9.25	0.708	2.739	10400
6	9.28	0.700	2.714	10393
7	10.22	0.680	2.682	8058
8	9.59	0.702	2.258	8517
9	10.37	0.654	2.109	8125
10	9.20	0.695	1.959	8274
11	9.90	0.580	1.567	8834
Mean	9.34	0.678	2.41	10242
Std. Dev.	0.55	0.034	0.359	0.645

and perpendicular to the length to avoid load eccentricity and premature failure. The tests were conducted according to the ASTM D143 standard procedure on an MTS closed-loop servo-hydraulic 22,000 capacity testing machine at a displacement rate of 0.012 in/min. until the specimens failed in compression. The strain in the specimens was measured by a Dual-Sensor Strain Transducer model DSST-II (Measurement Technology, Inc., Roswell, GA) over a 2″ gage length. The DSST consisted of two independent strain gage bridge sensors joined together to form a single transducer which could be easily attached to the opposite sides of a specimen with its clip-on attachment. The signal from each sensor was read by an MTI-SD-101 Instrumentation System which summed the two signals to provide an average specimen strain over the gage length.

The load-deflection data were recorded on an X-Y plotter and Young's modulus and the ultimate compressive stress were computed for the twenty specimens. The ultimate compressive stress and Young's modulus corresponding to the eleven creep test specimens are presented in Table 3.1. The mean and the standard deviation of the ultimate compressive stress were 10242 psi and 645 psi, and the mean and the standard deviation for Young's modulus were 2.41×10^6 psi and 0.359×10^6 psi.

3.1.6 Load Level

In practice, the design stress level in wood structural elements is only a small percentage of ultimate stress of the material. In this study, a stress equal to 16% of the experimentally determined mean ultimate compressive stress was chosen for the creep tests to obtain a constant reference stress level. This resulted in a creep stress of 1675 psi, and a load of 370 pounds was applied to all the accelerated test specimens. The percentage stress level for individual specimens varied from 15% to 20% of the respective ultimate compressive stress levels. At such small stress levels, many wood species have shown linear viscoelastic behavior (see Chapter 2); therefore, it was assumed that southern pine behaves as a linear viscoelastic material at these stress levels.

3.1.7 Temperature and Relative Humidity Conditions

The accelerated compression creep tests were conducted at various temperature levels starting from the ambient temperature of 70°F. The required temperature range for accelerated creep tests was below the glass transition temperature (T_g) of wood because the creep response of structures is in the glassy response region of wood. However, the T_g of southern pine was not known and needed to be determined. The following is the method used to determine the T_g of southern pine.

A Polymer Laboratories' Dynamic Mechanical Thermal Analyzer (DMTA) interfaced to a Hewlett-Packard 9816 computer was employed to determine the glass transition temperature of kiln-dried southern pine at 9% moisture content. The DMTA allows one to accurately assess the effects of temperature and moisture content on the molecular motion of a material (Kelly et al., 1986) The DMTA is sensitive to the individual transitions of a heterogeneous material. Since the wood cell wall is composed of three polymeric components (cellulose, hemicellulose, lignin), the DMTA should be sensitive to the thermal transitions associated with the amorphous components of hemicellulose and lignin (Kelly et al, 1986).

The specimen geometry for the dynamic test on DMTA was a dual cantilever beam with the following dimensions: 0.118″ thickness, 0.236″ width across the radial face, and 0.55″ free length. The temperature scans were performed at a heating rate of 9°F (5°C) per minute, frequency of 1 Hertz, and strain level of 4% over a temperature range of 77°F to 482°F (25°C to 250°C). Both the log- storage modulus (log E′) and the internal friction (tanδ) vs. temperature plots were obtained as shown in Figure 3.1. The region where log E′ showed a transition and tanδ peaked characterized a thermal transition region in the material. Both plots revealed a glass transition at 260°F (127°C) for kiln-dried southern pine and this temperature was used to select a temperature range for the accelerated compression tests.

The T_g obtained from the dynamic test showed that the maximum temperature for creep tests can be up to 260°F. However due to the limited capacity of the air control unit that supplied conditioned air for the creep tests, the maximum air temperature in the accelerated tests was 150°F. Starting from the ambient temperature of 70°F, eight successive temperature steps of 10°F

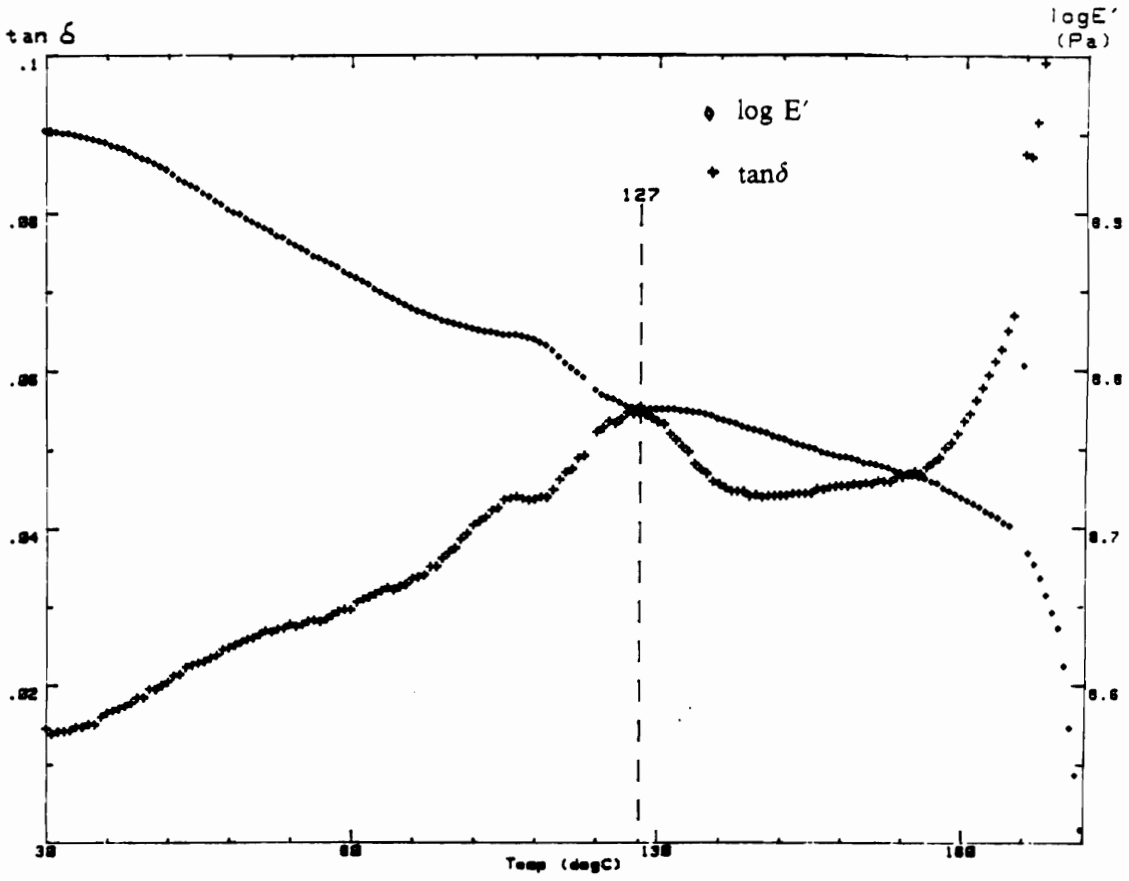

Figure 3.1. Glass transition temperature of kiln-dried southern pine

were used until the maximum temperature of 150°F was reached. The relative humidity of the accelerated test environment was adjusted at each temperature so that the Equilibrium Moisture Content (EMC) was maintained at 9% to produce constant moisture conditions within the test specimens. The humidity values were obtained from the Wood Handbook (1989), and Table 3.2 shows the temperature and the corresponding relative humidity (RH) used in the accelerated creep tests. The temperature and the relative humidity values obtained from the Wood Handbook were for sitka spruce. These data were used in the creep study because similar data for other specimens were not available. However, the moisture content of the specimens was monitored using the moisture content specimens located in the accelerated test environment as discussed later.

Heated air conditioned at the specified temperature and humidity levels was supplied by a PGC (Parameter Generation & Control Inc.) environmental chamber model 150/300 CFM CLIMATE-LAB-AA, 1985. The temperature of the conditioned air was maintained with $\pm$ 0.36°F accuracy and the relative humidity with an accuracy of $\pm$ 0.5%.

3.1.8 Test Duration

Each specimen was tested at each temperature level in the accelerated creep tests. Therefore, it was necessary to ensure that the creep deflection at the previous temperature level was recovered prior to the beginning of the test at the next temperature level. Based on the observations from a preliminary creep test program, the following creep and recovery periods were chosen for the accelerated creep tests.

The accelerated creep test duration was 17 hours at each temperature level except at the highest temperature (150°F). At 150°F, the test period for various test specimens was extended to time durations ranging from three to ten days to expand the extrapolation of the developed master curves. The recovery was observed for 40 hours at each temperature up to 140°F, and at 150°F, recovery data were collected for a duration equal to the corresponding creep test period.

Table 3.2 Temperature and relative humidity to maintain constant EMC (9%) in accelerated creep tests (Source: Wood Handbook 1987)

Temperature (°F)	Temperature (°C)	Relative humidity (%)
70	21.11	48
90	32.22	50
100	37.77	51
110	43.33	53
120	48.88	55
130	54.44	57
140	60.00	59
150	65.55	61

3.1.9 Strain Measurement with Bonded Strain Gages

The compressive creep strain in the accelerated tests was measured by strain gages bonded to the surface of the test specimens and connected in a Wheatstone bridge circuit. An electrical resistance strain gage consists of a strain-sensitive conductor mounted on a paper or plastic backing. The backing allows ease in handling the gage filament, presents a readily bondable surface for cementing gages to a test surface, and insulates the conductor from the surface of the test material (Perry, 1962). Strain gages used in this study were constantan alloy foil strain gages mounted on plastic backing and had the following characteristics: 0.24″ gage length, 120 ohm resistance, 2.05 gage factor, 5% maximum strain range, and -110°F to 350°F operating temperature range.

The gage factor is the ratio of the relative resistance change of the gage to the strain in the material to which the gage is bonded and is expressed as

$$F\,\varepsilon = \frac{\Delta R}{R} \qquad [3.1]$$

where

F = gage factor (supplied by the manufacturer)

ε = strain in the material (needed to be determined)

ΔR = resistance change of the gage (measured experimentally)

R = initial resistance of the gage (supplied by the gage manufacture)

The relationship in Eq. 3.1 was used to compute the strain in the wood specimens with the measured resistance change of the gages as discussed later. However, the key to successful strain measurements with strain gages is properly bonded gages, and extreme care should be taken in mounting them on a test surface.

Mounting Strain Gages on Wood Surfaces

Bonding strain gages to a surface of a material is a technique that must be acquired by experience. The key to satisfactory bonding of gages is a properly prepared material surface (Perry, 1962). The materials and equipment necessary for the gage installation were purchased from the

gage manufacturers (Measurement Groups, Inc., Raleigh, NC.) and their recommended procedure was followed in preparing the mounting surface and bonding the gages to the wood specimens with a two part epoxy adhesive AE-10. The AE-10 adhesive is a "100% solid epoxy system allowing high elongation (10%) and operating temperatures from -320°F to 200°F". After the gages were properly mounted, three foot long 430-FST type lead wires were soldered to the solder tabs of the gages for connecting the gages to a Wheatstone bridge circuit. The lead wires were stranded, silver-plated, copper wires with teflon insulation, and assembled as a four conductor twisted cable with a braided shield in a teflon jacket.

The AE-10 adhesive is highly resistant to moisture and is therefore, recommended by the manufacturers for permanent installations (i.e., over one year). However, since wood is a hygroscopic material, extra protection for strain gages from moisture was provided by a DOW CORNING 3140 RTV silicone rubber coating which cured in 24 hours at ambient conditions.

3.1.10. Measuring Compressive Strains with Strain Gages

A specimen subjected to a compressive force may experience bending deflection due to load eccentricity. The bending effect can influence the measured compression data. In addition, the temperature sensitivity of the gages and lead wires that connect the gages to the Wheatstone bridge can lead to temperature induced apparent strains. Moreover, the self-temperature compensating gages used in this study show extremely low sensitivity to temperature when bonded to test surfaces with thermal expansion coefficients similar to that of the gage material. However, when bonded to wood, dissimilar thermal expansion of the gage and the wood produces temperature induced apparent strains in the gages. This apparent strain can affect the measured compression data. Thus, a strain gage arrangement for measuring pure compressive strain should provide cancellation of any bending and thermal effects from the Wheatstone bridge output. The method used to achieve these conditions is discussed next.

Figure 3.2 shows the gage lay out and Wheatstone bridge arrangement designed to eliminate bending and temperature effects and to obtain compression creep data. Here, the active specimen is the loaded specimen and the dummy is a stress-free (unloaded) specimen and both specimens are exposed to same environmental conditions. Two gages were bonded on the opposite sides of each specimen as shown in Figure 3.2.(a) and the gages were arranged in the Wheatstone bridge powered with 2 Volts dc as shown in Figure 3.2.(b). In this bridge, the active gages (1 and 3 in Figure 3.2(a)) as well as the dummy gages (2 and 4) are on opposite legs of the Wheatstone bridge. The bridge was powered by a multi-channel strain gage conditioner and amplifier system model 2100 (Vishay Intertechnology, Inc., Raleigh, NC).

The principle of the Wheatstone bridge states that if the resistance of the opposite legs, for instance, R_1 and R_3 in Figure 3.2(b), undergo changes of the same sign (+ or -), these effects on the bridge output are additive, whereas the resistance changes of opposite sign are numerically subtractive. The reverse is true for resistance changes on adjacent legs of the bridge, such as, R_1 and R_4. Here, the same sign of resistance changes are subtractive and opposite sign changes are additive. This principle was used to arrange gages in the Wheatstone bridge shown in Figure 3.2(b) to cancel the bending and temperature effects from the bridge output. According to this principle the two gages bonded on opposite sides of the active specimen led to cancellation of bending effects and doubled the sensitivity of the output to compression (compared to a single gage). The dummy gages provided elimination of thermal effects. More details on these compensations are presented later in this section.

The data collection was started by powering the bridge, loading the active specimen, and reading the bridge output voltage. In the creep tests, the bridge output voltage corresponding to the resistance change of the gages, induced by the load acting on the specimen, was recorded. Then the output voltage was converted to the strain in the specimen using the relationship between the gage factor and the strain expressed in Eq.3.1 in conjunction with the equation for the Wheatstone bridge output (Eq.3.2) as discussed in the next section.

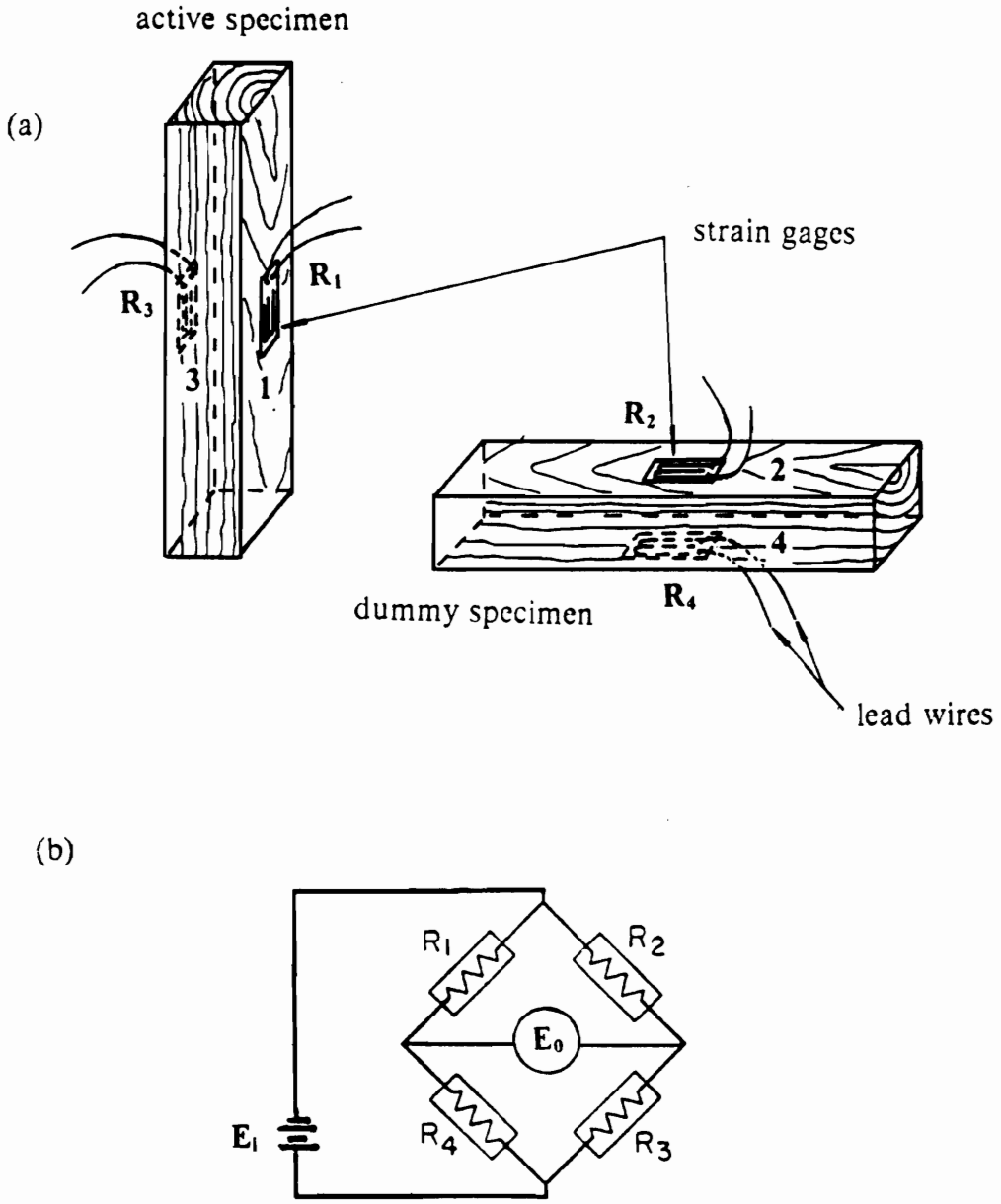

Figure 3.2. Creep strain measurement: (a) active and dummy gages (b) Wheatstone bridge circuit

Computation of Compressive Strain in the Specimen

The relationship between the bridge output voltage and the resistance of the gages in the Wheatstone bridge shown in Figure 3.2(b) can be expressed as (Perry, 1962):

$$\frac{E_0}{E_i} = \left[\frac{R_1}{(R_1 + R_2)}\right] - \left[\frac{R_4}{(R_3 + R_4)}\right] \qquad [3.2]$$

where

E_0 = bridge output voltage (measured experimentally)

E_i = bridge excitation voltage (2 volts dc.)

R_1, R_3 = resistance of the active gages (known)

R_2,R_4 = resistance of the dummy gages (known)

When the active specimen is loaded in compression and both active and dummy specimens are being exposed to the same constant temperature, the active gages (1 and 3 in Figure 3.2) undergo resistance changes of the same sign (ΔR) and the resistance of the dummy gages remain unchanged. The Wheatstone bridge output for this configuration can be expressed as:

$$\frac{E_0}{E_i} = \left[\frac{(R_1 + \Delta R)}{(R_1 + \Delta R) + R_2}\right] - \left[\frac{R_4}{(R_3 + \Delta R) + R_4}\right] \qquad [3.3]$$

Since all gages have equal initial resistance ($R_1 = R_2 = R_3 = R_4$), and from Equation 3.1

$$\frac{\Delta R}{R} = F\ \varepsilon \qquad [3.4]$$

where

F = gage factor

ε = strain in the test material

Equation 3.3 can be rewritten as:

$$\frac{E_0}{E_i} = \frac{F\ \varepsilon}{2 + F\ \varepsilon} \qquad [3.5]$$

From Eq.3.5, the strain in the specimen can be computed as:

$$\varepsilon = \frac{2\ E_0}{F\ (E_i - E_0)} \qquad [3.6]$$

The strain in the specimen, ε, was computed from Eq. 3.6 with experimentally measured bridge output voltage, E_i.

Elimination of Bending Effects from the Bridge Output: If the active specimen subjected to an axial compressive force also experiences bending deflections, the resistance changes of the two active gages are of opposite signs ($+\ \Delta R$ and $-\ \Delta R$) whereas, the resistance of the dummy gages remain unchanged. Substituting resistance changes due to bending into Equation 3.2

$$\frac{E_0}{E_i} = \left[\frac{(R + \Delta R)}{(R + \Delta R) + R}\right] - \left[\frac{R}{(R - \Delta R) + R}\right] \qquad [3.7]$$

Simplifying Equation 3.7

$$\frac{E_0}{E_i} = -\frac{\left(\frac{\Delta R}{R}\right)^2}{4 - \left(\frac{\Delta R}{R}\right)^2} \qquad [3.8]$$

Substituting Eq.3.4 into Eq.3.8

$$\frac{E_0}{E_i} = -\frac{F^2 \varepsilon^2}{4 - F^2 \varepsilon^2} \qquad [3.9]$$

According to Eq.3.9, the output becomes approximately zero due to the negligible square term of the micro-strain, indicating the elimination of bending effects.

Cancellation of thermal effects from the bridge output: When both active and dummy gages are subjected to a temperature change of ΔT, all four gages experience similar resistance changes, ΔR, due to the temperature change. When ΔR is substituted into Equation [3.2] where all the initial

resistances are similar, the bridge output, E_0, becomes zero indicating that the effects of the temperature change are cancelled from the measured data.

3.1.11 Data Acquisition

In the accelerated creep tests the bridge output voltage (E_0) was read by a data acquisition system consisting of a data translation board model DT2805 (Data Translation, Inc., Marlboro, MA) and a portable IBM-PC computer. A software package was developed at the laboratory for automatically reading creep data at various user specified time intervals and storing the data on a magnetic tape.

3.1.12 Accelerated Compression Test Apparatus

The short-term accelerated creep tests were conducted in an insulated, 5′ long, 2′ wide, and 2′ high test chamber. A 3.5″x3.5″ angle iron attached to the bottom of the test chamber served as the base for the tests as shown in a schematic diagram in Figure 3.3. A test fixture consisted of two 1″x2″x6″ aluminum bars connected with two 3/8″ threaded rods. Each threaded rod passed through a 0.5″ diameter hole in the chamber base as shown in Figure 3.3. A three foot long lever arm was attached to the bottom aluminum bar and a fulcrum was located on the bottom of the test chamber. This arrangement allowed for load application and removal from outside the chamber.

The specimen was placed between the top aluminum bar and the angle iron base. A 1″ diameter by 0.375″ thick spherical washer arrangement was placed underneath the specimen to allow for uniform load application over the entire cross section of the specimen. The load was applied by hanging a weight on the free end of the lever arm. A preliminary experiment was conducted to verify that the lever arm arrangement applied the required force (370 pounds) to the specimen. A 1000 pound capacity calibrated Universal Flat Load Cell model FL1OU-3SPKT was placed underneath the spherical seat, and the weight hanging on the lever arm was adjusted until the voltage

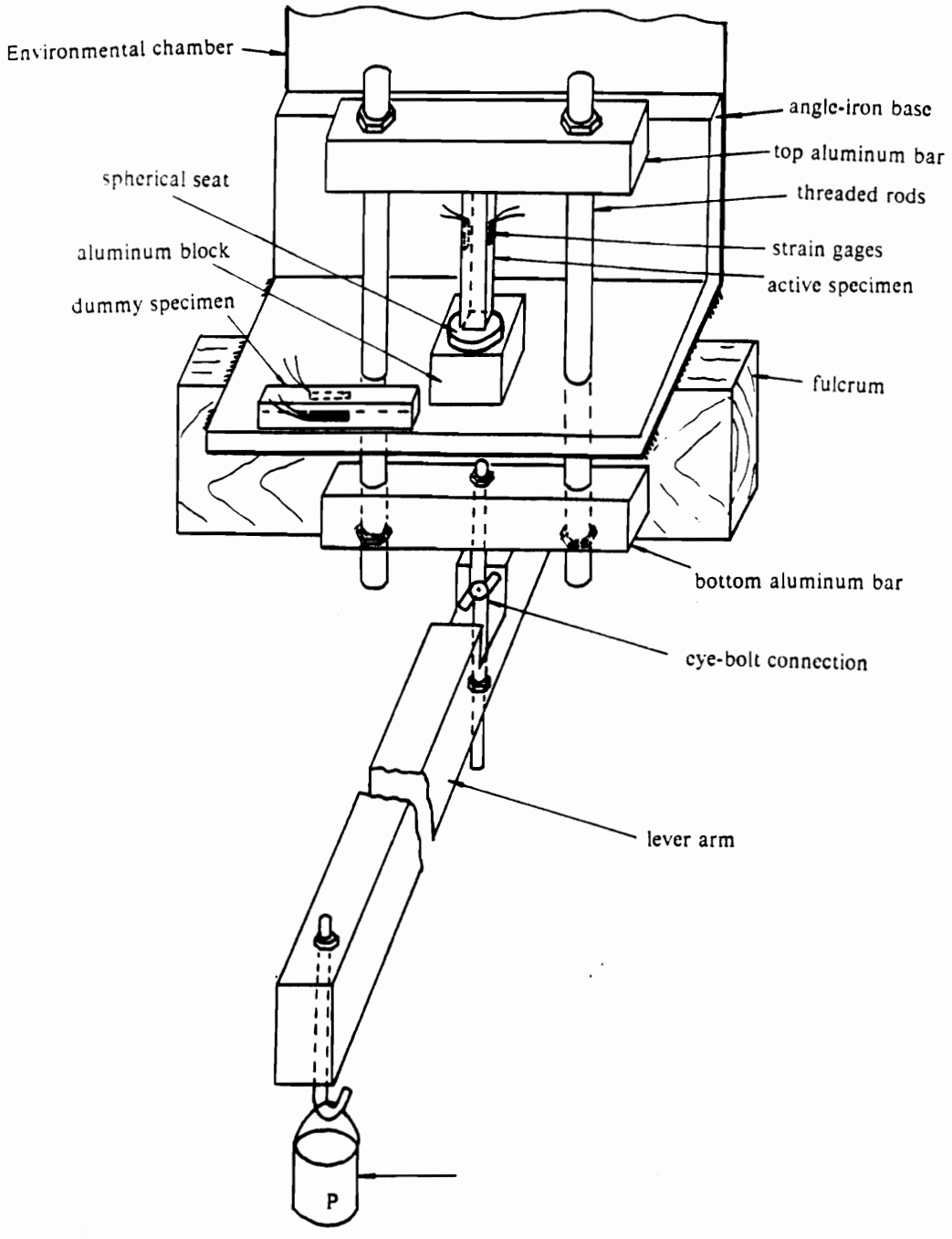

Figure 3.3. Schematic diagram of accelerated test fixture

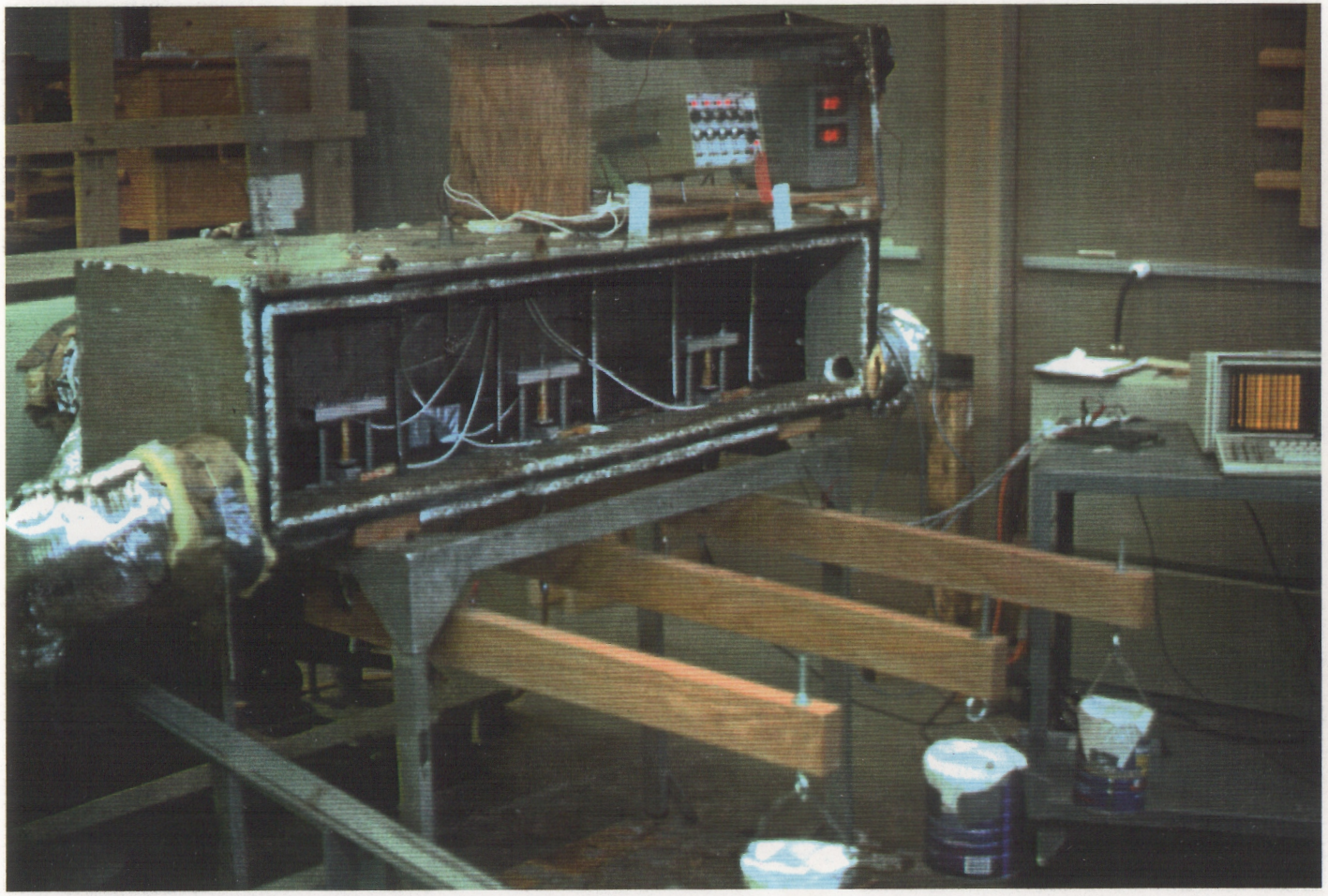

Figure 3.4. Short-term accelerated test arrangement

output from the load cell corresponded to 370 pounds. The lever arm calibration showed that the lever advantage was approximately 1:20. Once the required force was verified, the load cell was replaced with an Aluminum block of equal thickness to retain the geometry of the test fixture as shown in Figure 3.3.

Three similar test fixtures were assembled in the test chamber for testing three specimens simultaneously as shown in Figure 3.4. Five thermometers were placed in the chamber to measure the temperature distribution within the chamber. In addition, a humidity and temperature transmitter model HMP 135Y (Vaisala Products, Finland) located inside the chamber provided a digital readout of the relative humidity and the temperature in the chamber. The temperature measurement range of the transmitter was from 32-320°F with an accuracy of $\pm$0.36°F and the relative humidity range was from 0-100% with $\pm$ 1% accuracy.

3.1.13 Accelerated Test Procedure

A set of preliminary accelerated creep tests was conducted in the chamber to test the applicability of TTSP to wood by testing a wood specimen, with the active and dummy gage arrangements already discussed, at temperature levels ranging from 70°F-130°F with 10°F steps. The prescribed load of 370 pounds was applied to the specimen and creep data were recorded for 17 hours and recovery data for 35 hours. Since a master curve could be developed from these preliminary data, the creep tests were continued on all the prepared wood specimens following the procedure discussed next.

Three pairs of active and dummy specimens were instrumented with bonded electrical resistance strain gages, and the gages and the specimens were coated with the moisture protective coatings discussed previously. Prior to placing the specimens in the test fixtures, each specimen pair (active and dummy) was weighed (with attached lead wires) to monitor moisture gain or loss during the experimental program. In addition, three moisture content specimens, also with a

moisture protective coating, were placed in the chamber near the test fixtures for the duration of the experiments.

The active specimens were centered in the test fixtures and the dummies were located as close to the active specimens as possible as shown in Figure 3.4, and the chamber door was closed and tightly sealed. The lead wires were connected to the Wheatstone bridge supplied by the strain gage conditioner and amplifier system and the bridge output wires were connected to the data translation board of the data acquisition system.

To improve the stability of the strain reading from strain gages, the specimens were subjected to a mechanical conditioning scheme at the highest test temperature. The temperature in the chamber was raised to 150°F and the humidity was adjusted, according to Table 3.2, to obtain an EMC of 9%. The unloaded specimens were conditioned for 24 hours to achieve thermal equilibrium, after which the loads were applied to the active specimens which were subjected to a 17 hour creep period. The mechanical conditioning scheme was concluded by removing the loads and observing the specimen recovery at the same temperature until the recovery was complete as evidenced by the return of the voltage reading on an external voltmeter to the initial reading shown prior to the creep tests. Upon completing the mechanical and thermal conditioning scheme, creep tests were conducted in the following manner.

The creep test procedure was started by conditioning the specimens at ambient temperature and humidity conditions (70°F, 49% RH) for 24 hours. Then, the loads were applied, the data acquisition system was activated, and the bridge output voltage was recorded for 17 hours. The frequency of the data collection was as follows: every second for 200 seconds, every 10 seconds for 3000 seconds, every 100 seconds for 30,000 seconds, and every 1000 seconds 31,000 seconds. After the creep period, the loads were removed and the recovery data were recorded for 48 hours. The frequency of the recovery data collection was: every second for 200 seconds, every 10 seconds for 3000 seconds, every 100 seconds for 30,000 seconds, every 1000 seconds for 29,000 seconds, and every 10,000 seconds for 130,000 seconds.

Next, the temperature was raised to the next higher level and the humidity of the conditioned air was adjusted to achieve 9% EMC. Then the unloaded specimens were conditioned for 24 hours.

At this point, the completion of recovery from the previous creep test was checked by an external voltmeter as discussed previously, and if the specimens were still recovering, the thermal conditioning was extended until the recovery was complete. Then, the loads were applied and creep data were collected for 17 hours after which 48 hour recovery tests were performed. The test procedure was repeated up to 140°F in 10°F steps. At 150°F, the test duration was extended to three to ten days for various sets of test specimens. Some specimens were tested only up to 140°F. For these specimens, the test duration was extended to longer periods at 140°F. The purpose of this extension was to expand the extrapolation of the developed master curves.

Upon completing the recovery test at 150°F, one set of accelerated tests was finished, and the active and the dummy specimen pairs as well as the three moisture content specimens were weighed to determine if any moisture change occurred during the test period. Then, another three pairs of active and dummy specimens were located in the test fixtures and the whole test procedure was repeated until all the specimens were tested. The results of the accelerated tests and developed master curves are presented in the next section.

3.2 Development of Long-term Creep and Recovery Curves (master curves)

Long-term creep and recoverable compliance curves were developed from the accelerated creep and recovery data obtained from the eleven test specimens. The observations from the accelerated creep and recovery tests are presented and discussed in section 3.2.1. The development of the master curves is described and the information related to the master curves, such as, shift factors, are presented in section 3.2.2. In section 3.2.3., power functions are developed for each creep and recovery master curve using a nonlinear regression analysis technique. Finally, regression relationships are developed to predict the model parameters from Young's modulus of wood in section 3.2.4.

In this section, the results are presented in the following manner. For each specimen, accelerated creep and recovery curves and the corresponding master curves are presented along with the

corresponding shift factor data. In this way, all the information related to one specimen is complete before the presentation of the results for other specimens. The typical results for three specimens are reported in the text and the detailed observations for the other specimens are reported in Appendix A.

3.2.1 Accelerated Test Results

Accelerated creep and recovery data were collected at temperature levels ranging from 70-150 °F as discussed in section 3.1.13.. In the preliminary investigation, the temperature range was from 70°F - 130°F. Creep and recovery tests on twelve specimens were conducted from ambient to 150 °F, and tests on four specimens were performed up to 140°F. The accelerated tests could be successfully conducted only on eleven out of seventeen test specimens for the reasons discussed in the next paragraph. The difference between the moisture content of the test specimens at the beginning and the end of the accelerated test procedure was approximately 0.5%.

The data collection from the first six specimens was not successful. In these tests, two sets of three test specimens were tested one after the other at each temperature level. This procedure resulted in experimental difficulties and erroneous data. Therefore, the results from these six specimens were discarded. Consequently, in the subsequent experiments, tests on one set of three specimens were completed at all the temperature levels prior to the tests on another set.

The accelerated data were in the form of Wheatstone bridge output voltage and were stored on magnetic tapes. For the data analysis, the voltage output data ($E_0(t)$) were first converted to strain in the specimen (ε_t) using the relation expressed in Equation 3.6 as

$$\varepsilon(t) = \frac{2\,E_0(t)}{F\,(E_i - E_0(t))} \qquad [3.10]$$

where;

F = gage factor = 2.05

E_i = bridge excitation voltage (2 volts dc.)

Then the compliance, D(t), was computed from

$$D(t) = \frac{\varepsilon(t)}{\sigma} \qquad [3.11]$$

where

σ = applied creep stress (1670 psi)

The creep and recoverable compliance at each temperature level were plotted against log-time and these curves for three selected specimens (Nos. 2, 9, and 4) are shown in Figures 3.5(a)-(b), 3.7(a)-(b), and 3.9(a)-(b). The curves for the other eight specimens are included in Appendix A. Since numerous data points were collected at frequent intervals, curves were formed automatically when the data were plotted. For the creep and recovery curves, the initial elastic reading corresponds to a time period equal to five times the load application period to avoid the impact of the loading on the initial data. The data at 80°F overlapped with the data at the 70°F ambient temperature. Therefore, the curves for 80°F were eliminated from the data sets.

The Figures 3.5, 3.7, 3.9, and those in Appendix A, show that the temperature has a considerable influence on the compression creep behavior of wood. For example, the time dependent compliance and the initial elastic compliance increase with temperature. Creep rate is low at low temperature levels; however, the creep rate increases rapidly at high temperature levels. It is evident that for a given load duration, higher temperatures produce higher creep rates and higher magnitudes of creep. At all temperatures, the creep rate at a given time is faster than the the corresponding rate of recovery showing a delay in the recovery of the creep deflection. These results are consistent with the observations of other researchers studying the effects of temperature on the creep behavior of wood (see Chapter 2).

The accelerated creep and recovery curves were used to form master curves based on TTSP, and the procedure used is discussed in the next section.

3.2.2 Master Curve Formation Procedure

The formation of master curves based on the time temperature superposition principle is illustrated for the data presented in Figure 3.5(a) and the resultant curve master curve is shown in Figure 3.6(a). The procedure used to form master curves is described as follows: First, 70°F was chosen as the reference temperature to correspond to the typical interior temperature in buildings. Then, keeping the curve at 70°F stationary, the curve at 90°F was shifted along the log-time axis, until it smoothly joined the curve at 70°F. Next, the other curves at successively higher temperature levels were shifted in a similar fashion until all the curves joined to form a master curve as shown in Figure 3.6(a).

The distance each curve was shifted is called horizontal shift factor, $\log a_T$ (see chapter 2). The shift factor for each creep curve segment shown in Figure 3.5(a) is presented in Table 3.3. In addition to horizontal shifting, most curves required a vertical shift to form the master curve. The distance each curve needs to be shifted vertically is called the vertical shift factor, a_s, and these values for the curve sections shown in Figure 3.5(a) are also presented in Table 3.3. More discussion on horizontal and vertical shift factors are presented later in this section.

Generally, the curve segments shown in Figure 3.5(a) joined well with the master curve as shown in Figure 3.6(a). However, the end sections of most master curves did not perfectly match with the master curve but this error was less than a compliance value of $4x10^{-9}$(1/psi) (Figure 3.6(a)). For comparison of the long- term creep and recovery behavior, the master curve developed for recovery is also presented in Figure 3.6(a) along with the creep master curve. The master curves for the other ten specimens were formed using the same procedure as that used for the example specimen. Therefore, for clarity, only the final curve (i.e., without unmatched curve segments) is presented for the remaining specimens. The master curves for two more specimens are presented in Figures 3.8(a) and 3.10(a). The curves for the other eight specimens are reported in Appendix A immediately next to the corresponding accelerated test curves.

The master curves show that creep increases exponentially with time. The recovery master curves lagged behind the creep curve demonstrating the delayed recovery of the long-term creep

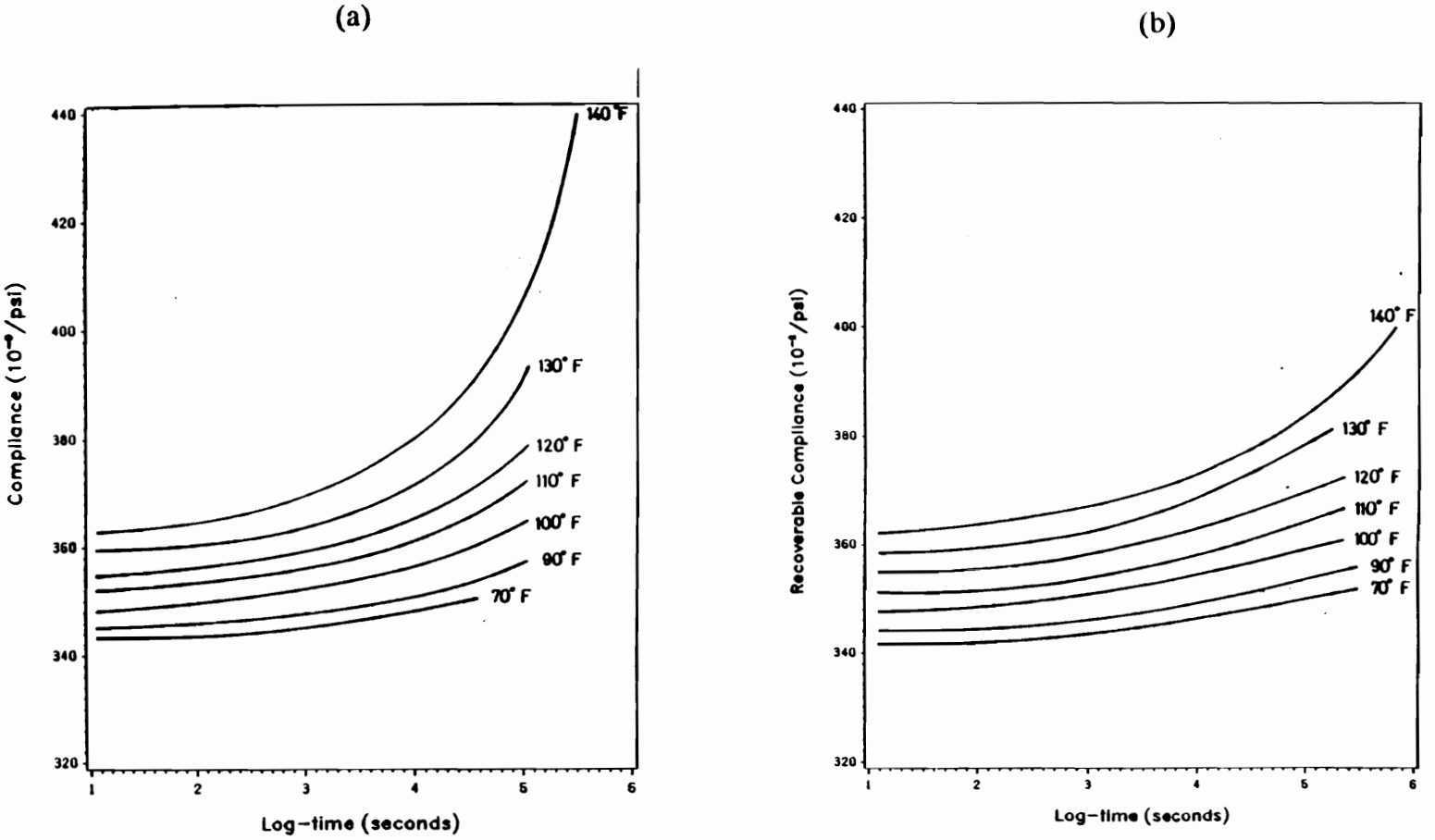

Figure 3.5. Short-term accelerated data for specimen No.2: (a) creep data (b) recovery data

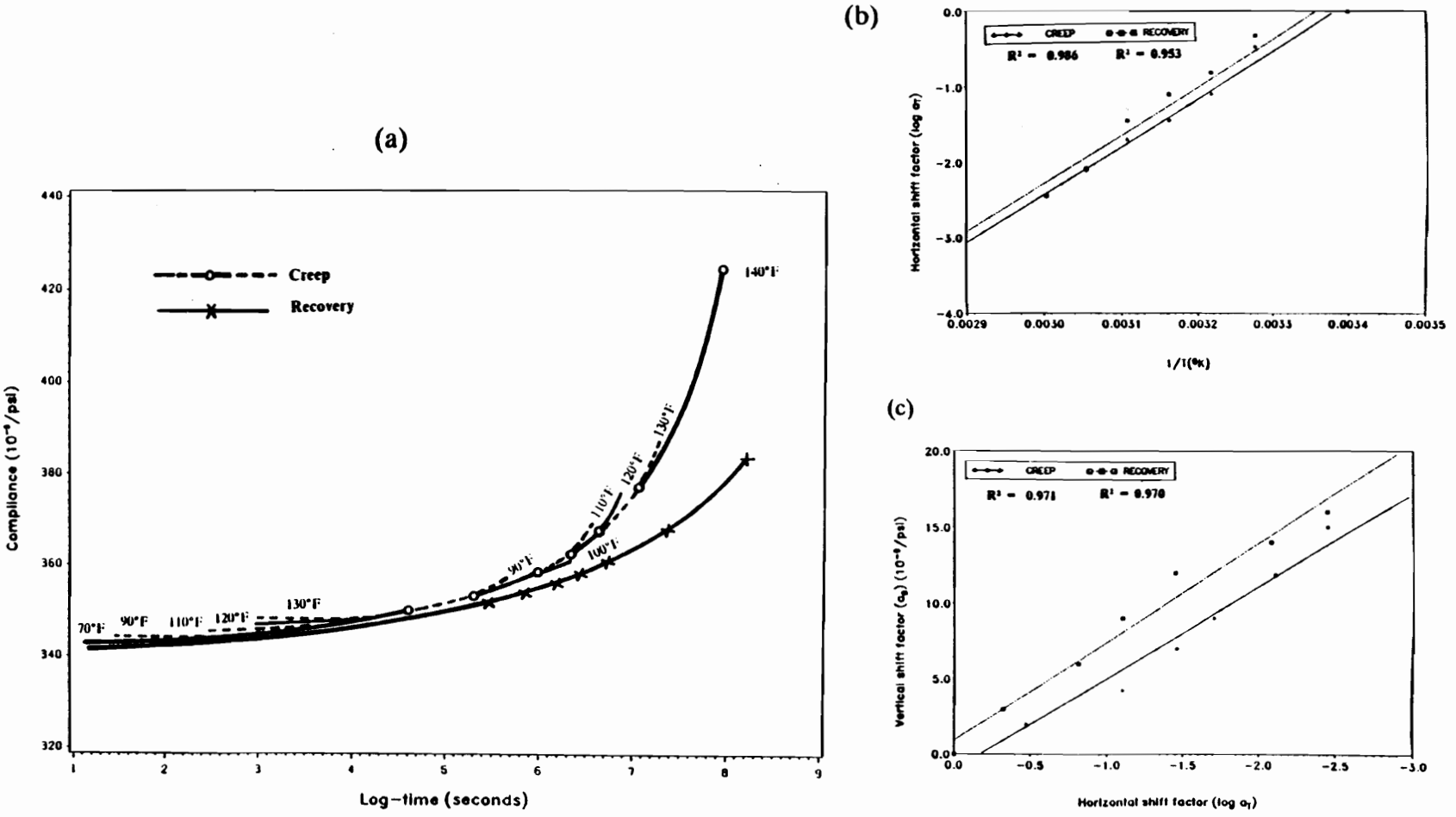

Figure 3.6. Master curves and shift factor data for specimen No.2: (a) creep and recovery master curves (b) horizontal shift factor vs. temperature (c) vertical vs. horizontal shift factors

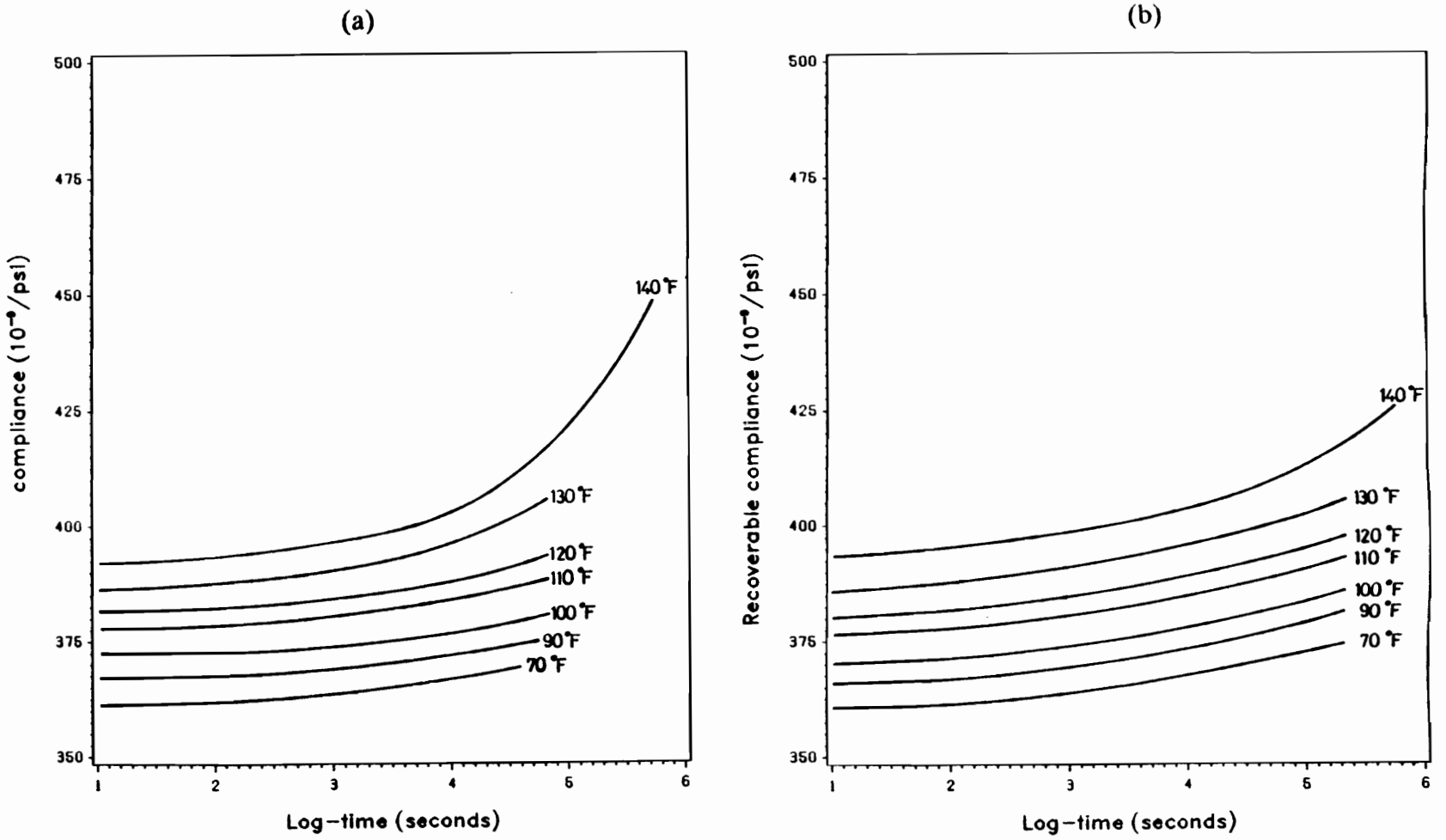

Figure 3.7. Short-term accelerated data for specimen No.4: (a) creep data (b) recovery data

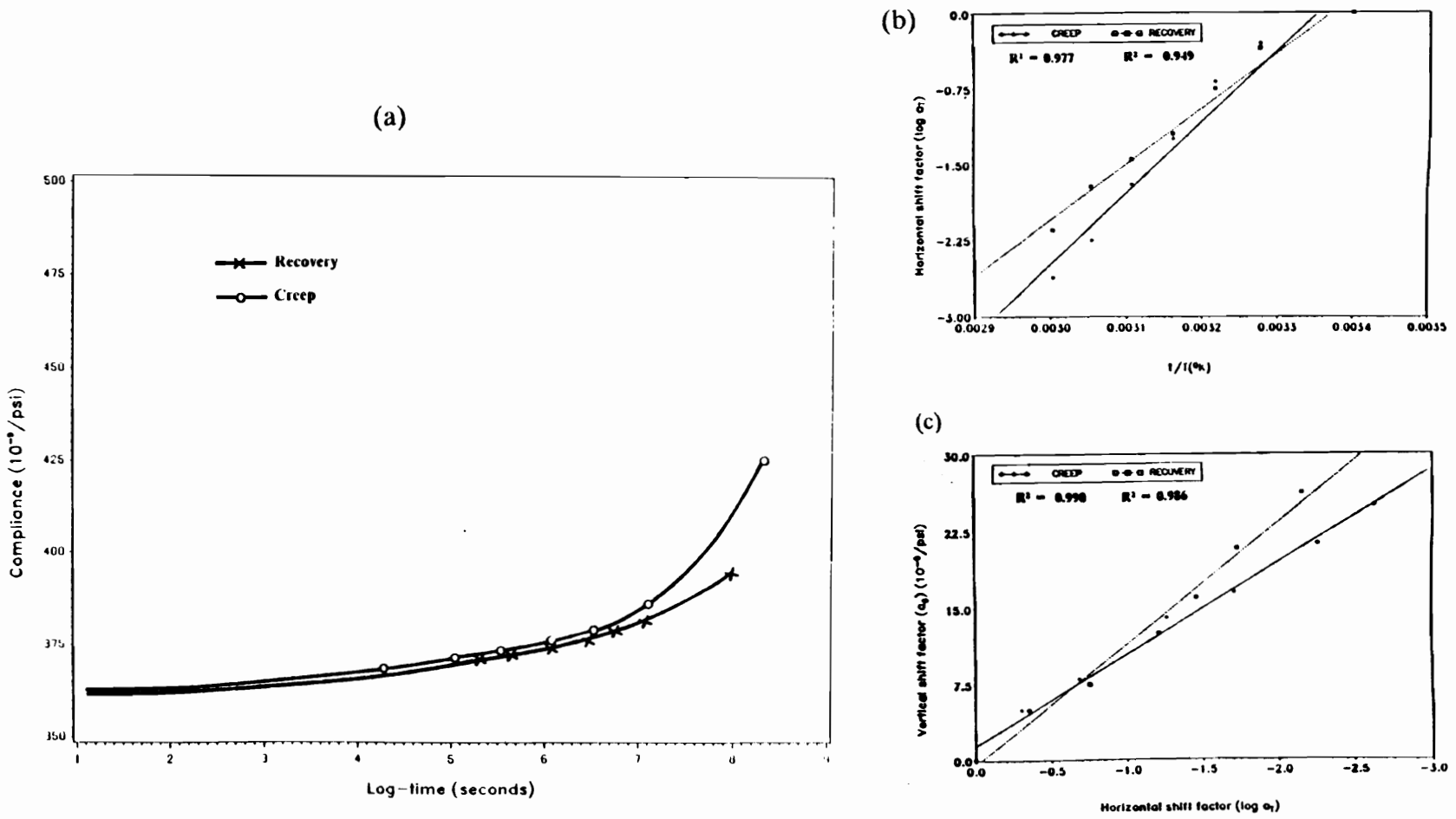

Figure 3.8. Master curves and shift factor data for specimen No.4: (a) creep and recovery master curves (b) horizontal shift factor vs. temperature (c) vertical vs. horizontal shift factors

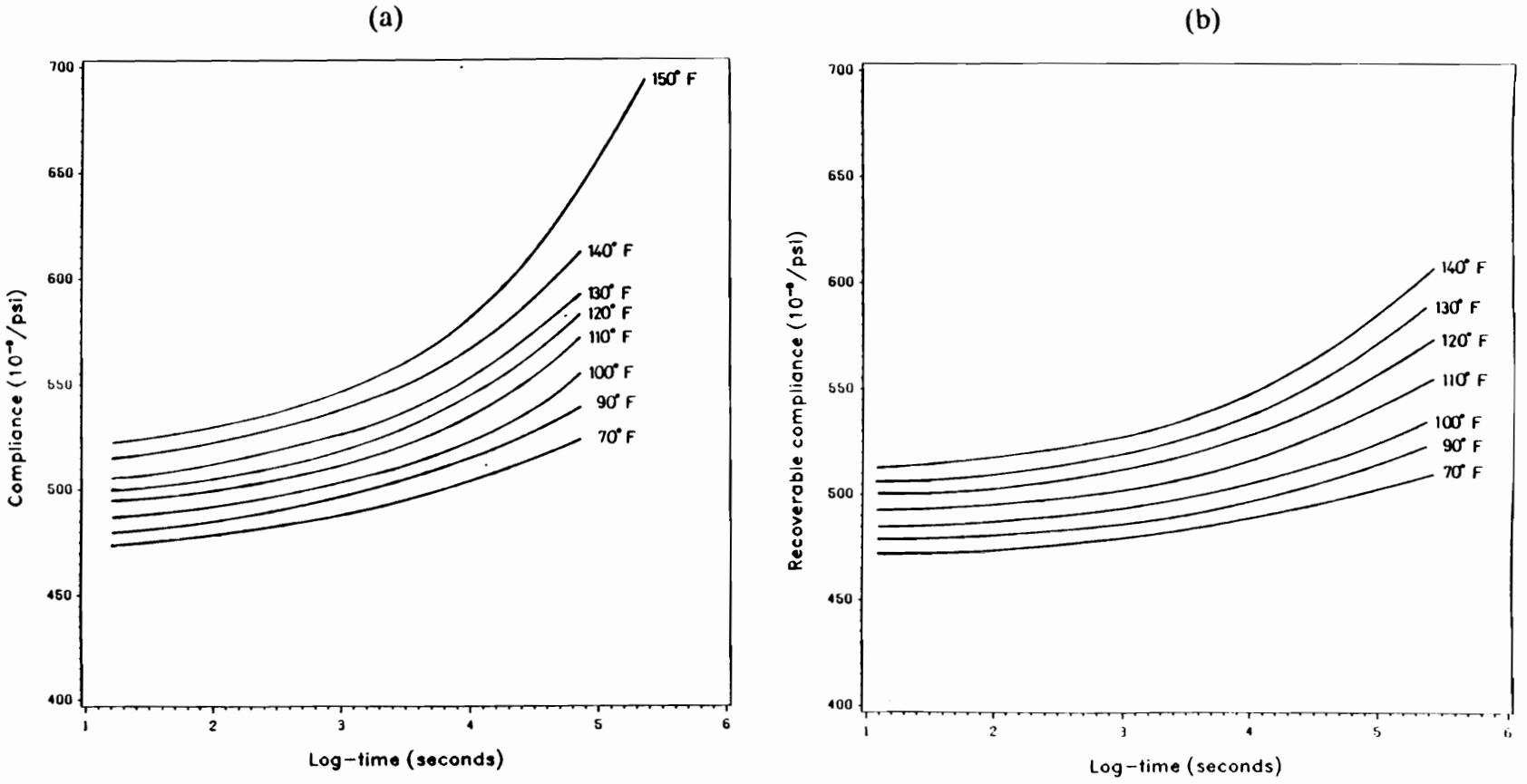

Figure 3.9. Short-term accelerated data for specimen No.9: (a) creep data (b) recovery data

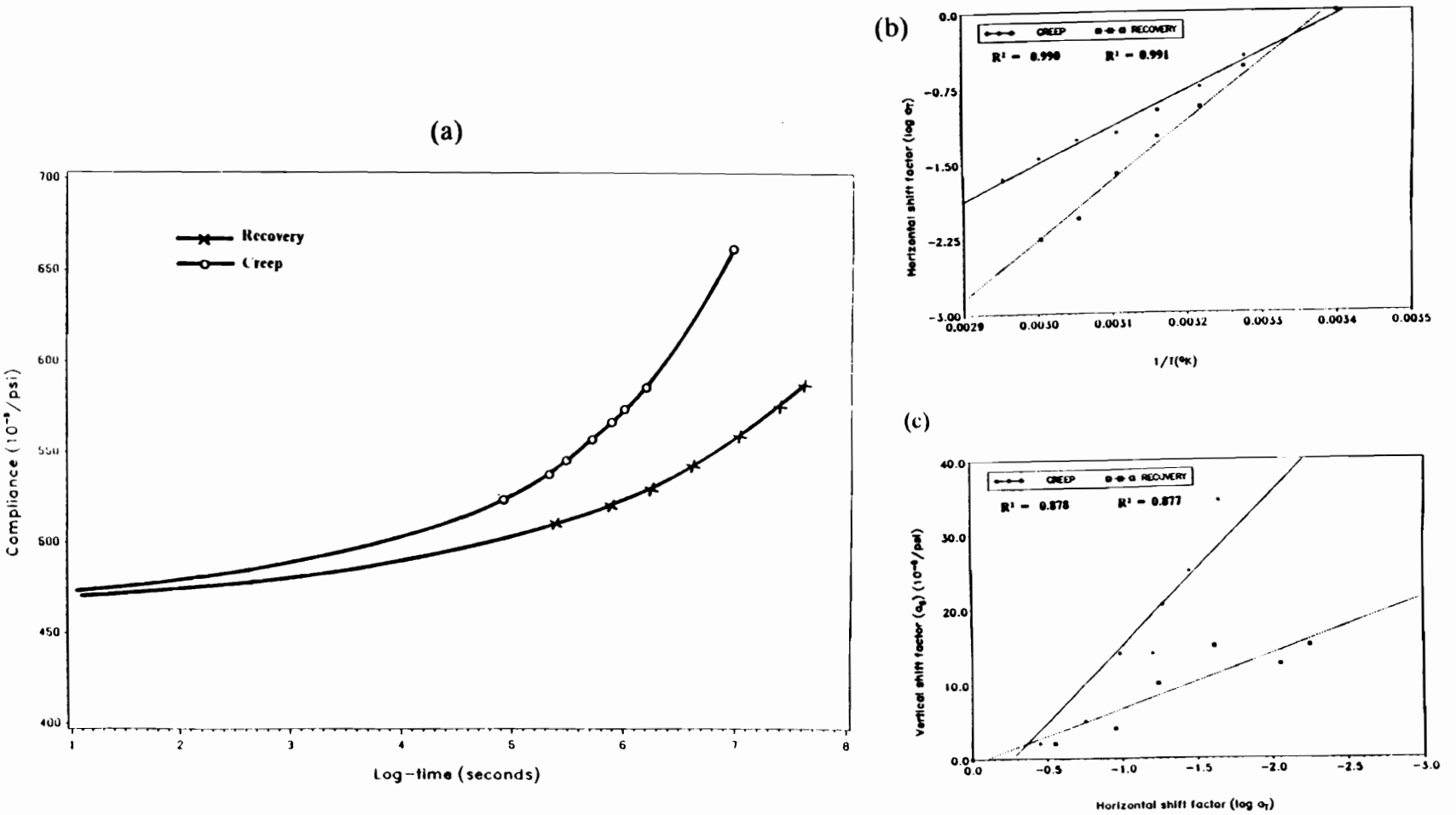

Figure 3.10. Master curves and shift factor data for specimen No.9: (a) creep and recovery master curves (b) horizontal shift factor vs. temperature (c) vertical vs. horizontal shift factors

Table 3.3. Horizontal ($\log a_T$) and vertical (a_s) shift factors for master curve No. 2

T°F	$\log a_T$ (log-sec)	$a_s(10^{-9}/\text{psi})$
90	0.47	2.0
100	1.10	4.25
110	1.45	7.0
120	1.70	9.0
130	2.11	11.9
140	2.45	15.0

deformation. The extrapolation and the maximum relative compliance (i.e., the ratio of the creep compliance to the elastic compliance) of the master curves for creep and recovery of all the accelerated specimens are summarized in Table 3.4. The table shows that the short-term accelerated data can be used to predict: (1) a long-term creep response of 0.23 years to 6.4 years (20 to 230 fold projection), and (2) a long-term recovery response of 0.84 years to 4.5 years (45 to 135 fold projection). The maximum relative compliance for creep varies from 17% to 60% and that for recovery ranges from 10% to 17%.

The results shown in Figures 3.5 to 3.10 and in Appendix A indicate that the master curves could be formed from accelerated data. The correctness of the master curve formation can be tested with the relationship between the horizontal shift factor and the temperature as discussed in Chapter 2. Since the predicted long-term response is within the glassy response region of wood, the shift factor must follow the Arrhenius formulation expressed in Eq. 2.21 as

$$\log a_T = \frac{\Delta E}{2.303\,R}\left[\frac{1}{T} - \frac{1}{T_R}\right] \qquad [3.12]$$

where

ΔE = activation energy (KCal/mole)

T = test temperature (Kelvin)

T_R = reference temperature (70°F = 294°K)

R = gas constant (1.986 KCal/mole/kelvin)

According to Eq. 3.12, the relationship between horizontal shift factor, $\log a_T$, and the reciprocal of the absolute temperature, $\frac{1}{T}$, must be linear. To investigate this relationship, $\log a_T$ was plotted against $\frac{1}{T}$. The plots for three specimens are presented in Figures 3.6(b), 3.8(b), and 3.10(b), respectively. Similar plots for the other eight specimens are shown next to the corresponding master curves in Appendix A.

The General Linear Model (GLM) procedure (SAS, 1985) was used to study the linearity of the relationship between $\log a_T$ and 1/T. The coefficient of determination (R^2), residual plot, mean square error, and the F- test for the significance of the models were used to test the linear regression

Table 3.4. Extrapolation time and maximum relative compliance from master curves

Specimen No.	E (10^6 psi)	Creep		Recovery	
		Extrap. (years)	Rel. creep (%)	Extrap. (years)	Rel. creep (%)
1	2.961	3.20	28.09	0.80	10.49
2	2.911	2.55	22.56	4.54	11.93
3	2.811	5.00	31.00	3.21	10.84
4	2.766	6.40	17.18	2.55	10.71
5	2.739	1.23	27.46	1.61	12.22
6	2.714	3.80	32.37	5.80	11.43
7	2.682	0.77	38.98	3.21	21.21
8	2.258	2.50	34.25	2.03	21.69
9	2.109	0.32	39.61	1.27	22.04
10	1.959	3.20	62.33	0.84	17.32
11	1.567	0.23	60.30	-	-

model. The results showed that very good linear regression models could be developed for creep and recovery of all the specimens with R^2 ranging from 0.889 and 0.995. The regression models superimposed on the data, as shown in Figures 3.6(b), 3.8(b), 3.10(b), and in Appendix A, indicate a strong linear relationship between $\log a_T$ and 1/T. The linear relationship between $\log a_T$ and 1/T indicates that the Arrhenius formulation was satisfied. However, the true validity of the master curves can be tested only by comparing the master curve predictions with long-term experimental results. Chapter 4 is devoted to testing the validity of the master curves with long-term creep tests.

The $\log a_T$ and 1/T relationship was also used to compute the activation energy ,ΔE, for creep and recovery. From the Arrhenius expression (Eq.3.12), the slope, $\tan \alpha$, of the $\log a_T$ vs. 1/T plot can be computed as

$$\tan \alpha = \frac{\Delta E}{2.303R} \qquad [3.13]$$

From Eq. 3.13, one obtains

$$\Delta E = \tan \alpha \; 2.303 \; R \qquad [3.14]$$

The parameter ΔE was computed for creep and recovery of each specimen from Eq. 3.14 using the slope, $\tan \alpha$, of the developed regression models. The activation energy for all the specimens is presented in Table 3.5. As can be seen from Table 3.5, the mean and the coefficient of variation (CV) of the activation energy for creep and recovery are very similar. For example, the mean and the CV of the activation energy for creep are 27.099 KCal/mole and 21.1%, respectively, and these parameters for recovery are 28.184 KCal/mole and 18.8%. The term ΔE for creep and recovery should be similar because the temperature dependent response of both creep and recovery is governed by the same activation mechanism. The activation energy obtained from this study is compared with data reported in the literature in the next section.

Very limited information is available on the activation energy of wood. Salmen (1984) reports that for water saturated wood or for insitu lignin the activation energy is approximately 98 KCal/mole. He states that, in general, the activation energy varies from about 9.5 KCal/mole and

Table 3.5 Activation energy (ΔE) for creep and recovery

Specimen No.	ΔE (KCal/mole)	
	Creep	Recovery
1	23.12	24.78
2	29.05	29.17
3	26.09	33.58
4	32.28	25.33
5	22.53	21.70
6	32.23	36.72
7	28.56	35.37
8	33.27	25.08
9	16.77	26.93
10	20.47	23.18
11	33.72	-
Average	27.10	28.18
CV (%)	21.1	18.8

upwards depending upon the glass transition temperature of the material. In an ongoing study, Hoffman (personal communications) found an activation energy of 15.5 KCal/mole for a cross-linked lignin alkylene oxide copolymer tetsed on DMTA. The activation energy for dry wood is not available; however, for dry wood the activation energy should be lower than that for wet wood because of the slower time dependent response of the dry material to the temperature. The term ΔE obtained in this study is lower than that reported for wet wood by Salmen and is close to that found by Hoffman. However, a true comparison can be made only with the activation energy data obtained for dry wood.

The relationship between the vertical and horizontal shift factors can be used to detect changes in the activation mechanism within the temperature range used in the accelerated tests. Hiel (1984) states that the discontinuity in the slope of this plot indicates a change from one activation mechanism to another. Therefore, the vertical shift factor (a_ε) was plotted against the horizontal shift factor ($\log a_T$) for creep and recovery of each specimen. The plots for three specimens are shown in Figures 3.6(c), 3.8(c), and 3.10(c). The plots for other specimens are reported in Appendix A. It was difficult to detect any visual discontinuity in the slope due to the scatter of the data. A linear regression analysis was performed using the GLM procedure (SAS, 1985) to determine if the relationship between a_ε and $\log a_T$ is linear. The same criteria as those used in the previous regression analysis were used to test the goodness of fit of the regression models. The analysis results revealed a strong linear relationship between a_ε and $\log a_T$, with the R^2 ranging from 0.859-0.989 as reported on each plot. These results indicate that there was no change in the activation mechanism within the temperature range used for the accelerated tests.

3.2.3. Mathematical Representation of Master Curves

In the previous section, master curves were developed for creep and recovery of eleven accelerated test specimens. In this section, power functions are developed for creep and recoverable

compliance master curve of each specimen using a nonlinear regression analysis technique (SAS, 1985).

Power models have been widely used to represent the creep behavior of wood (see Chapter 2); therefore, an exponential model of the following form was assumed for the developed master curves:

$$\frac{D_{crp}}{D_0} = P_1 \, t^{P_2} \qquad [3.15]$$

where

D_{crp} = creep compliance (1/psi)

D_0 = initial compliance (1/psi)

P_1, P_2 = parameters to be estimated

t = time (hours)

The creep compliance was divided by the initial compliance as shown in Eq. 3.15 to obtain relative creep. It has been customary to use relative creep in creep modeling as evidenced by the studies of Itani et al. (1985), Gressel (1985), and others (see Chapter 2) because of its usefulness in comparative studies. The power model expressed in Eq. 3.15 was developed for each creep and recovery master curve using nonlinear regression analysis. In the following section, nonlinear regression analysis is discussed and the developed nonlinear models are presented.

Nonlinear Regression Analysis Procedure

In nonlinear regreession analysis, the parameters, P_1 and P_2 in Eq. 3.15 can be estimated from methods, such as the modified Gauss-Newton and the Levenberg-Marquardt procedures, for computing nonlinear least square estimates. These methods require an initial guess for the estimated parameters and use iterative procedures to find parameter estimates that minimize the residual sum of squares (Kulasiri, 1990).

The Statistical Analysis System (SAS,1985) facilitates a procedure called NLIN for parameter estimation of nonlinear regression models. The NLIN provides four iterative techniques: modified

Gauss-Newton, Marquardt, gradient, and false position method to estimate the parameters. In this study, Marquardt method was used because of its wide applicability in nonlinear analysis. The criteria for the goodness of fit of the models were the MSE, R^2, statistical significance of the parameters, and the residual plots.

Development of Nonlinear Regression Models for Creep and Recovery Master curves

A digitizer interfaced to a personnel computer was used to generate compliance-time data from the master curves and store them on a magnetic tape. Then, the NLIN procedure (SAS, 1985) was used to find the parameters P_1 and P_2, shown in Eq. 3.15, for creep and recovery master curves of the eleven specimens.

The P_1 and P_2 parameters for each curve obtained from the analysis are shown in Table 3.6 along with the corresponding R^2 and MSE. As shown in Table 3.6 the R^2 is above 0.99 for all the curves, and the MSE is very low. The high R^2 is expected because the data came from smooth master curves. The relative compliance predicted from the model was plotted against the original data for each creep and recovery curve, and a near perfect agreement was found between the original and predicted data. Thus, the nonlinear regression analysis results indicate that the developed power models represent the master curves very well.

3.2.4. Predicting Model Parameters from Wood Properties

Each nonlinear regression model developed in the previous section is valid for a specimen with unique material properties. However, in practical situations, the material properties of wood structural elements vary within a structure. Therefore, to apply the developed long-term response models to practical situations, a method is necessary to predict the model parameters for a range of material properties. The usual approach is to develop regression models between the model parameters and a material property, such as, Young's modulus and specific gravity. The regression models developed in this study are discussed next.

Table 3.6. Power model parameters for creep and recovery master curves

Specimen	E	Creep				Recovery			
No.	($x10^6$ psi)	P_1	P_2	MSE ($x10^{-5}$)	R^2	P_1	P_2	MSE ($x10^{-5}$)	R^2
1	2.961	0.00904	0.3346	1.18	0.999	0.01469	0.2191	0.42	0.998
2	2.911	0.00402	0.3943	1.77	0.999	0.01099	0.2238	0.28	0.999
3	2.811	0.01948	0.2440	1.80	0.999	0.01664	0.1822	0.78	0.998
4	2.766	0.00589	0.3088	1.67	0.997	0.01661	0.1864	0.62	0.998
5	2.739	0.00753	0.3899	2.08	0.998	0.01768	0.2019	1.02	0.997
6	2.714	0.00603	0.3765	0.75	0.999	0.01301	0.1990	1.23	0.996
7	2.682	0.02305	0.3236	5.05	0.999	0.02258	0.2204	0.45	0.999
8	2.258	0.18681	0.2839	10.9	0.996	0.02412	0.2243	0.78	0.999
9	2.109	0.04207	0.2829	0.98	0.999	0.01991	0.2527	2.62	0.997
10	1.959	0.02031	0.3325	18.3	0.998	0.02107	0.2387	1.46	0.998
11	1.567	0.03899	0.3308	2.24	0.998	-	-	-	-

The GLM procedure (SAS,1985) was used to find the relationship between the model parameters and the Young's modulus or specific gravity of the accelerated test specimens. The criteria used in the previous linear regression analysis were used to test the goodness of fit of the model. As reported in Table 3.1, the Young's modulus of the test specimens varied from 1.567×10^6 psi to 2.961×10^6 psi and the specific gravity from 0.580 to 0.727.

A weak correlation was found between P_1 and the specific gravity ($R^2 = 0.20$). A better correlation was found between P_1 and the Young's modulus, E, as shown in Figures 3.11(a) and 3.11(b) where the regression line is super imposed on the data for creep and recovery. The R^2 for the regression models between the P_1 and E for the creep and recovery was 0.62 and 0.50, respectively. The mean and the coefficient of variation (CV) of P_1 for creep were 0.01774 and 47%, respectively, and the mean and CV for recovery were 0.0177326 and 18%, respectively. The data and the model show a negative correlation of P_1 with the Young's modulus. Considering the variability of wood these relationships were considered to be acceptable.

The following are the regression models developed for predicting P_1 from the Young's modulus, E (psi),

$$P_1(\text{creep}) = 0.0749 - 2.291 \times 10^{-8} \ (E) \qquad [3.16]$$

$$(R^2 = 0.626)$$

$$P_1(\text{recovery}) = 0.0391 - 0.827 \times 10^{-8} \ (E) \qquad [3.17]$$

$$(R^2 = 0.50)$$

The GLM results showed a weak relationship between the parameter P_2 and the Young's modulus (E) ($R^2 = 0.30$). A weaker correlation was found between P_2 and specific gravity ($R^2 = 0.13$). The mean and the CV of P_2 for creep were 0.3358 and 11.9%, respectively, and these values for recovery were 0.2148 and 10%, respectively. Considering the low variability of P_2 and its weak correlation with the material properties, it was decided to suggest the average value of P_2 for use in the model. The recommended values for P_2 are:

$$P_2 \text{ (creep)} = 0.3358$$

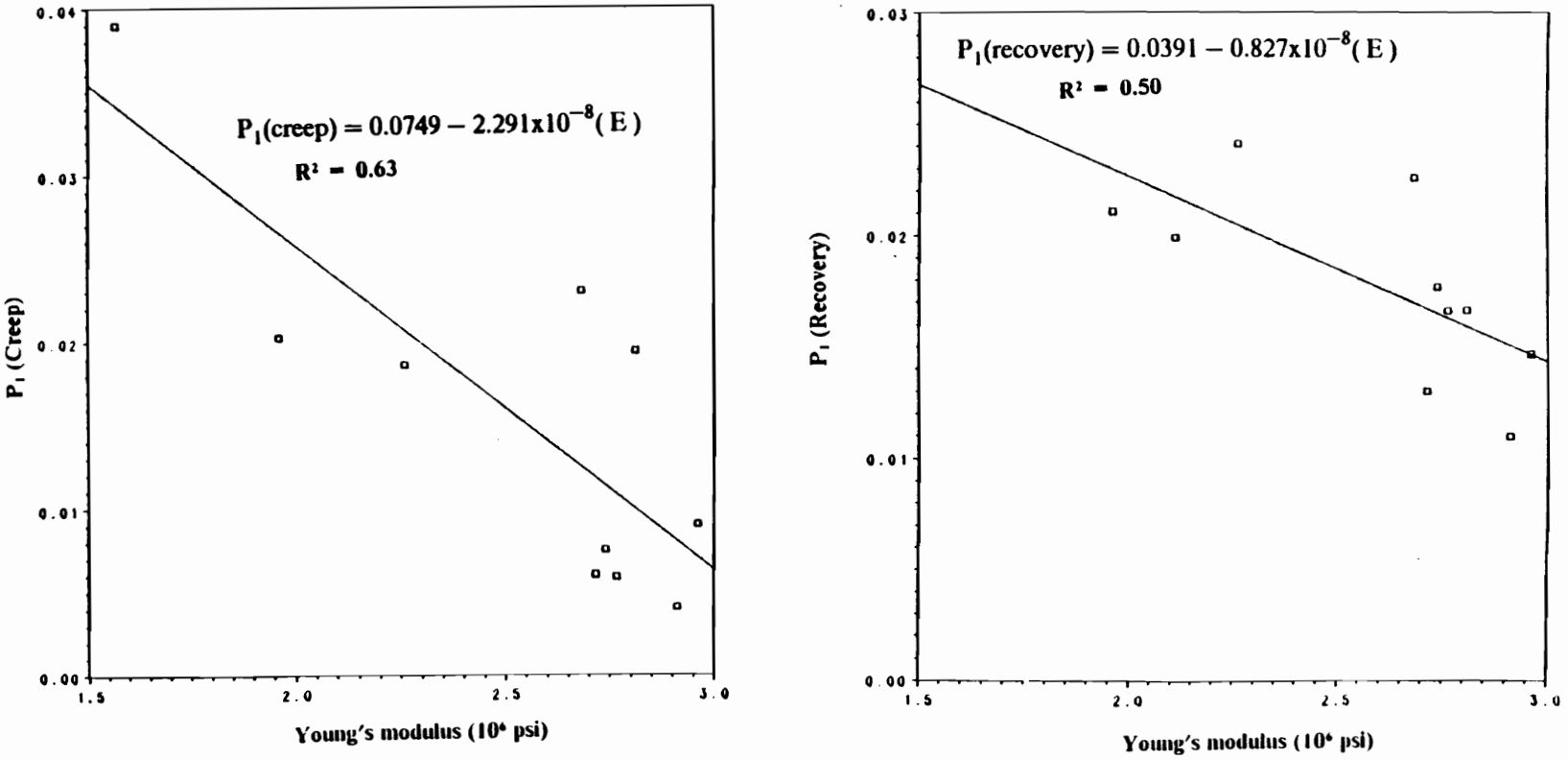

Figure 3.11. Relationship between P_1 and Young's modulus: (a) creep (b) recovery

P_2 (recovery) = 0.2148

The relationships expressed in Eqs. 3.16 and 3.17 for P_1 and the recommended average values for P_2 are valid only for the range of elastic modulus shown in Table 3.1.

This concludes the master curve formation and the results presented in this section are summarized as follows. Master curves were developed from accelerated creep and recovery data to predict the long-term response of wood under interior normal exposure conditions. The linear relationship between the horizontal shift factor and temperature satisfied the Arrhenius formulation which describes the relationship between the shift factors and temperature below glass transition temperature. The activation energy for creep and recovery was very similar with an average value of 28 KCal/mole. The strong relationship between the horizontal and vertical shift factors indicates that there was no change in the activation mechanism within the temperature range of 70°F to 150 °F. Power functions were developed to represent the master curves using a nonlinear regression analysis technique. The model parameter, P_1, showed a fair correlation with Young's modulus and regression models were developed for predicting P_1 for creep and recovery. The other model parameter, P_2, was poorly correlated with material properties, therefore; the average values were recommended for P_2.

Chapter 4

Testing Validity of Developed Long-term Creep Models

In Chapter 3, master curves were developed from accelerated data to predict the long-term creep and recovery response in compression parallel to the grain of southern pine exposed to interior ambient environmental conditions ($\simeq$70°F, $\simeq$9% MC). In this Chapter, the creep response predicted from eight master curves is compared to ten month creep data collected from the eight corresponding long-term test specimens tested at interior exposure conditions. The chapter is divided into two sections: In section 4.1, long-term experiments are discussed. The master curve predictions are compared with long-term experimental data in section 4.2.

4.1 Long-term Compression Creep Tests

The long-term compression creep tests were conducted on wood specimens end matched with those used in the short-term accelerated tests, and the specimen preparation was discussed in section 3.1.3. The specimen dimensions were 1/2in. x 1/2in x 3in.. Eight specimens were tested for long-

term compression and this number was based on the capacity of the long-term creep measuring system.

Load Level: The long-term creep stress level was 1670 psi (load = 370 pounds) which was the same as that used in the accelerated tests.

Temperature and Relative Humidity Conditions: The creep tests were performed in the laboratory where the average temperature and the average relative humidity were 70° F, and 50%, respectively.

Test Duration: The test duration was ten months and no recovery data were collected from the tests.

Strain Measurement: The compressive creep strain in the long-term creep test specimens was measured with bonded strain gages, using the same Wheatstone bridge circuit as that used in the accelerated tests. However, the bridge was powered with 2 volts dc by a portable strain indicator model P-3500 (Measurements Group, Inc., Raleigh, NC). The indicator was powered with 9 volts dc by an external adaptor connected to the ac power line.

Data Acquisition: The long-term compressive creep strain (in micro-strains) was manually read directly from the liquid crystal digital display on the strain indicator. A Switch and Balance unit model SB-10 (Measurements Group, Inc., Raleigh, NC) which allowed the sequential reading of the strain gage output from ten channels using a single strain indicator was used to connect all the long-term test specimens to the strain indicator.

4.1.1 Long-term Creep Test Apparatus

Long-term creep tests were conducted at laboratory ambient conditions of 70°F temperature and 50% relative humidity for ten months. The test fixtures and the method of load application were identical to those in the accelerated creep tests. However, the test apparatus was not enclosed in a chamber but was exposed to ambient environment in the laboratory.

Figure 4.1. Long-term creep test arrangement

Two 8.5′ long 3.5″x3.5″x1/4″ steel angle-iron sections prepared to serve as the base test frame for the long-term creep tests were welded and anchored to a steel frame as shown in Figure 4.1. Eight testing fixtures along with the lever arms were assembled on the test frame and the lever arms were calibrated as discussed previously in the section 3.1.12. (Chapter 3) on accelerated creep test apparatus.

4.1.2 Test Procedure

Each of the eight pairs of active and dummy specimens were instrumented with bonded strain gages and coated with the moisture protective coatings. The active specimens were placed in the test fixtures and the dummy specimens were placed near the active specimens. The gages on each specimen pair were arranged in a Wheatstone bridge circuit through the switch and balance unit which connected the bridges to the strain indicator.

The loads (370 pounds) were applied to the specimens and the creep strain was read from the strain indicator for ten months. Strain data were collected frequently in the first few hours, four times a day for one week, twice a day for 5 months, daily for 3 months, and weekly for the rest of the test duration.

When strain gages are used for long-term strain measurements, it is possible for the null balance point of the strain measuring system to shift with time. This phenomenon is called zero drift. The zero drift due to the instability of the strain measuring system can be detected by reversing the positions of the active and dummy gages in the Wheatstone bridge. This reverses the sign of the indicator reading from positive to negative and the difference in the magnitude of the readings corresponding to the original and reversed gage positions is attributed to the zero drift in the strain measuring system (Perry, 1962). In this study, a reading for the reversed gage positions was taken whenever a creep reading was taken for the original gage positions.

A few days after the long-term creep test had begun, an unexpected variation was observed in the creep strain data. The exact reason for the fluctuation was not known but was attributed to the

changes in the test environmental conditions. Although the temperature and relative humidity inside the laboratory were controlled at 70°F and 50%, respectively, the conditions were affected by the frequent opening of laboratory doors, including a high bay garage door. To explore the reason for the fluctuation, a detailed investigation was conducted as follows.

- A hygro-thermograph (Bacharach Instrument, Inc., Pittsburgh, PA) was located near the test specimens to continuously record the ambient temperature and humidity data.

- To determine if the moisture content of the test specimens changed during the long-term creep tests, five moisture content specimens, coated with the moisture protective coating, were located near the active specimens, and their weights were measured for eight months at each time the creep readings were taken from the loaded specimens.

- A pair of wood specimens with the dimensions and gage arrangement similar to those used in creep tests were left unloaded in the creep test environment, and the gages were connected to the Wheatstone bridge on a vacant channel of the Switch and Balance unit. A strain reading was taken from this bridge circuit whenever creep strains in the loaded specimens were read.

- Another two unloaded wood specimens with the dimensions and gage arrangement similar to those used in creep tests were placed in an environmental chamber where the temperature and the relative humidity were strictly controlled at 21°C and 60%, respectively. The output from this bridge was monitored for six months.

- An unloaded aluminum specimen, with the gage arrangement as already discussed, was connected to a vacant channel of the SB-10 unit and left unloaded in the creep test environment. A strain reading was taken from this specimen simultaneously with the strain readings from the loaded specimens.

4.2 Long-term Creep Test Results and Validity of Master Curves

In this section, long-term results are discussed (section 4.2.1) and the measured creep data are compared with the response predicted by the long-term creep models developed in Chapter 3 (section 4.2.2).

4.2.1 Long-term Creep Test Observations

The long-term strain data did not show any zero drift in the strain measuring system used for the creep tests. Therefore, the reading corresponding to the normal gage positions in the Wheatstone bridge was taken as the true strain in the specimen.

The measured strain was converted to compliance by dividing the strain by the creep stress level (1670 psi) and was plotted against time as shown in Figure 4.2(a) for a typical long-term test specimen. The data from the other eight specimens followed the same trend. In the first few days of the creep tests, the creep reading from all the specimens increased continuously with time. Then, the reading started to fluctuate with an overall upward trend as shown in Figures 4.2(a). For example, the measured compliance varied by as much as $\pm 27 \times 10^{-9}$/psi which in some cases amounted to about 30% of the observed creep compliance. However, the fluctuation subsided three months after the tests started. Then, the reading steadily increased during the last seven months with minimum observed variation of the data.

The pair of unloaded (stress-free) wood specimens located in the creep test environment also showed an apparent strain (i.e., strain due to factors other than mechanical loading) which fluctuated cyclically from the zero reading as shown in Figure 4.2(b). The apparent compliance followed the trend of the creep data and it was as high as $\pm 30 \times 10^{-9}$/psi on some occasions (Figure 4.2(b)). Both apparent and creep compliance plots show similar peaks and variation with time. These observations indicate that the variation of the creep data was due to apparent strains induced by changes in the environmental conditions.

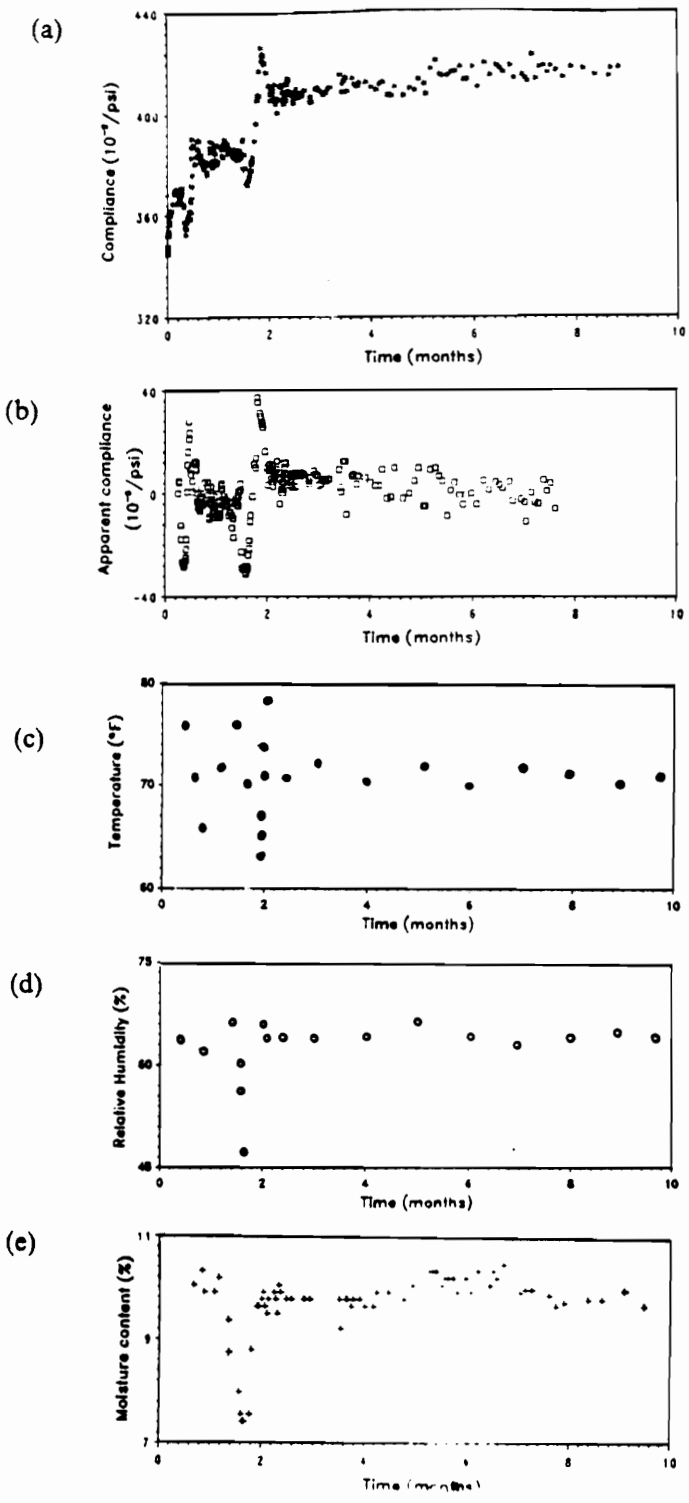

Figure 4.2. Effect of environmental conditions on long-term data: (a) long-term compliance (b) compliance induced by changes in environmental conditions (c) temperature (d) relative humidity (e) moisture content

The reading from the unloaded wood specimens placed in the environmental chamber where the temperature and the relative humidity were strictly controlled remained unchanged through out the test period. This proves that the fluctuation of apparent strain in the stress-free wood specimens located in the creep test environment was due to the fluctuations of temperature and humidity in the long-term test environment.

Effect of temperature, humidity, and moisture content on measured creep and apparent data

Variation of Temperature and Relative Humidity: The hygro-thermograph showed a variation in the temperature and relative humidity (Figure 4.2(c) and (d)) indicating that the test environmental conditions were not constant. The fluctuation of the temperature and humidity was greater on very cold winter days and also when the variation of the outside environmental conditions was rapid. A temperature change as high as 14°F and a humidity variation as high as 21% were observed in the test environment. Short periods of constant conditions occurred periodically but only for three to four days consecutively.

The results shown in Figures 4.2(c) and (d) indicate that both apparent and creep data were affected by temperature change alone on some occasions and mostly by humidity change on other occasions. However, the greatest influence was exhibited when both temperature and relative humidity varied simultaneously as evidenced by the maximum variation of the apparent compliance ($\pm 30 \times 10^{-9}$/psi) and creep compliance ($\pm 27 \times 10^{-9}$/psi) under these conditions. Here, temperature varied from 63°F to 77°F and humidity fluctuated from 47% to 66%. Under the same conditions, the moisture content of the specimens also showed the maximum variation as discussed next.

Variation of EMC: The moisture content variation of all the moisture content test specimens showed the same trend, and the moisture change in a typical specimen is illustrated in Figure 4.2(e). The moisture content dropped from 10.4% to 7.4% about six weeks after the tests had begun. Then, the moisture content reached about 10% and fluctuated between 10.6% and 9.4% ($\Delta MC = 1.2\%$) through out the rest of the test period. The comparison of the apparent and creep

compliance data with the variation of the moisture content in the specimens, indicate that the largest variation in the compliance data occurred in the same two week period when the moisture content of the specimens fluctuated most.

The nature of the fluctuation of the creep data can be explained by using the results from the unloaded aluminum specimens. The reading from the gages bonded to the unloaded aluminum specimen placed in the creep test environment did not show any apparent strain during the entire long-term test period. This indicates that the Wheatstone bridge arrangement used in this study provided complete temperature compensation for the aluminum specimen.

In general, a self-temperature compensating gage shows a temperature induced apparent strain when bonded to a material with the coefficient of thermal expansion (α) different from that of the gage. The thermal coefficient of expansion (α) is a measure of the dimension change of a body due to temperature changes. The α of aluminum is 12.5×10^{-6}/ °F and the α for the gage is 6.0×10^{-6}/ °F. The difference between the α values would have produced a temperature induced apparent strain if only one gage had been used in the Wheatstone bridge. However, the zero reading from the bridge with four bonded gages indicates that apparent strain at all gage locations in the aluminum specimen was similar leading to zero net output. This is possible only when each gage location of the test material shows similar response to temperature changes (i.e., uniform thermal expansion throughout the specimen)

For wood, the thermal coefficient of expansion in the longitudinal direction varies only from $(1.7\text{-}2.5) \times 10^{-6}$/°F. Therefore, temperature induced apparent strains are produced at each gage location. However, if the α of wood is constant for all the specimens, the apparent strain induced at each gage location is similar and must be cancelled in a bridge arrangement where dummy gages are used to compensate for temperature as shown in section 3.1.10. in Chapter 3.

The effect of moisture change on the measured compression data indicate that the apparent strain has also been induced by the variable shrinkage/swelling characteristics of the wood at the gage location. In addition, moisture content change within the loaded specimens can lead to mechano-sorptive creep. Thus, the reason for the apparent strain in stress-free wood specimens subjected to the test environmental conditions was due to the dissimilar apparent strains experi-

enced by each of the active and dummy gages in the Wheatstone bridge due to the non-uniform thermal and shrinkage/swelling properties of wood at the gage locations.

A quantitative analysis was conducted to study the effect of variable thermal and shrinkage properties of wood at gage locations on the measured creep data. A detailed discussion is included in Appendix B and a summary of the results are presented here. The computations show that the combined effect of temperature change of 10°F and 3% change in moisture content, as observed in the creep test environment, produce an apparent compliance as high as 57×10^{-9}/psi. This apparent compliance compares very well with the maximum variation of the creep compliance observed under these conditions. The results also show that the shrinkage/swelling has a tremendously greater effect than the thermal expansion on the observed variation of the compliance data. For example, 96% of the total apparent compliance was induced by moisture change.

4.2.2 Comparison of master curves with long-term creep experimental data

A detailed discussion of the long-term creep experimental observations was presented in the previous section. In this section, the long-term data are compared with the response predicted by the creep models developed in Chapter 3.

It is evident that the collected long-term creep data contains temperature and moisture induced apparent strains in addition to creep strains. However, the master curves were for constant environmental conditions. Although a gage arrangement was designed to eliminate apparent strains and read pure compression data in the long-term test specimens, the performance of the gages was influenced by the variation of the response of wood at the surface where the gages were bonded. Therefore, to obtain creep due to compression, these effects should be eliminated from the measured data.

Considering the similar variation in creep and apparent compliance (Figures 4.2(a) and (b)) a FORTRAN program was developed to eliminate the apparent strain from the measured creep data. However, much improvement could not be achieved because the peaks and the variation of the

apparent and creep data did not coincide at a given time. This is because the variation took place over a duration of time (i.e., several weeks). Therefore, the uncorrected data were compared with the predicted response.

The comparison between the master curves and the experimental creep data presented here is not the best comparison because of the fluctuations of the experimental atmospheric conditions. A true comparison can only be made with experimental data containing only creep effects. Regardless, the master cures were superimposed on the data as shown in Figures 4.3 to 4.6.

The figures show that the master curves followed the trend of the data. The curve for specimen No.9 matched very well with the experimental data. However, the creep response predicted by all the other master curves was below the corresponding experimental data. It is clear from the figures that the creep data and all the master curves agreed well in the first few weeks when there was no fluctuation of the environmental conditions. However, the curves started to deviate from the data as soon as the long-term data began to fluctuate with the changing environmental conditions. From then on, the measured long-term response was considerably greater than the predicted response due to the tremendous fluctuation of the collected data during the first three months. The overall effect of the fluctuation of the data during this period was to significantly increase the average strain reading. Therefore, a high overall creep response was measured even during the latter seven months when the fluctuation of the data was minimum.

The relative creep compliance at the end of the long-term test period (10 months) was computed from the long-term data and the master curves. A discrepancy of 28% to 50% was found between the experimental and predicted response indicating that the fluctuation of the experimental data significantly affected the comparison.

In summary, the master curves and the long-term data followed the same trend. The overall experimental response was affected by the variable thermal expansion and shrinkage behavior of wood at the gage locations in response to the fluctuating environmental conditions during the first three months. However, the master curve predictions were for constant environmental conditions. Consequently, a good comparisons between the experimental and predicted creep response was not found. Therefore, the long-term strain measuring technique must have minimum sensitivity to the

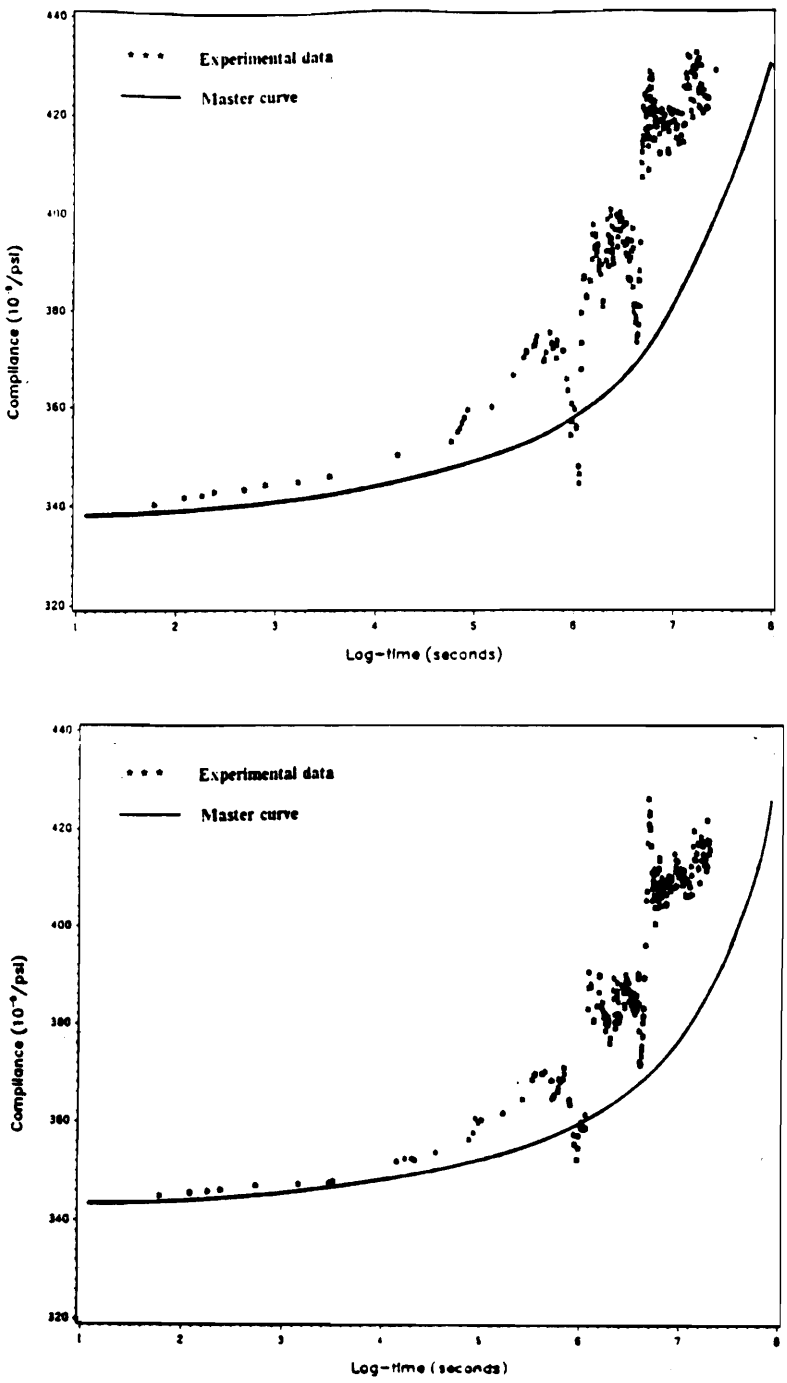

Figure 4.3. Predicted vs. experimental creep compliance: (a) specimen pair No. 1 (b) specimen pair No. 2

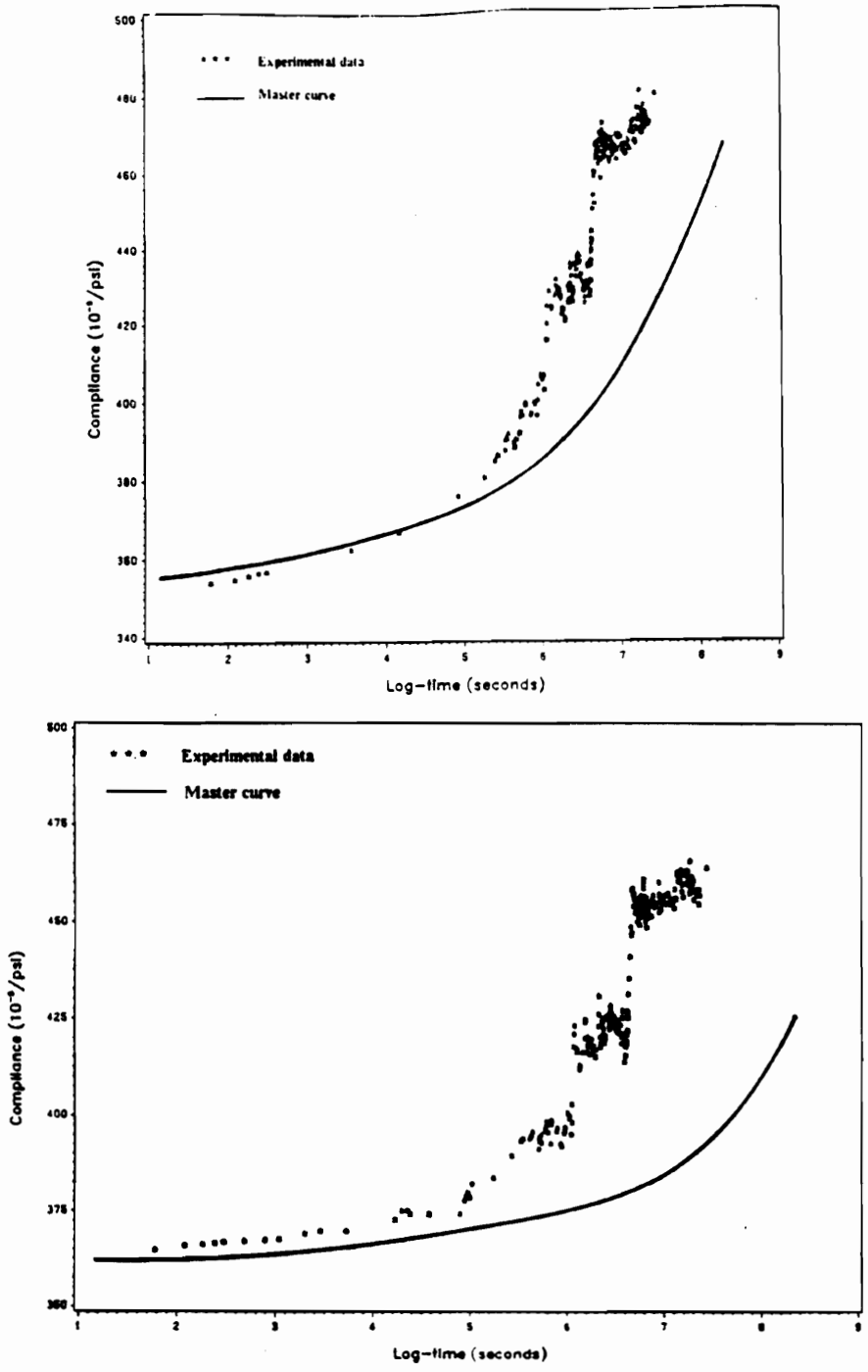

Figure 4.4. Predicted vs. experimental creep compliance: (a) specimen pair No. 3 (b) specimen pair No. 4

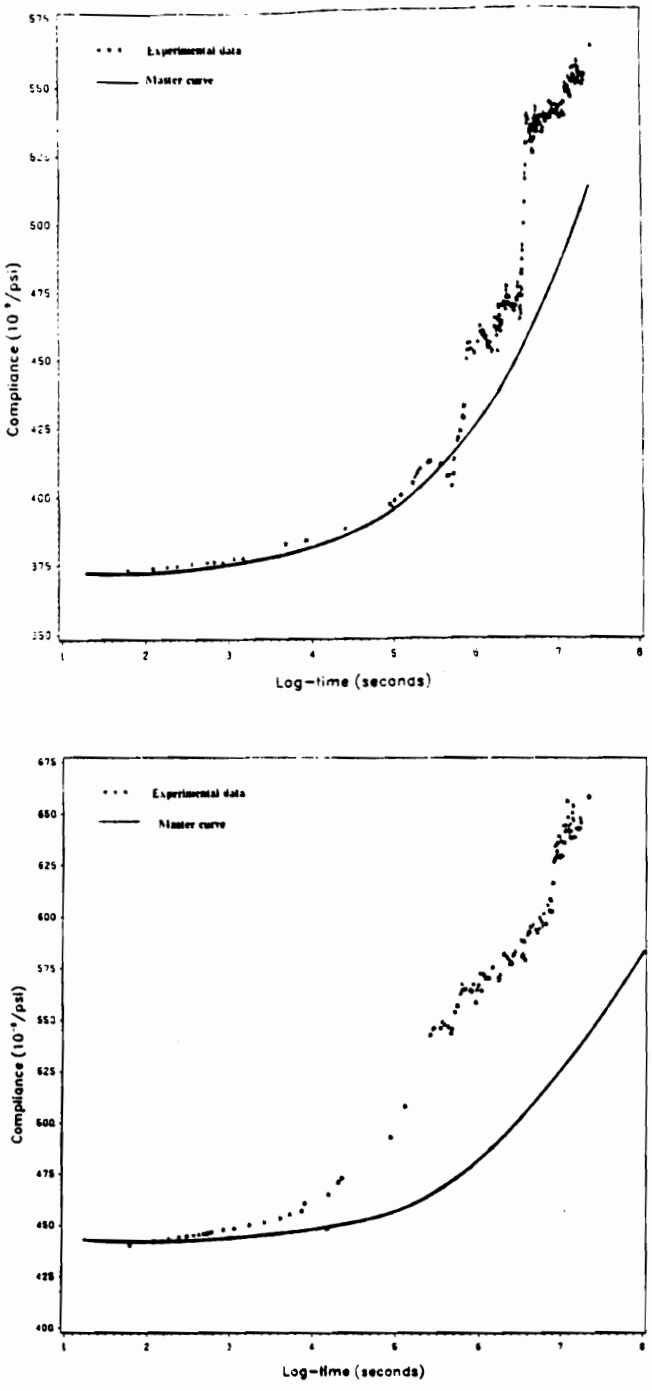

Figure 4.5. Predicted vs. experimental creep compliance: (a) specimen pair No. 7 (b) specimen pair No. 8

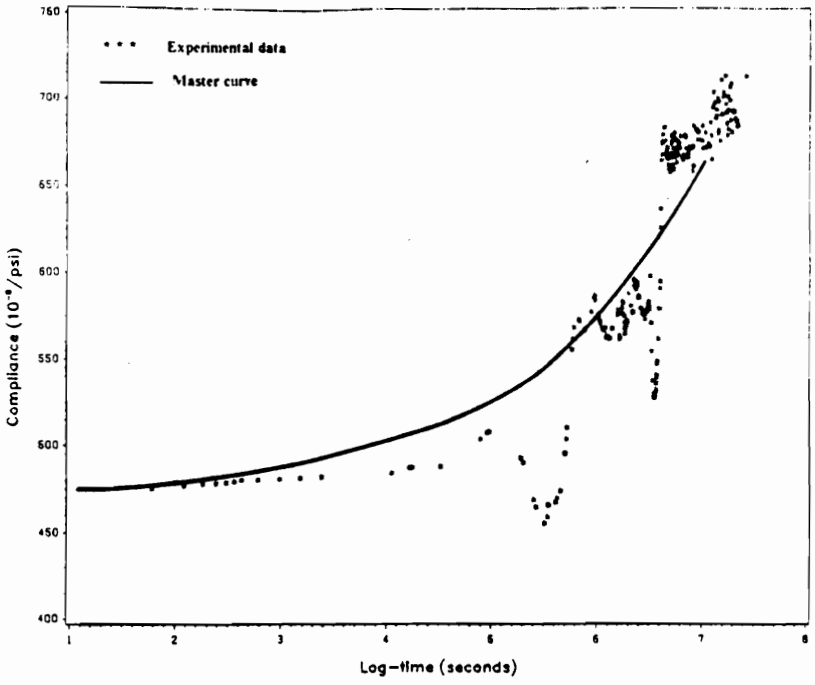

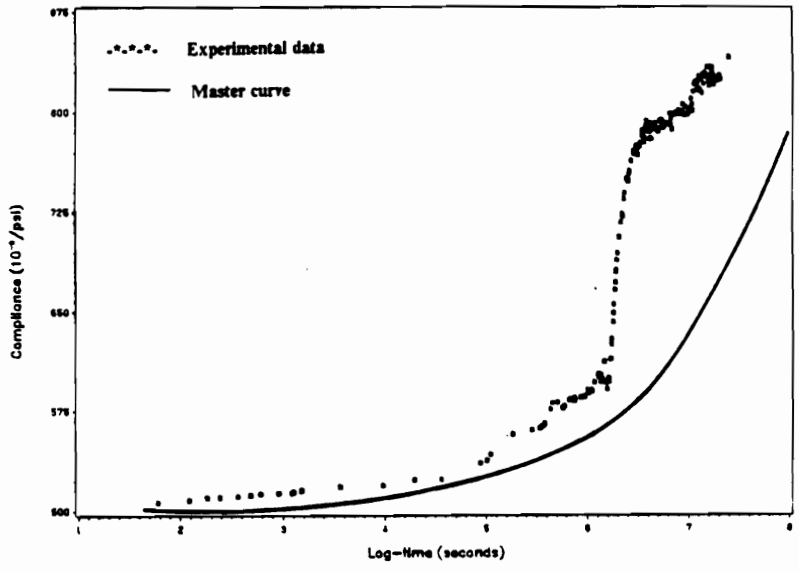

Figure 4.6. Predicted vs. experimental creep compliance: (a) specimen pair No. 9 (b) specimen pair No. 10

localized variable thermal expansion and shrinkage effects at the surface of wood and measure overall response of the volume of the specimen. For example, a metallic clip gage may economically and accurately measure strain over a longer gage length than that used in this study. Since in clip gages, the strain gages are bonded to metallic surfaces, and a large gage length can be obtained, the apparent strains induced by the localized variation of the thermal and shrinkage/swelling properties of wood can be minimized.

Chapter 5

Creep Behavior of Shallow Wood Arches

The objective of the study presented in this Chapter was to demonstrate the application of the finite element method in conjunction with the TTSP based long-term creep models (Chapter 3) to predict the creep behavior of wood structures. The chosen example structrue was a shallow arch. In shallow structures, creep can magnify geometric nonlinearity leading to snap-through buckling.

Creep experiments on shallow arches were conducted for two months and the proposed method was used to predict the creep response of the arches. However, the finite element analysis revealed that modeling of the experimentally tested arches was difficult due to the tremendous sensitivity of the arches to the geometry and the presence of various other factors influencing the experimental measurements. Therefore, the creep tests and experimental results are discussed (section 5.1) and the problems associated with finite element modeling of the arches are reported (section 5.2). The best approximate arch model was used to conduct creep analysis; however, creep response showed an inconsistent trend providing more evidence to the complexity of modeling the experimental behavior. Therefore, it was difficult to make valid comparisons between the predicted and experimental creep behavior.

5.1 Creep Tests on Shallow Wood Arches

The geometry of the chosen configuration of the shallow arch is shown in Figure 5.1 and this geometry was based on experimental considerations. The member cross section dimension and the length were 1″x1″ and 15″, respectively, and the rise of the arch was approximately 1″. This configuration resulted in a rise to span ratio of 1 to 30 and an incline angle of 3.82 degrees. The creep tests were performed in the laboratory environmental conditions (70°F, 50% RH) in specially designed test apparatus. A load was applied at the peak of the arches and the arch deflection was recorded for two months.

5.1.1 Preparation of Arch Members

Arch members were prepared from the same batch of kiln-dried southern pine lumber used in the compression creep tests so that each arch consisted of end matched members. First, 1″x1″x44″ defect free sections were prepared and each section was cut in half length wise to prepare the end matched members. Then, 4″ long pieces were cut from the ends of each member to determine the ultimate compressive strength, Young's Modulus, moisture content, and specific gravity. Ideally, the length of each member should have been 15″; however, due to the space occupied by the steel joints (section 5.1.4), the required length of the wood members was 13.125″ to retain the specified rise to span ratio. The ends of the members were cut square and perpendicular to the length to avoid load eccentricity. After the desired member geometry was obtained, they were coated with Daran wrap to minimize the moisture interaction with the environment. A total of ten arches were prepared for creep tests.

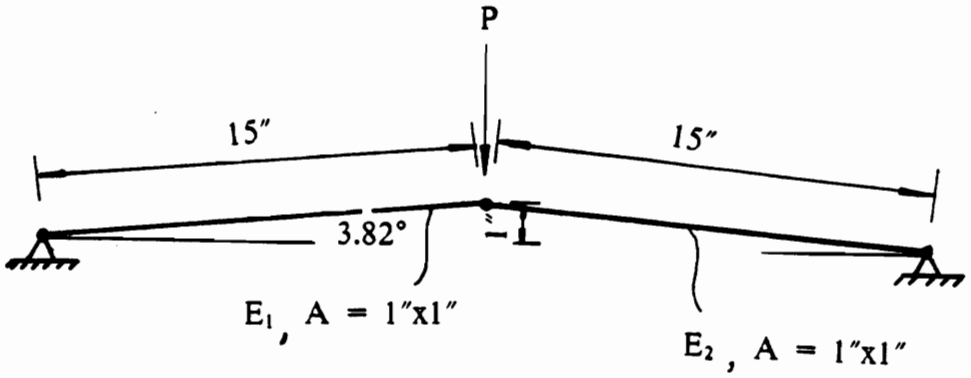

Figure 5.1. Geometry of the shallow arch

5.1.2 Material Properties of Arch Members

The ASTM D143 standard static compression tests were conducted on 4″ long specimens cut from each end of the arch members to obtain the ultimate compressive strength and the Young's modulus. The test procedure was similar to the static compression test method described in Chapter 3. The ultimate stress and Young's modulus of an arch member was computed from the properties of the two end specimens cut from the same member. After the compression tests, these test specimens were used to determine the specific gravity and the moisture content based on oven dry method. The physical and mechanical properties of the arch members are presented in Table 5.1. The mean and the coefficient of variation of the measured properties were as follows: Young's modulus: 2.288×10^6psi, and 12.7%, specific gravity: 0.566 and 8.75%, and moisture content: 9.97% and 2.67%.

5.1.3 Load Level

Four load levels were used in the creep tests: 35 pounds were applied to 2 arches, fifty pounds to five arches, 70 pounds to two arches, and 100 pounds were applied to one arch (Table 5.2). These load levels represented a range of 29 to 72% of short-term elastic buckling loads determined experimentally as discussed in section 5.1.5.

5.1.4 Arch Test Fixture

The arch test fixture consisted of a 4′ long angle-iron base and three steel pin joints manufactured in the laboratory. The peak joint of an arch was assembled by joining two 4″ long square steel "shoes" with a 0.5″ diameter pin as shown in Figure 5.2(a). The shoes were prepared by welding four 4″ long, 0.1835″ thick, and 1.375″ wide steel sections. The ends of the shoes closer to the pin were closed and two opposite sides of the shoes were extended 1″ for assembling the two

Table 5.1 Moisture content, specific gravity, and Young's modulus of arch members

Arch No.	Moisture content (%)		Specific gravity		Young's modulus (10^6psi)	
	member 1	member 2	member 1	member 2	member 1	member 2
1	10.11	10.09	0.619	0.612	2.6117	2.4425
2	9.67	10.02	0.595	0.591	2.5193	2.3453
3	9.92	10.00	0.511	0.513	2.1534	2.2439
4	10.12	9.92	0.540	0.529	2.1209	2.4628
5	9.40	9.34	0.575	0.579	2.0255	1.9315
6	10.32	10.32	0.643	0.641	1.9203	2.5546
7	10.23	10.21	0.540	0.536	2.2487	2.1415
8	10.10	10.00	0.491	0.493	2.0813	2.0766
9	9.96	10.09	0.629	0.610	2.4086	2.7012
10	9.71	9.98	0.565	0.519	2.1561	2.1191

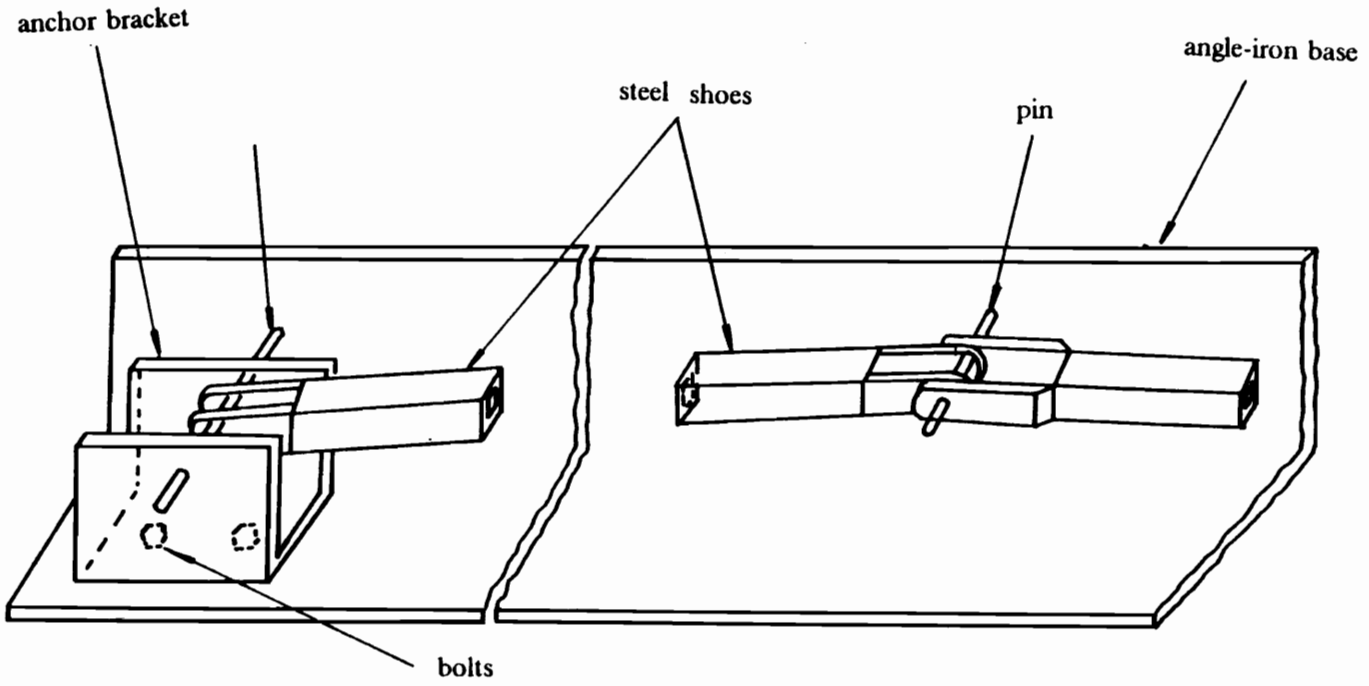

Figure 5.2. Arch test fixture: (a) peak joint (b) base joint

parts with a pin (Figure 5.2(a)). The inner cross section of the shoes was 1″x1″ so that the arch members could be inserted into the shoes and rested against the closed ends. A base joint shown in Figure 5.2(b) consisted of a square shoe, similar to that used in the peak joint, and an anchor bracket joined with a 0.5″ diameter pin. The anchor bracket was manufactured by welding two 4″ long 3.5″x3.5″ angle-iron pieces. The anchor bracket was fastened to the angle-iron base with two 0.5″ diameter bolts with a 190 foot-pound torque applied by a pneumatic wrench.

5.1.5 Elastic Buckling Load of Arches

The elastic buckling load of a three-pin arch is the maximum static peak load which causes snap-through buckling of the arch. Knowing this load ensured that the applied creep load did not exceed the elastic buckling load, and the creep load levels could be represented as percentages of the buckling load.

The elastic buckling load of an "ideal" three-pin arch can be computed from Equation 2.90 (Chapter 2) expressed as:

$$P_{cr} = \frac{2\ A\ E\ \alpha^3}{3\sqrt{3}} \qquad [5.1]$$

where;

P_{cr} = short-term elastic buckling load

A = area of the members

E = Young's modulus of the members

α = original arch angle

However, since ideal conditions are difficult or impossible to achieve and because wood is a highly variable material, experimental tests were conducted on each arch prepared for creep tests to obtain its elastic buckling load. The theoretical buckling loads were computed from Equation 5.1, however, for comparing the theoretical and experimental values. Member stresses at snap-through buckling were computed and found to be about 35% of the proportional limit stress in

compression and about 39% of the Euler buckling load of the compressed members. The static test procedure used to obtain the experimental short-term elastic buckling load of the arches is discussed next.

Static Arch Test Procedure

The arches were assembled in the test fixtures so that the rise was approximately 1″ and the base length was 30″. An arch assembly was placed on a 22,000 pound capacity MTS servo-hydraulic test machine and a 50 pound pre-load was applied at the peak for removing any slack in the test fixture. The pre-load was removed and the rise was measured with a vernier caliper with 0.001″ accuracy and the base length with a ruler with 1/32″ accuracy. Then, a ramp load was applied at the apex at a rate of 100 pounds/min until the snap-through buckling occurred. The load-deflection curve was recorded continuously on an X-Y plotter and the elastic buckling loads for all the arches were obtained in this manner.

The experimental buckling loads were compared with theoretical buckling loads obtained from Eq. [5.1] to gain confidence in the measured values. However, a maximum of 40% discrepancy was found between the two buckling loads as shown in Table 5.2. The possible sources of errors were investigated and the cause of the discrepancy was attributed to the base joints. The computations based on Eq.5.1 showed a significant influence of the base support deflection on the elastic buckling load as shown in Table 5.3. For example, 0.006″ horizontal movement of the supports reduced the buckling load by 26%. Therefore, static tests on several arches were repeated with 0.0001″ accuracy dial indicators attached to the anchor brackets of the base joints to determine whether the joints actually deflected during a test. Deflections ranging from 0.002 to 0.005 were observed; however, the indicator returned to zero after the snap-through buckling occurred. This indicated that the base joint behaved as a pin-joint supported by an elastic spring. Therefore, it was decided to read joint deflections during the creep tests on arches and include these in the finite element modeling.

Table 5.2 Theoretical and experimental short-term elastic buckling load of arches and creep load levels

Arch No.	rise (in)	$P^{\#}_{max}$ (lb) (theoretical)	P_{max}(lb) (exprimental)	$\Delta P^{\$}_{max}$ (%)	P_{creep} (lb)	P_{creep} (%) of P_{max}(exp)
1	0.940	240	126	47.5	35	27.8
2	0.909	208	110	47.1	35	31.8
3	1.044	286	152	46.8	50	32.9
4	1.022	280	134	52.1	50	37.3
5	1.009	232	100	56.9	50	50.0
6	1.031	280	166	40.7	50	30.1
7	1.054	294	159	45.9	50	31.4
8	1.056	280	172	38.6	70	40.7
9	1.034	322	159	50.6	70.5	47.5
10	1.039	274	138	49.6	100	72.5

- P_{max} is the elastic buckling load of arches
$ - ΔP_{max} is the difference between theoretical and experimental buckling loads computed as a percentage of the theoretical value

Table 5.3 Effect of support deflection on the short-term elastic buckling load of wood arches

Joint deflection (in)	rise (in)	$P_{cr}^{\$}$ (%)
0.000	1.000	100
0.001	0.985	95.61
0.002	0.969	91.21
0.003	0.954	86.88
0.004	0.930	82.00
0.005	0.922	78.44
0.006	0.906	74.33
0.007	0.889	70.29
0.008	0.872	66.32

$ - The elastic buckling load as a percentage of the buckling load corresponding to zero support deflection

5.1.6 Creep Test Procedure

In the creep tests, each arch test fixture was anchored to a wooden frame as shown in Figure 5.3 and placed in the laboratory where ambient temperature and relative humidity were 70°F and 50%, respectively. After assembling the arches, the anchor brackets of the base joints were spot-welded to the angle-iron base to eliminate any joint displacements during creep tests. A 0.0001″ accuracy dial indicator was attached to one base joint of each arch to measure the joint deflection with respect to the angle-iron base. An aluminum block was inserted into the peak joint and an eye-bolt was threaded into the aluminum block for the load application. A 0.001″ accuracy dial indicator was used to measure the creep deflection of the apex with respect to the angle iron base as shown in Figure 5.3.

A creep test was started by applying a 15 pound pre-load to eliminate slack in the test fixture. Then, the pre-load was removed, rise (Table 5.2) was measured with a vernier caliper, and the creep load was applied smoothly by means of a hydraulic jack in about one minute. The deflection readings were taken from both dial indicators for two months. The frequency of the data collection was as follows: every minute for 10 minutes, every 30 minutes for 5 hours, every hour for 6 hours, twice a day for a week, daily for three weeks and once in two days for the rest of the test duration.

5.2 Experimental Creep Response and Finite Element Analysis

5.2.1 Experimental Observations

The peak deflection data were plotted as a function of time for two typical arches as shown in Figures 5.4(a) and 5.4(b). The general behavior of the other eight arches is similar to that of the example arches. As soon as the arches were loaded, an elastic peak deflection and an elastic support deflection were observed and these were higher for higher load levels. Then, the peak deflection

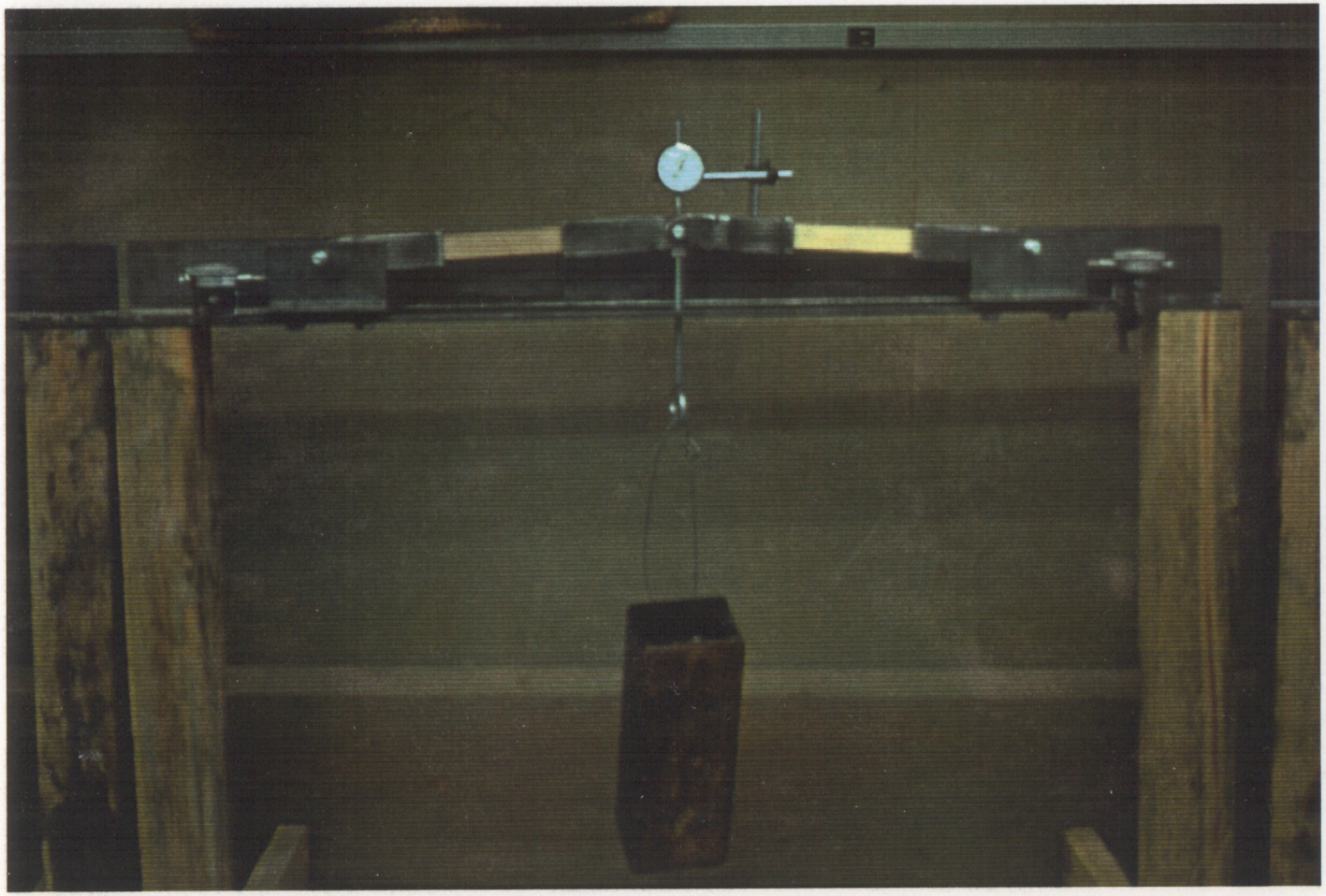

Figure 5.3. Arch creep test arrangement

increased exponentially with time. The arch loaded at 100 pounds snapped-through 200 hours ($\simeq$9 days) after the tests began. The other arches sustained the load in the two month test period, but higher load levels produced larger creep deflections. The relative creep (i.e., ratio of creep deflection to initial elastic deflection) varied from 16% to 61% depending on the rise of the arch and the load level.

Several days after the tests had begun, the peak deflection data started to fluctuate as evidenced by Figures 5.4(a) and 5.4(b). Similar fluctuations were observed in the data collected from the other eight arches. Although not shown here, the support deflection also fluctuated through out the test period. For example, the dial indicators showed a support deflection even when there was no change in the peak deflection. However, theoretically, the supports should deflect only when the arch creeps and should always increase with time due to the increasing horizontal thrust. There was a definite influence of the changes in environmental conditions on the measured readings. This is evident from the Figures 5.4(a) and 5.4(b) which exhibited very similar fluctuations of the peak deflection. For example, the creep increased rapidly during the first eight days. Within the next 20 days there was near zero creep. The creep rate increased again during the next twelve days after which creep reading decreased for eight days. The decrease in the peak deflection indicates an upward movement of the peak of the loaded arches. This means that the thermal and moisture effects can produce a pressure large enough to lift the loaded arches. A critical study of the variation in the test environmental conditions was conducted in Chapter 4. It was found that the laboratory environmental conditions were not constant. Therefore, the effect of fluctuating temperature and relative humidity on the measured data was investigated.

It was explained in section 5.1.5 that the arches were extremely sensitive to the geometry, particularly, to the rise. Therefore, the geometry changes induced by factors other than creep have a great impact on the collected data. Some of these factors are the expansion and contraction of the steel supports and steel shoes surrounding the wood members, in addition to the moisture induced shrinkage/swelling and thermal expansion/contraction of the wood. Using the previously shown thermal expansion and shrinkage coefficients for wood (Appendix B), it can be shown that the combined effect of extreme fluctuations of the temperature by 10°F and the moisture content

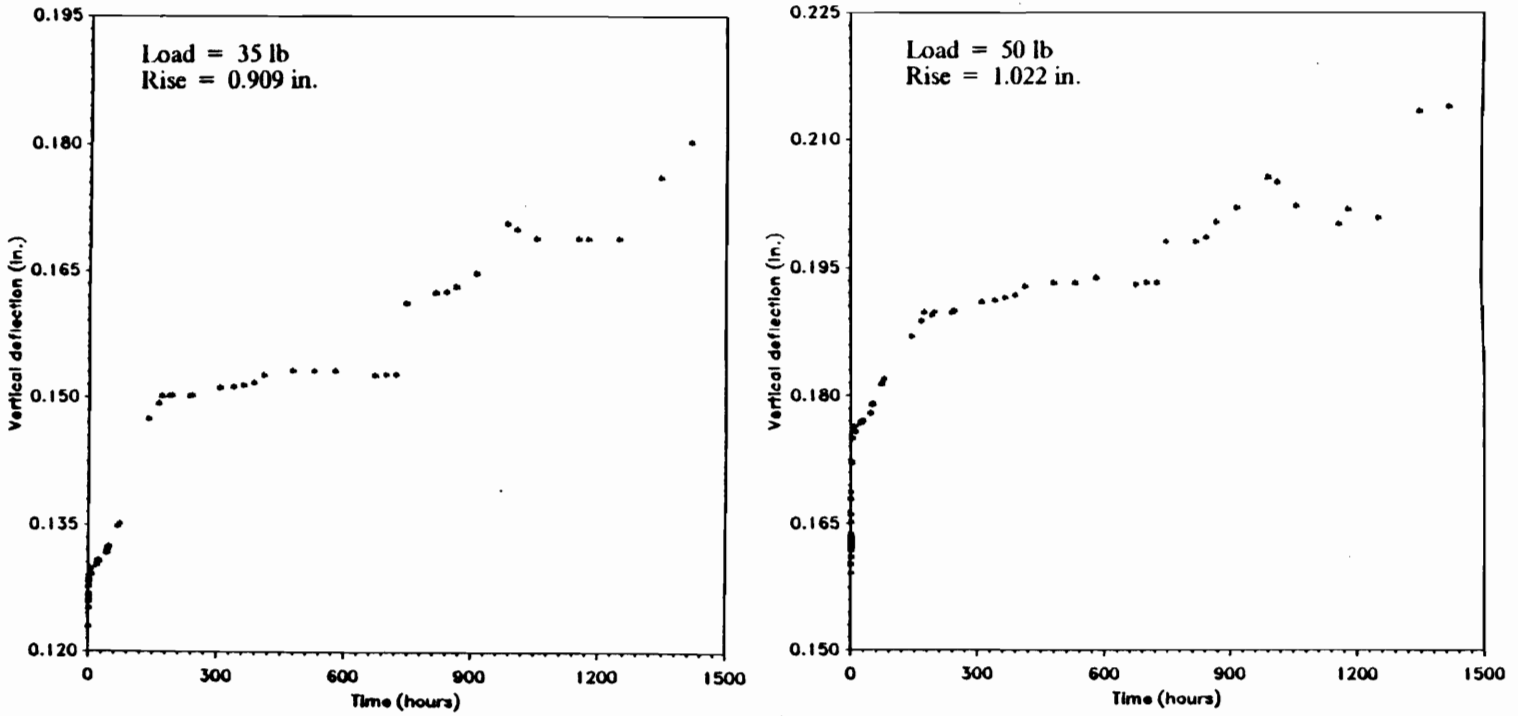

Figure 5.4. Arch creep test data: (a) deflection for 35 lbs (b) deflection for 50lb

by 2% can cause about 0.002" change in the effective length of the arch members. This leads to 3% change in the rise resulting in a 15% change in the peak deflection. The dial indicator read these additional geometry changes caused by the variable temperature and humidity, and indicated a variable creep response.

The temperature and relative humidity data collected during the long-term compression creep tests (Chapter 4) indicated that there were no extreme fluctuations of the environmental conditions during the period of creep tests on arches. Still, the influence of changing environment was evidenced by the fluctuation of the collected shown in Figures 5.4(a) and (b).

4.3.2 Finite Element Analysis

Computer Program

ABAQUS, a very powerful and general purpose finite element program (FE), was used to conduct the creep analysis of wood arches (ABAQUS, 1989). ABAQUS is specially tailored for nonlinear analysis with its key features of automatic time integration and iteration. It is considered as one of the easiest to use and one of the most computationally efficient FE computer programs (Davalos, 1989).

Selection of model elements

The element selected to model the wood members was a 2-D (B21) beam element. The B21 element has two nodes and linear interpolation functions. Each support was modeled by a zero length linear elastic spring (SPRING1). One node of the spring element is fixed to the ground and the other node is connected to a node on the beam element. The only degree of freedom of the spring element is the horizontal translation. The arch model consisted of two hinged beam elements and two zero length springs as shown in Figure 5.5.

Required model input

The program requires the data for the nodal points, elements, loads, and boundary conditions, and creep model parameters. Keyword cards, such as, NODE, ELEMENT, LOAD,

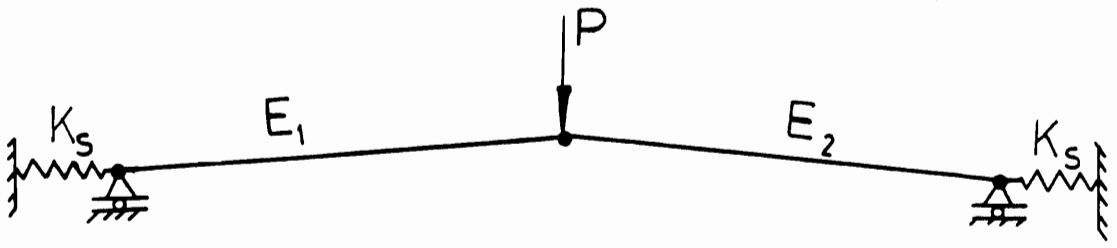

Figure 5.5. Model of the experimental arches

BOUNDARY,VISCO), are defined for the convenient data input. In addition, nodes and elements can be conveniently grouped using the "SET" parameter definitions.

Nodal data: For the beam elements, coordinates of each node must be specified. The required nodal input for the spring element is the number of the node attached to the beam element. There is no dimension associated with the zero length spring elements.

Element data: For the beam elements, the two nodes that define the element must be given. In addition, the program requires the geometry of the cross section and the cross sectional dimensions. Material property definition (i.e., ELASTIC) for each material type and the material properties are also required element input data. For the spring element, the degree of freedom of the node connected to beam element and the spring stiffness must be defined.

Creep Parameters

In the program, the creep behavior is defined by the parameter definition VISCO. The required input parameters are the coefficients A, n, and m in the creep rate expression (Eq. 2.11) given by,

$$\dot{\varepsilon}_{cr} = A\,\sigma^{n}\,t^{m} \qquad [5.1]$$

These parameters were obtained from the developed creep models (Chapter 3) expressed in Eq. 3.15 as,

$$\frac{D_{cr}}{D_0} = P_1\,t^{P_2} \qquad [5.2]$$

The parameter P_1 for each arch member was predicted from the experimentally determined Young's modulus (Table 5.1) of arch members using the regression model expressed in Eq. 3.16 (Chapter 3). For parameter P_2, the previously recommended value of 0.3358 was used. The expression in Eq. 5.2 was converted to creep strain rate in the form of Eq. 5.1, and the coefficients A, n, and m were obtained to define the creep behavior of each arch member.

Creep analysis on ABAQUS is based on the initial strain method discussed in Chapter 2. In the creep analysis, ABAQUS uses the α method (Chapter 2) for the integration of the creep rate expression given in Eq. 5.1.

Load data: The concentrated load applied at the peak node must be defined by the direction of the load with respect to the global axes.

Boundary condition data: The boundary condition of all the boundary nodes must be specified in terms of the nodal degree of freedom.

Program Output

The nodal displacements and stresses and strains for a group of nodes and elements can be obtained through the "SET" parameter definition. For a 2-D element, the stresses and the strains at five points through the thickness is provided by the program.

Elastic Analysis of Arches

An elastic analysis was conducted to compare the predicted and the experimental initial elastic response of the tested arches to gain confidence in the model. Young's modulus of the members were the values determined experimentally. First the arch supports were modeled as pin joints with restricted translation to study the influence of the joints. The results showed that the predicted elastic peak response is only 15% to 25% of the experimental response indicating that 80% to 85% of the experimental observation was due to the flexibility of the arch test fixture.

Next, the arches were modeled with zero length springs attached to the supports (Figure 5.5). The spring stiffness was computed from the horizontal thrust in the supports and the measured support deflection. The measured support deflection varied from 0.001" to 0.004" and the computed stiffness ranged from 150,000 lb/in to 480,000 lb/in. The peak response predicted by the model was 45% to 66% of the experimental elastic peak response. This indicates that either the support deflection measurement was inaccurate or other factors, such as, imperfections in the members and the system, affect the response of the arches.

A sensitivity study was conducted using ABAQUS to determine the influence of the rise, spring stiffness, Young's modulus, and the member length on the system response. It was found that the arch response is most sensitive to the rise. For example, 6% change (1/16") in the rise causes 38% change in the elastic deflection, and this relationship was nonlinear. However, the it was found that the rise was measured accurately with less than 1% error. The effect of the length and Young's modulus were as follows: 1% change in the length and the Young's modulus cause 2.5% and 1%, respectively, changes in the elastic deflection. However, the influence of these parameters within their allowable measurement errors did not explain the large discrepancy between the predicted and the experimental elastic behavior.

There was a nonlinear relationship between the elastic peak deflection and the spring stiffness. The average sensitivity of the response to the spring stiffness was that 1% change causes 2% change in the elastic deflection. Since the spring stiffness was the only uncertain parameter, it was assumed that the support deflections were measured incorrectly, and the springs in the finite element model were calibrated so that the predicted elastic peak response agreed with the measured deflection. The calibrated spring stiffness ranged from 57,000 lb/in to 108,000 lb/in and the predicted support deflection was between 0.004" and 0.14". The results indicated that the support deflection should be three to five times larger than the measured values.

Numerous attempts were made to obtain a more accurate experimental measurement of the joint deflection; however, the values required by the finite element model were not achieved. Therefore, it appears that there are other factors influencing the system response. These can be the imperfection in the wood members and the arches. For example, slight crookedness in the wood members can increase the system deflection due to P-Δ effect in the members. Moreover, imperfection in the system geometry can cause out-of-plane bending and twisting in the members. Although there were no apparent bending and twisting in the members, the presence of unrecognized bending and twisting can affect the response because the measured peak deflections are on the order of 0.1 to 0.03 inches and the system response is extremely sensitive to the geometry. However, due to the lack of measurable evidence of the other factors influencing the experimental data,

it was difficult to improve the finite element model. Regardless, creep analyses were conducted using the developed creep models (Chapter 3) to test the predicted creep response.

Creep Analysis

Since the model with the calibrated spring was the best approximation for the arches, it was used in two month creep analyses of the experimentally tested arches. As discussed previously, the experimental data included temperature and moisture effects and the model does not account for these effects. Since the effect of changing environmental conditions on the arch response at a given time was difficult to estimate, no corrections were made on the experimental data.

The finite element results showed that the difference between the predicted and the experimental creep response decreased as the load increased. For example, the difference between the predicted and the measured creep deflection for arches loaded with 35 pounds was 77% and for those loaded with 50 pounds was 63%. According to the finite element results, the arch subjected to 100 pounds snaps in six hours. However, in the experiments, the snap-through buckling in the arch occurred nine days after the tests were begun.

The results showed that the model tremendously underestimated the creep response at the lowest load level and considerably overpredicted the behavior at the highest load level. Creep analysis results revealed an inconsistent trend in the creep behavior which cannot be explained by the creep model. The results strongly indicated that the calibrated spring model did not account for the total experimental response. Therefore, it was impossible to conduct valid comparisons between the predicted and the experimental creep response.

In summary, the experimental behavior of arches were affected by factors including the flexibility of the test fixture, and temperature and moisture changes within the arches. As the best approximation, a calibrated spring model was developed; however, since there seemed to be other unknown factors influencing the system behavior, a comparable creep response was not predicted by the model. Moreover, the creep comparison was even more complicated by the effect of the changes in the test environmental conditions on the experimental data. Therefore, it is impossible to draw valid conclusions regarding the creep response predicted by the finite element model.

Chapter 6

Summary, Conclusions, and Recommendations

Summary

Long-term creep and recovery models were developed to predict the compression parallel-to-grain behavior of southern pine exposed to constant environmental conditions (≃70°F, ≃9%EMC). The developed models were based on the time temperature superposition principle (TTSP) which states that the long-term response of a polymer at a lower temperature is equivalent to the short-term response at a higher temperature. To apply the TTSP to wood, short-term accelerated compression creep (17 hour) and recovery (35 hour) tests were conducted on small clear wood specimens within a temperature range of 70°F to 150°F and constant moisture conditions of 9%. The strain was measured using bonded electrical resistance strain gages.

The short-term compliance data for all temperature levels were plotted against log-time on the same plot. Then the curve segments at successively higher temperatures were shifted along the log-time scale with respect to the curve segment at 70°F so that the curve sections smoothly join

to form a master curve applicable to 70°F and 9% MC. In general, all the curves joined well to construct the master curves. The master curves predicted 0.23 year to 6.4 year response of wood in compression.

The requirement that the horizontal shift factors below the glass transition temperature must follow the Arrhenius formulation was met by the experimental shift factors. The activation energy for creep and recovery computed from the slope of this linear relationship was about 28 KCal/mole. The linear relationship between the vertical and horizontal shift factors indicated that there was no change in the activation mechanism in the test material within temperature range used in the accelerated tests.

The developed long-term creep and recovery compliance curves were represented by power functions using a nonlinear regression analysis technique. A linear regression model was developed to predict one model parameter from Young's modulus of wood. The other model parameter showed weak correlations with material properties; therefore, an average value obtained in the study was recommended.

To test the validity of the developed long-term creep models for predicting creep response of wood exposed to normal interior environmental conditions in buildings, ten month compression tests were conducted in a heated/cooled interior laboratory environment. The long-term test specimens were end-matched with those in accelerated tests. During the first three months, the long-term data fluctuated due to the variations in the test environmental conditions affected by outside severe winter weather conditions. The fluctuation of the data was more dramatic under changing Equilibrium Moisture Content (EMC) than under variable temperature. Although a bonded strain gage arrangement was designed to eliminate the effects of factors other than creep from the measured data, the strain measuring technique was sensitive to the variability of the thermal expansion and shrinkage/swelling in the surface of wood where the strains were measured.

The comparison between the master curves and the long-term data indicated that the master curves followed the trend of the data. However, the fluctuation of the experimental data led to 28% to 50% discrepancy between the predicted and the experimental response. This was because the master curves predict creep of wood exposed to constant environmental conditions whereas the

long-term data contained additional geometry changes in the surface of wood and mechanosorptive effects caused by fluctuating environmental conditions.

Creep behavior of shallow arches was studied to demonstrate the application of the finite element method incorporating the TTSP based master curves to predict creep in wood structures. Shallow three-pin arches were constructed and tested at various load levels for two months in a heated/cooled interior laboratory environment. One arch failed (i.e., snapped-through) nine days after the test began showing that creep can cause instability failures in shallow structures. The creep response of the other arches was larger for higher load levels. There was a definite influence of the changing environmental conditions on the measured data; however, it was difficult to make corrections for these effects.

The arches were modeled as three-pin structures with the base pins supported by zero-length linear elastic springs. The finite element analysis indicated that the response of the arches was extremely sensitive to the arch geometry, particularly to the rise. The elastic analysis showed that the predicted elastic response of the arches was considerably lower than the measured response. Therefore, the spring stiffness was calibrated until the predicted elastic response agreed with the experimental measurements. However, the predicted support deflections were much larger than those measured experimentally.

Creep analysis was performed using a finite element model incorporating the developed creep equations. However, due to complexity in the creep experimental apparatus, the numerical prediction were not validated empirically.

Conclusions

This study supports the following conclusions:

1. The time temperature superposition principle can be used to develop master curves for predicting the long-term response of kiln-dried southern pine loaded in compression parallel-to-

grain and exposed to constant environmental conditions (70°F and 9% EMC). This conclusion is based on the fact that master curves were developed from short-term data and the shift factors followed the Arrhenius formulation.

2. One model parameter which describes the creep response of wood in constant environments was shown to be linearly related to Young's modulus of wood. This finding was used to develop equations that predict the creep response of wood from the material property.

3. The activation energy for creep and recovery of kiln-dried southern pine within the temperature range of 70°F and 150°F was calculated as 28 KCal/mole.

4. The fluctuating interior environmental conditions caused localized geometry changes in the wood specimens, particularly at the surface where the strain gages were attached, due to changing moisture content in the specimens. Since wood experiences mechanosorptive creep under changing moisture conditions, the long-term creep specimens exhibited more creep than that predicted from the short-term accelerated tests in which the total volume of the specimens was maintained at constant equilibrium moisture content conditions. Therefore, for all but one specimen, the master curves consistently under-predicted the compliance of the long-term specimens.

5. Creep can cause instability failures in shallow wood arches. One experimental arch "snapped through" in the course of this study.

6. The finite element method incorporating the creep models can be used to predict the long-term response of wood structures. However, due to the complexity of the creep experimental apparatus, the numerical creep predictions could not be validated empirically.

Recommendations

- The creep master curves based on TTSP should be validated using a strain measuring technique which has minimum sensitivity to thermal expansion and shrinkage effects at the surface of wood but is capable of measuring the overall response of the specimen. In the measurement of small strains, a clip gage can be a viable option. A preliminary test should be conducted at interior environmental conditions on a wood specimen fitted with both bonded and clip gages to compare the effect of environmental conditions on the performance of the two strain measuring techniques. An advantage of the clip gages is that they can be used to measure the overall response of the volume of a specimen over the gage length.

- The validity of the developed recoverable compliance curves should be tested by collecting long-term recovery data from test specimens subjected to creep in compression. The recovery models are needed to predict the effects of stress reversals in structures due to variable loading histories.

- The applicability of TTSP to large wood specimens should be tested. In large wood members, the fluctuating environmental conditions mainly affect the surfaces of the members. Therefore, if the strain is measured over the volume of the members, instead of at the surface, the effect of the fluctuations in the environmental conditions on the measured response can be minimized.

- As an extension to this study, it is advisable to investigate the applicability of the TTSP to predict the long-term response of southern pine in tension and shear. These models are useful in predicting the long-term response of structures under combined loading conditions.

- When the response of shallow structures is studied, it must be recognized that the system response is extremely sensitive to the geometry. Therefore, serious attention should be given to

the variables in the system and accurate methods must be used to measure the important parameters. Considering the tremendous horizontal thrust in the supports of shallow structures, the test fixture and the supports must be extremely stiff compared to the stiffness of the structure.

Literature Cited

ABAQUS, (Version 4.7-1), 1989, Hibbitt, Karlsson & Sorensen, Inc., 100 Medway Street, Providence, RI.

Aklonis, J.J., and W.J. MacKnight. 1983. Introduction to Polymer Viscoelasticity, Second Edition, John Wiley and Sons, New York.

American Institute of Timber Construction, 1985. Timber Construction Manual (TCM). Third Edition, John Wiley & Sons, Inc. New York.

Arima, T., 1967. The Influence of High Temperature on Compressive Creep of Wood. Journal of Japan Wood Res. Soc. 13(2):37-40.

Arima, T. 1972. Creep in Process of Temperature Changes: I Creep in Process of Constant, Elevated, and Decreased Temperature. Journal of Japan Wood Res.Soc. 18(7):349-353.

Bach, L., and R.E. Pentoney, 1968. Nonlinear Mechanical Behavior of Wood. Forest Products Journal 18(3):60-66.

Bathe, K.J., 1982. Finite Element Procedures in Engineering Analysis. Prentice-Hall, Inc., Engelwood Cliffs, New Jersey 07632

Bodig, J., and B.A. Jayne, 1982. Mechanics of Wood and Wood Composites, Van Nostrand Reinhold Company Inc., 135 West 50th Street, New York, N.Y. 10020.

Clauser, W.S., 1959. Creep of Small Wood Beams Under Constant Bending Load. Forest Products Lab, Forest Service U.S.D.A. Report No. 2150.

(CEMS) Creep of Engineering Materials and Structures. 1978. Edited by G. Bernasconi and G. Piatti. Seminar on Creep of Engineering Materials and Structures.

Davidson, R.W., 1962. The Influence of Temperature on Creep in Wood. Forest Products Journal, 12(8):377-381.

Ferry, J.D., 1980, Viscoelastic Properties of Polymers, Third Edition, Wiley, New York.

Flugge, W. 1975. Viscoelasticity. Second revised edition, Springer-Verlag.

Ganowicz, R. 1988. The influence of Cyclic Temperature Changes on Creep of glue-laminated beams. Proceedings of the 1988 International Conference on Timber Engineering in Seattle, Washington.

Gressel, P. 1984. Prediction of Long-term Deformation Behavior from Short-term Creep Experiments. Holz als Roh-und Werkstoff. 42: 293-301.

Grossman, P.U.A., and R.S.T. Kingston. 1963. Some Aspects of the Rheological Behavior of Wood. III Test of Linearity. Division of Forest Products, CSIRO, Melbourne.

Grossman, P.U.A. 1976. Requirements for a Model that Exhibits Mechano-sorptive Behavior, Wood Sci. and Tech. 10:163-168.

Hann, R.A., et al. 1970. Moisture Content of Laminated Timbers. U.S.D.A. Forest Service Research Paper, FPL 149, Forest Products Laboratory.

Hayman, B. 1981. Creep Buckling- A general View of the Phenomenon. Proceedings of the Third IUTAM Symposium on creep in structures. A.R.S. Ponter and D.R. Hayhurst, eds., Springer-Verlag, pp.289-307.

Hiel, C, A.H. Cardon, and H.F. Brinson, 1984, The Nonlinear Viscoelastic Response of Resin Matrix Composite Laminates, NASA Contrator Report, 3772.

Holzer, S.M., D. A. Dillard, and J.R. Loferski. 1989. A Review of Creep in Wood: Concepts Relevant to Develop Long-term Behavior Predictions for Wood Srtuctures, Wood and Fiber Science, Vol.21, No.4, pp. 376-392.

Hoyle, R.J.Jr., M.C. Griffith, and R.Y. Itani. 1985. Primary Creep in Douglas-fir Beams of Commercial Size and Quality. Wood Fiber, 17(3):300-314.

Humphries, M. and A.P. Schniewind. 1982. Behavior of Wood Columns under Cyclic Relative humidity. Wood Sc. 15(1):44-48.

Hunt, D. 1979. A Preliminary Study of Tensile Creep of Beech with Concurrent Moisture Changes. ICM 3, 3:299-308.

Itani, R.Y., M.C. Griffith, and R.J. Hoyle, Jr. 1986, The effect of creep on Long Wood Column Design and Performance. Journal of Structural Engineering, Vol 112, No. 5, 1986, pp.1097-1114.

Kani, I.M., R.E. McConnel, and T. See. The Analysis of a Single Layer Braced Dome.

Kelly, S.S., T.G. Rilas, and W.G. Glasser. 1986. Relaxation Behavior of the Amorphous Components of Wood

King, E.J. Jr, 1961. Time-Dependent Strain Behavior of Wood in Tension Parallel to Grain. Forest Products Journal, 11(3):156-165.

Kingston, R.S.T., and L.N. Clarke, 1961. Some Aspects of the Rheological Behavior of Wood: I. the Effects of Stress with Particular Reference to Creep. Australian Journal of Applied Sci. 12(2):211-227.

Kingston, R.S.T., and B. Budgen, 1972. Some Aspects of the Rheological Behavior of Wood, Part IV: Nonlinear Behavior at High Stresses in Bending and Compression. Wood sci. and Tech. 6:230-238.

Kitahara, K., and K. Yukawa, 1964. The Influence of Change in Temperature on Creep in Bending. Journal of Japan Wood Res.Soc. 10(5):169-175.

Kraus, H. 1980. Creep Analysis. John Wiley & Sons, Inc.

Kulasiri, G.D. , 1990, Simulation of Deep-bed Drying of Virginia-type Peanuts, Dissertation, VPI&SU, Blacksburg, VA 24061.

Leicester, R.H., 1971. Large Deflections of Timber Beams During Drying. Wood Sci. and Tech. 5(3):221-231.

Miller, D.G. and P. George, 1974. Effect of Stress level on the Creep of Eastern White Spruce in Bending. Wood Sci. 7(1):21-24.

National Forest Products Association, 1986. National Design Specification for Wood Construction. Washington, D.C.

Panshin, A.J., and C. de Zeeuw, 1980. Fourth Edition, McGraw-Hill, Inc.

Pentoney, R.E., and R.W. Davisdon. 1962. Rheology and the Study of Wood. Forest Products Journal, 12:243-248.

Perry, C.C. and H.R. Lissner, 1962, The Strain Gage Primer, Second Edition, McGraw-Hill, pp.62-73.

Povolo, F., and M. Fontelos. 1987. Time Temperature Superposition Principle and Scaling Behavior. Journal of Material Sci. 22(5):1530- 1534.

Rosen, S.L., 1971. Fundamental Principles of Polymeric Materials for Practicing Engineers. Barnes & Noble, Inc., New York.

Salmen, L. 1984. Viscoelastic Properties of in situ Lignin under Water Saturated Conditions. Journal of Materials Science, 19:3090-3096.

Schaffer, E.L., 1972. Modeling the Creep of Wood in a Changing Moisture Environment. Wood Fiber, 3(4):232-235.

Schaffer, E.L., 1972. Influence of Heat on the Longitudinal Creep of Dry Douglas-fir in R.W. Meyer and R.M. Kellog, eds. Structural Uses of Wood in Adverse Environments. Society of Wood Sci. and Tech. Van Nostrand Reinhold Company, New York. pp.20-52

Schniewind, A. P., 1968. Recent Progress in the Study of the Rheology of Wood. Wood Sci. and Tech. volume 2 pp.188-206.

Schniewind, A.P., and J.D. Barrett, 1972. Wood As a Linear Orthotropic Viscoelastic Material. Wood Sci. and Tech. 6:43-57.

Schniewind, A.P., 1967. Creep Rupture Life of Douglas-fir Under Cyclic Environmental Conditions. Wood Sci. and Tech. 1(4):278-288.

Szabo, T., and G. Ifju. 1969. Influence of Stress on Creep and Moisture Distribution in Wooden Beams Under Sorption Conditions. Wood Sci.2(3).

Timoshenko, S. 1930. Strength of Materials. D. Van Nostrand Company, Inc., 250 Fourth Avenue, New York.

Wood Handbook - Wood as an Engineering Material. 1987. U.S. Department of Agriculture, Washington D.C.

Yamada, T., T. Takemura, and S. Kadita. 1961. On the Rheology of Wood III. The Creep and the Stress Relaxaton of Buna. Journal of Japan Wood Res.Soc. 7(2):63-67. (As reported by Schniewind (8))

Youngs, R.L., 1957 October. Mechanical Properties of Red Oak Related to Drying. Forest Products Journal, pp.315-324.

Zar, J. H., 1984. Biostatistical Analysis. Second Edition. Prentice-Hall, Inc., Englewood Cliffs, N.J. 07632.

Appendix A.

Accelerated Data and Master Curves (Cont'd)

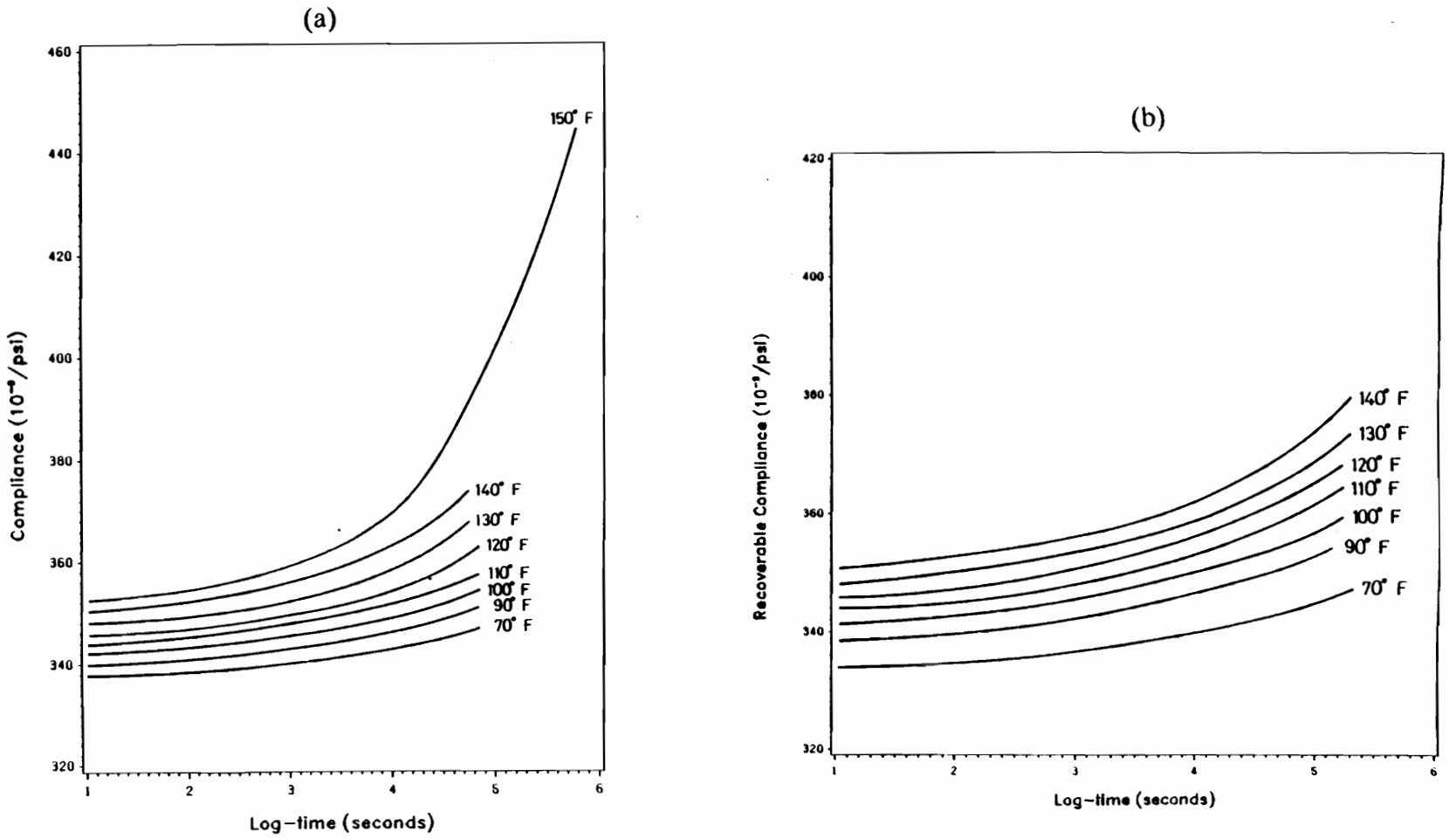

Figure A.1. Short-term accelerated data for specimen No.1: (a) creep data (b) recovery data

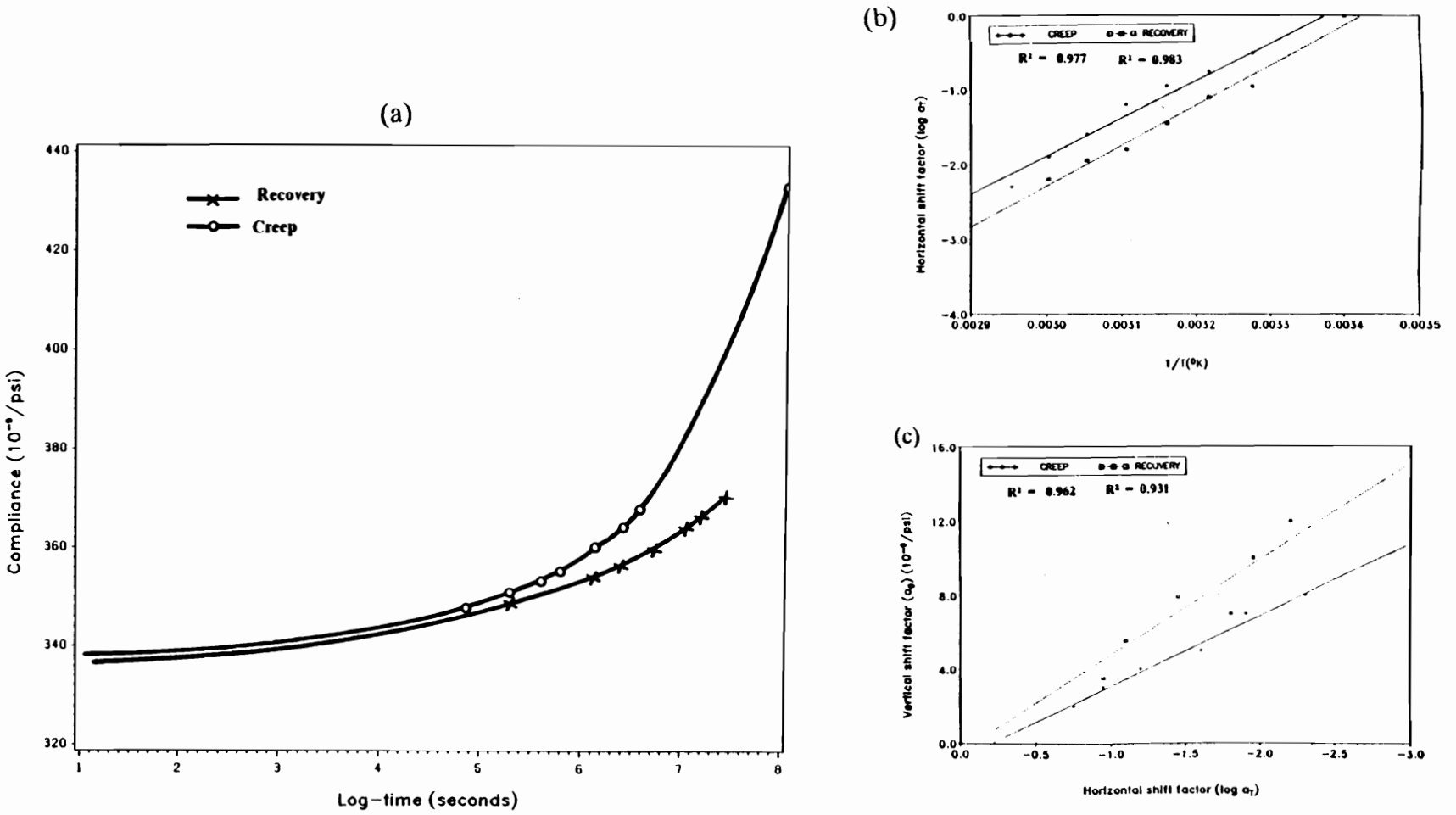

Figure A.2. Master curves and shift factor data for specimen No.1: (a) creep and recovery master curves (b) horizontal shift factor vs. temperature (c) vertical vs. horizontal shift factors

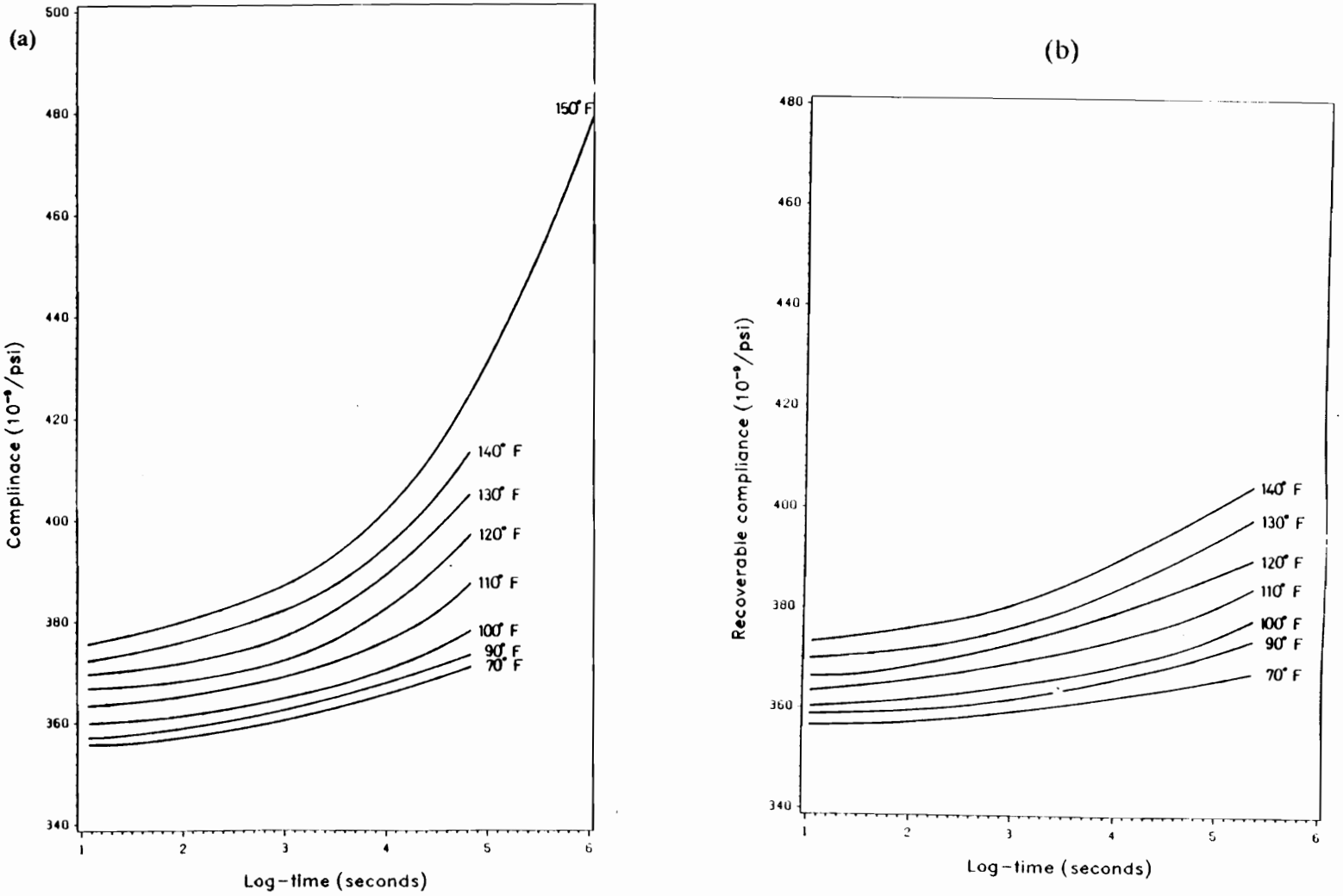

Figure A.3. Short-term accelerated data for specimen No.3: (a) creep data (b) recovery data

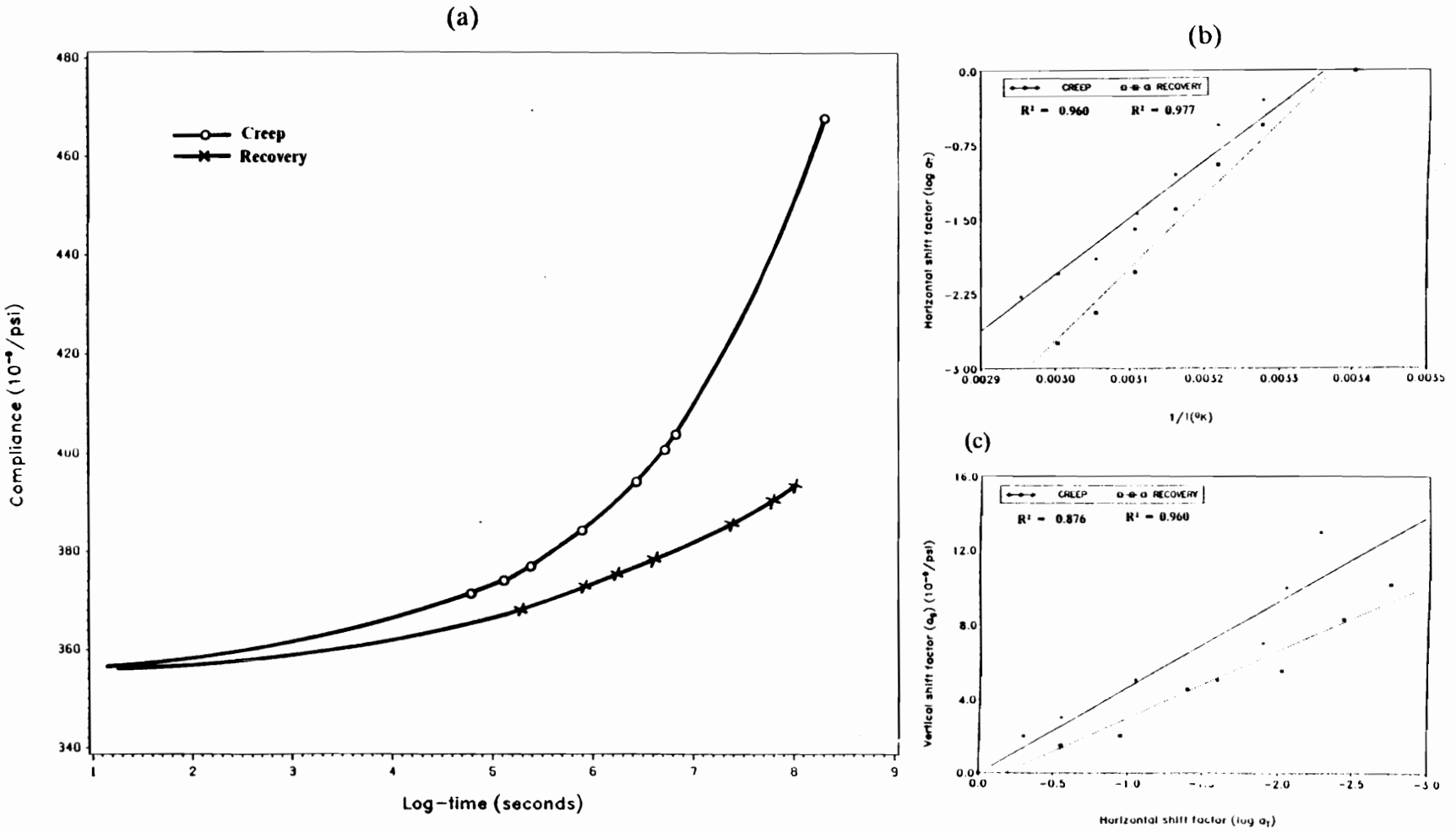

Figure A.4. Master curves and shift factor data for specimen No.3: (a) creep and recovery master curves (b) horizontal shift factor vs. temperature (c) vertical vs. horizontal shift factors

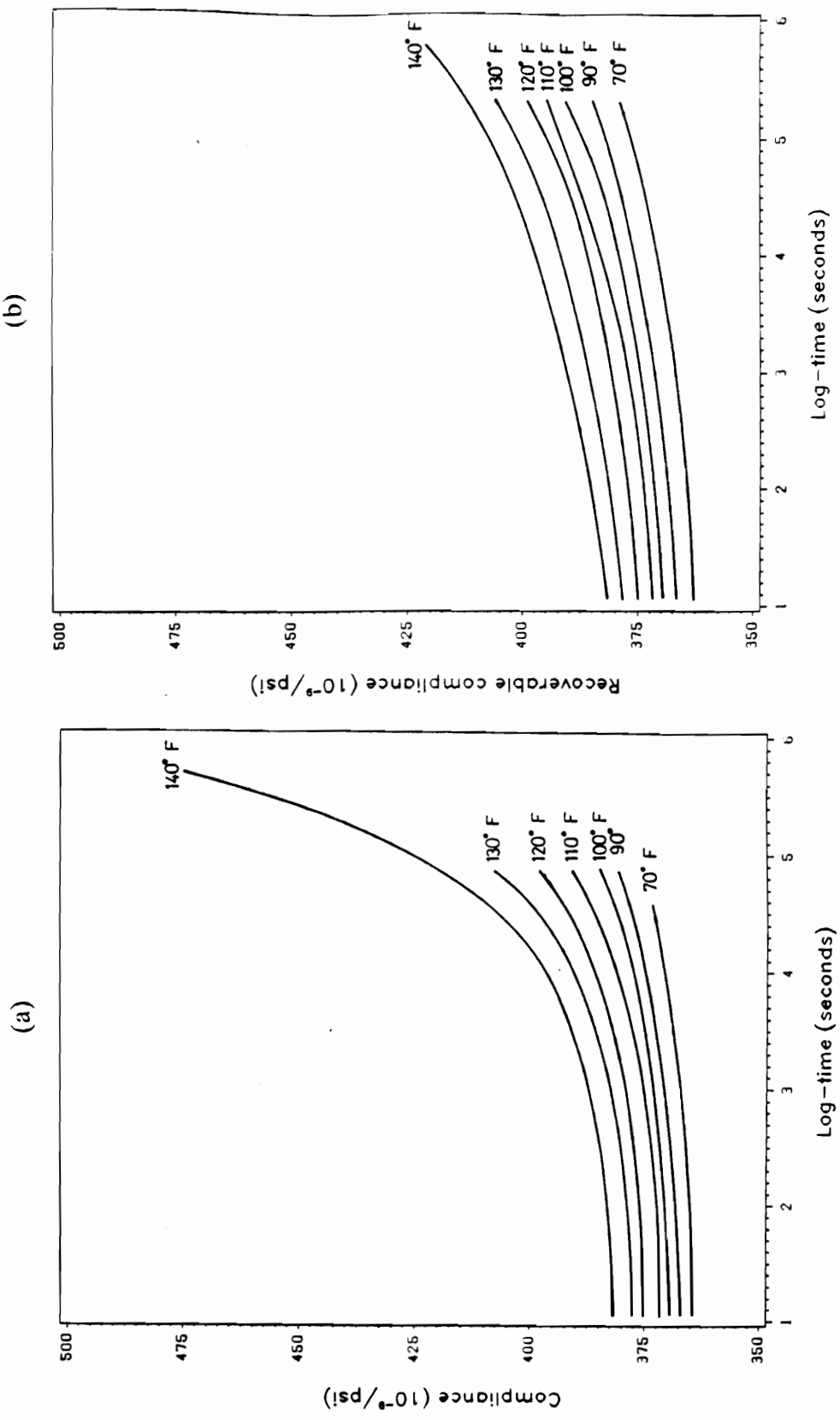

Figure A.5. Short-term accelerated data for specimen No.5: (a) creep data (b) recovery data

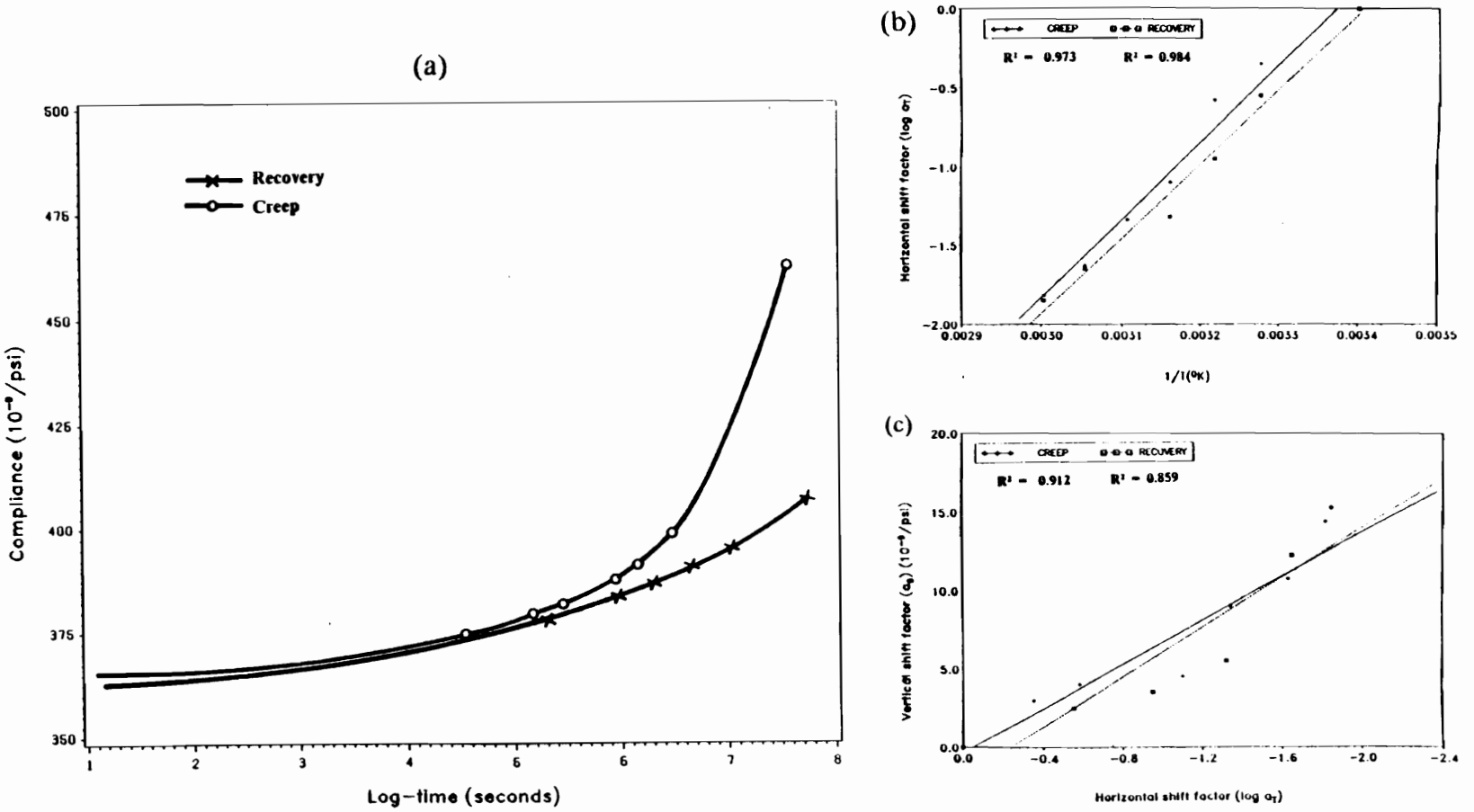

Figure A.6. Master curves and shift factor data for specimen No.5: (a) creep and recovery master curves (b) horizontal shift factor vs. temperature (c) vertical vs. horizontal shift factors

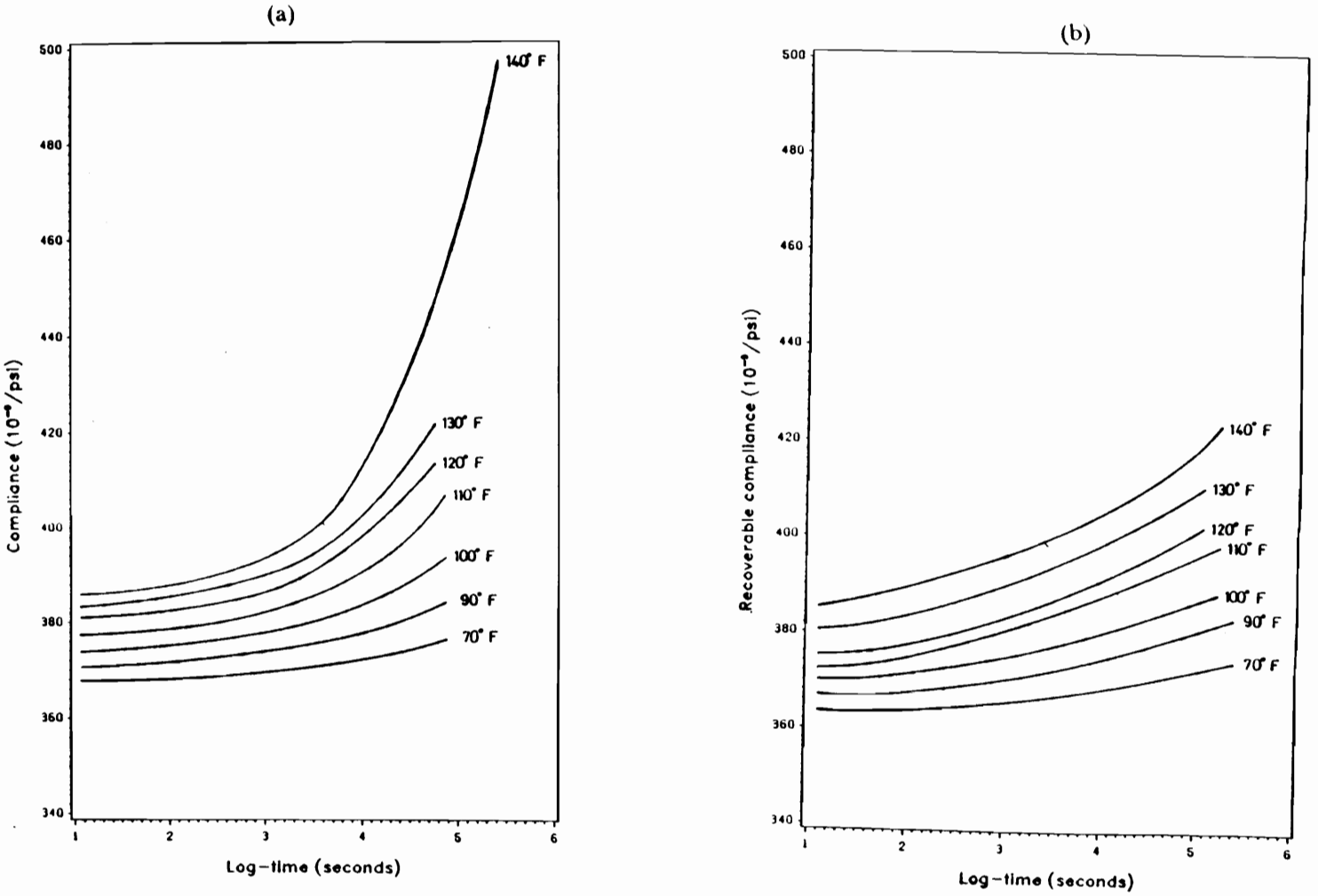

Figure A.7. Short-term accelerated data for specimen No.6: (a) creep data (b) recovery data

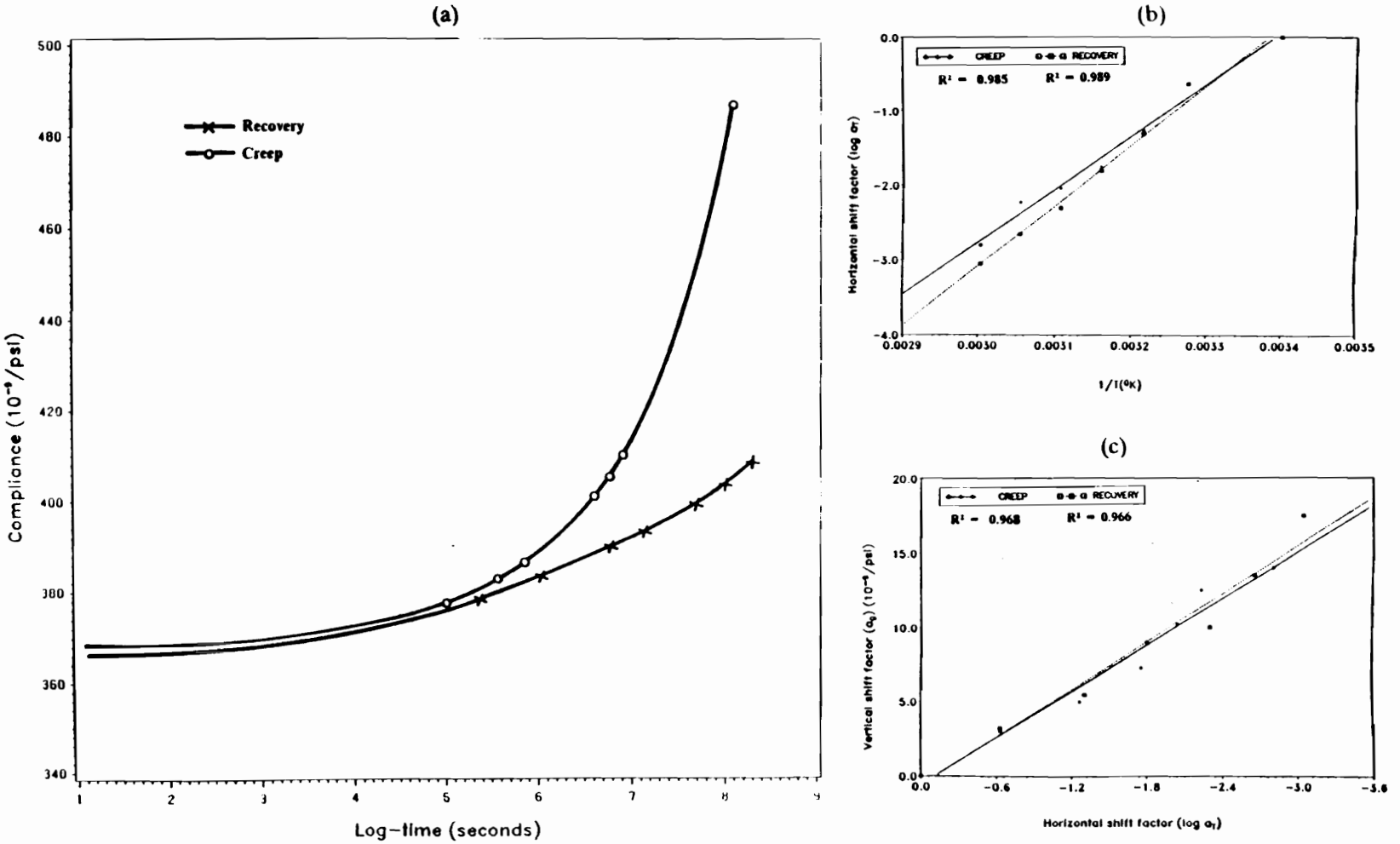

Figure A.8. Master curves and shift factor data for specimen No.6: (a) creep and recovery master curves (b) horizontal shift factor vs. temperature (c) vertical vs. horizontal shift factors

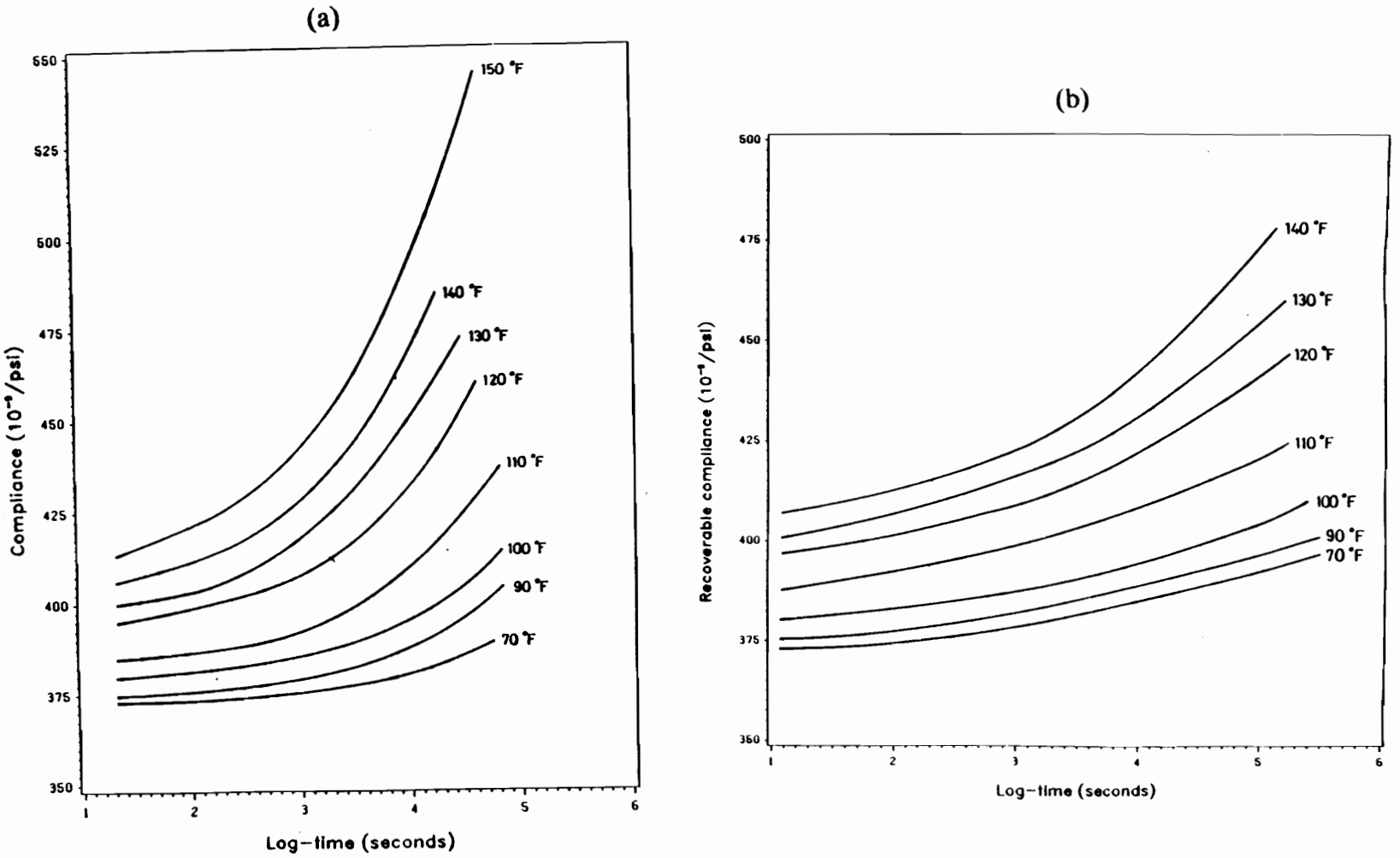

Figure A.9. Short-term accelerated data for specimen No.7: (a) creep data (b) recovery data

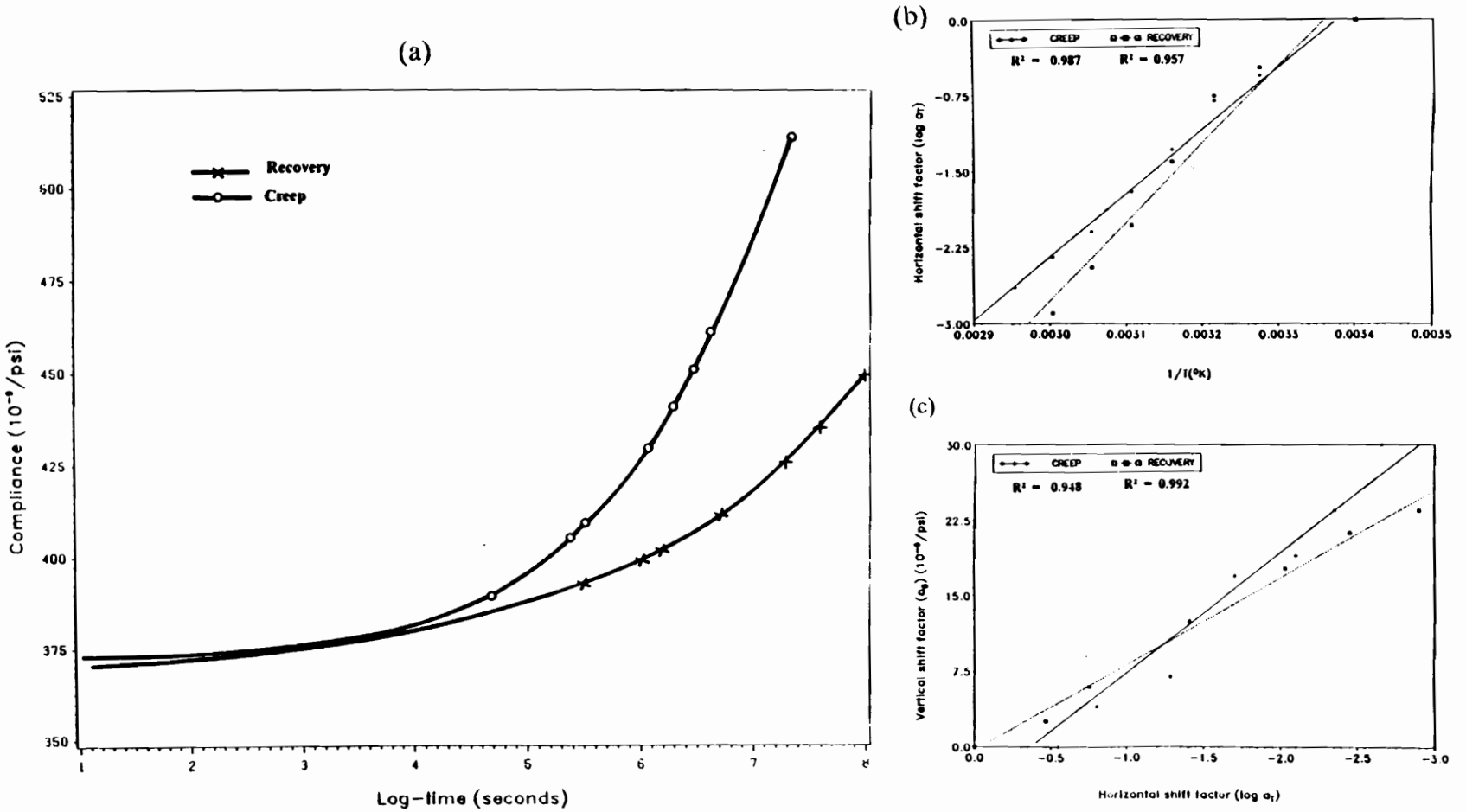

Figure A.10. Master curves and shift factor data for specimen No.7: (a) creep and recovery master curves (b) horizontal shift factor vs. temperature (c) vertical vs. horizontal shift factors

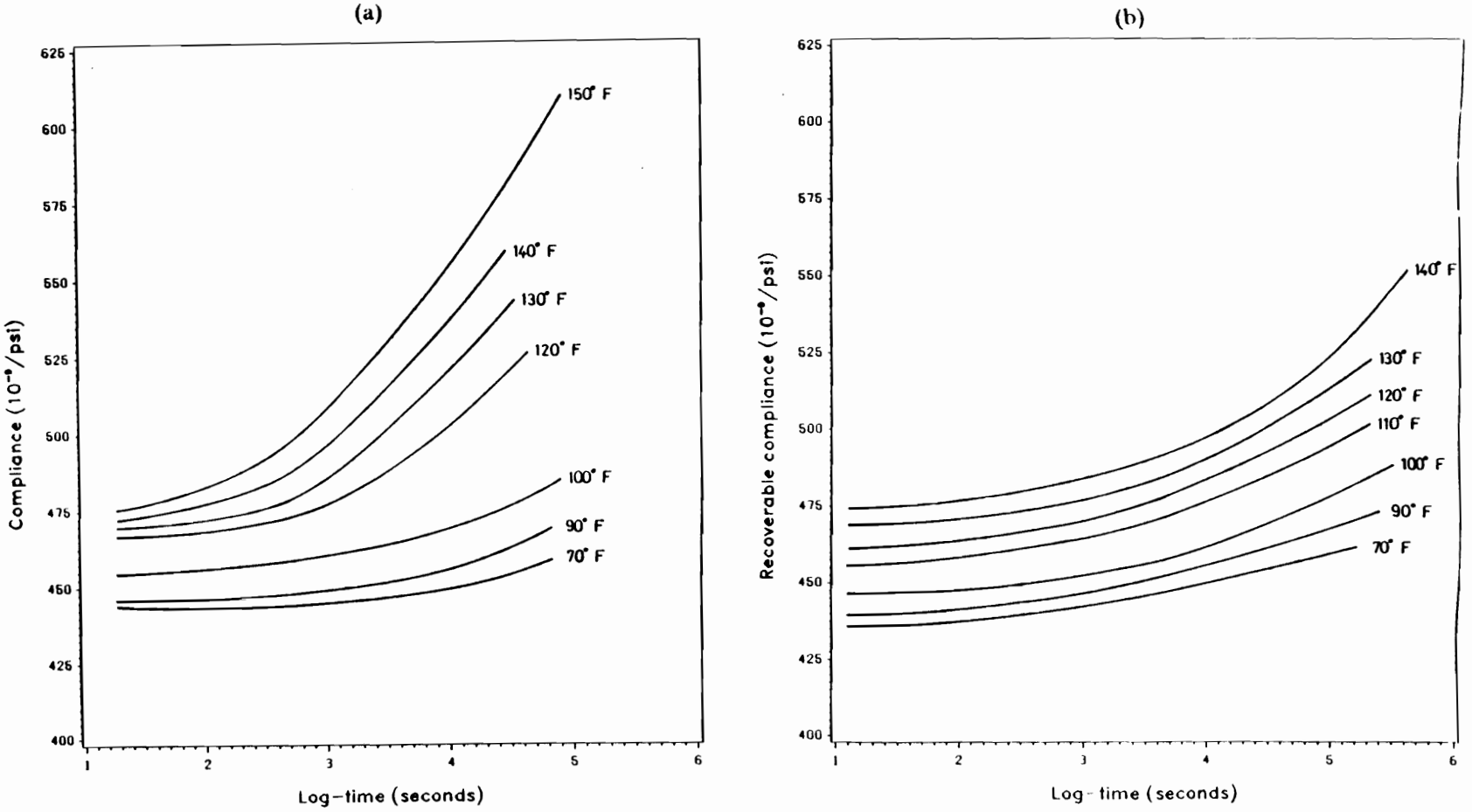

Figure A.11. Short-term accelerated data for specimen No.8: (a) creep data (b) recovery data

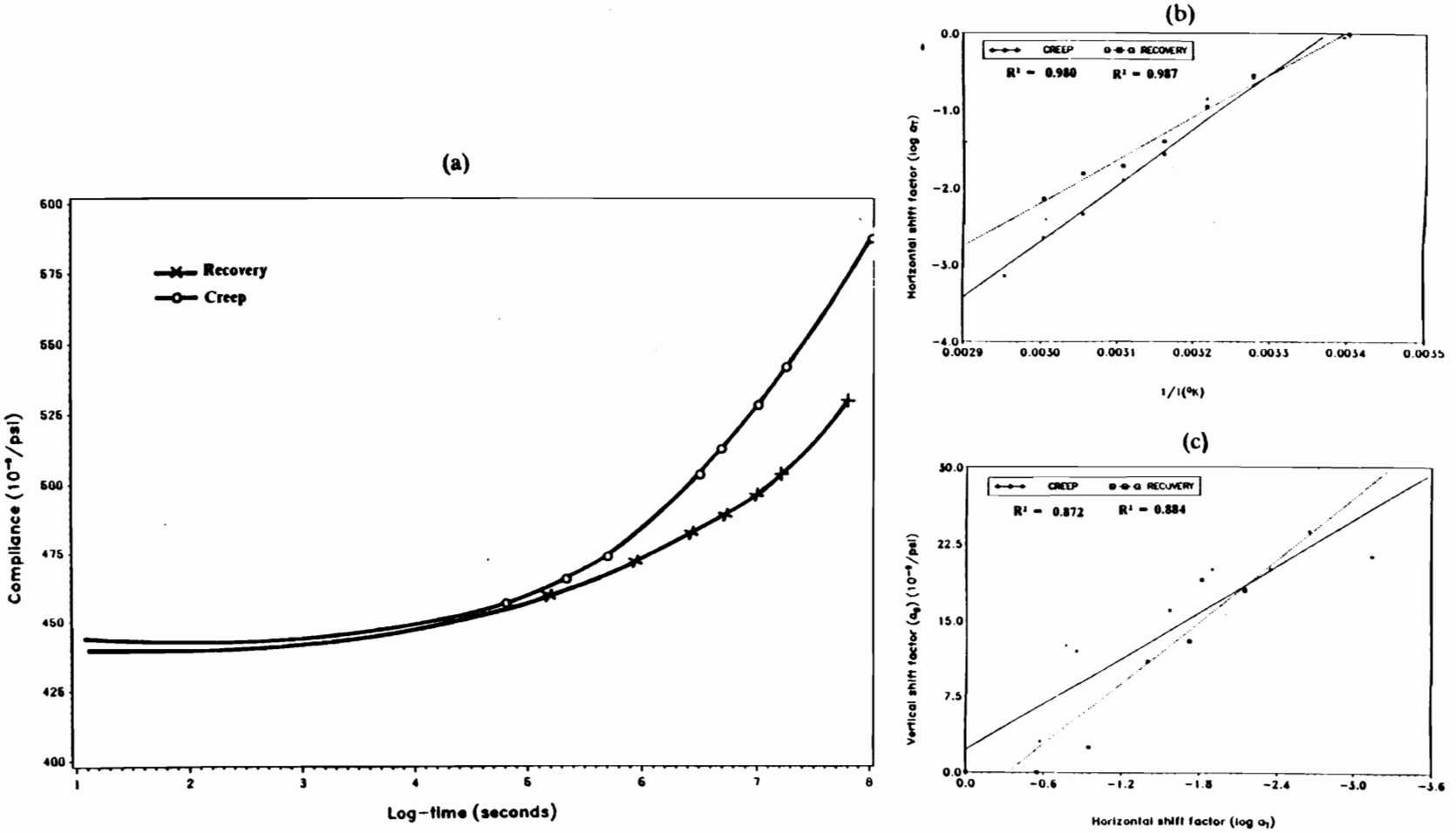

Figure A.12. Master curves and shift factor data for specimen No.8: (a) creep and recovery master curves (b) horizontal shift factor vs. temperature (c) vertical vs. horizontal shift factors

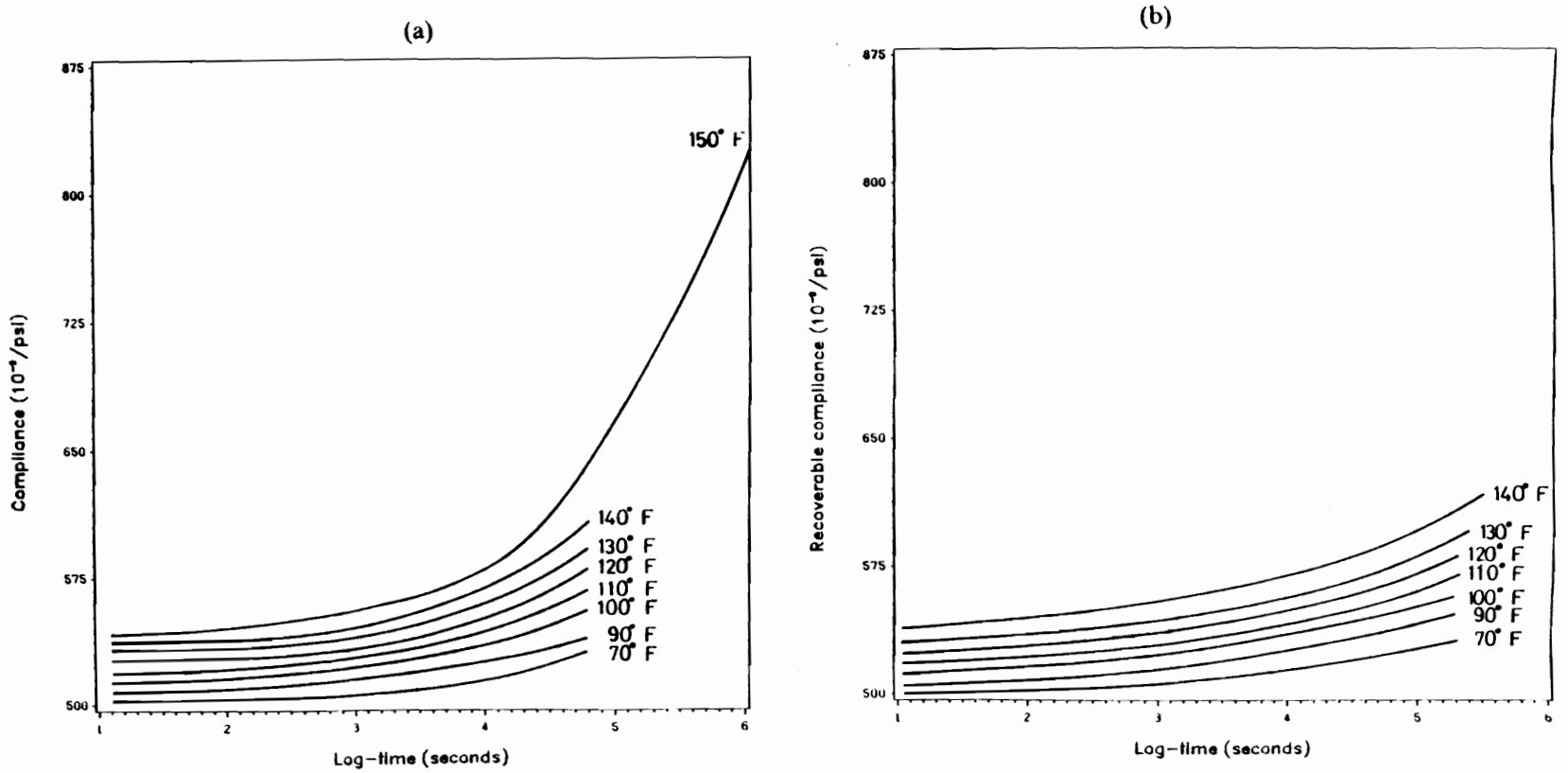

Figure A.13. Short-term accelerated data for specimen No.10: (a) creep data (b) recovery data

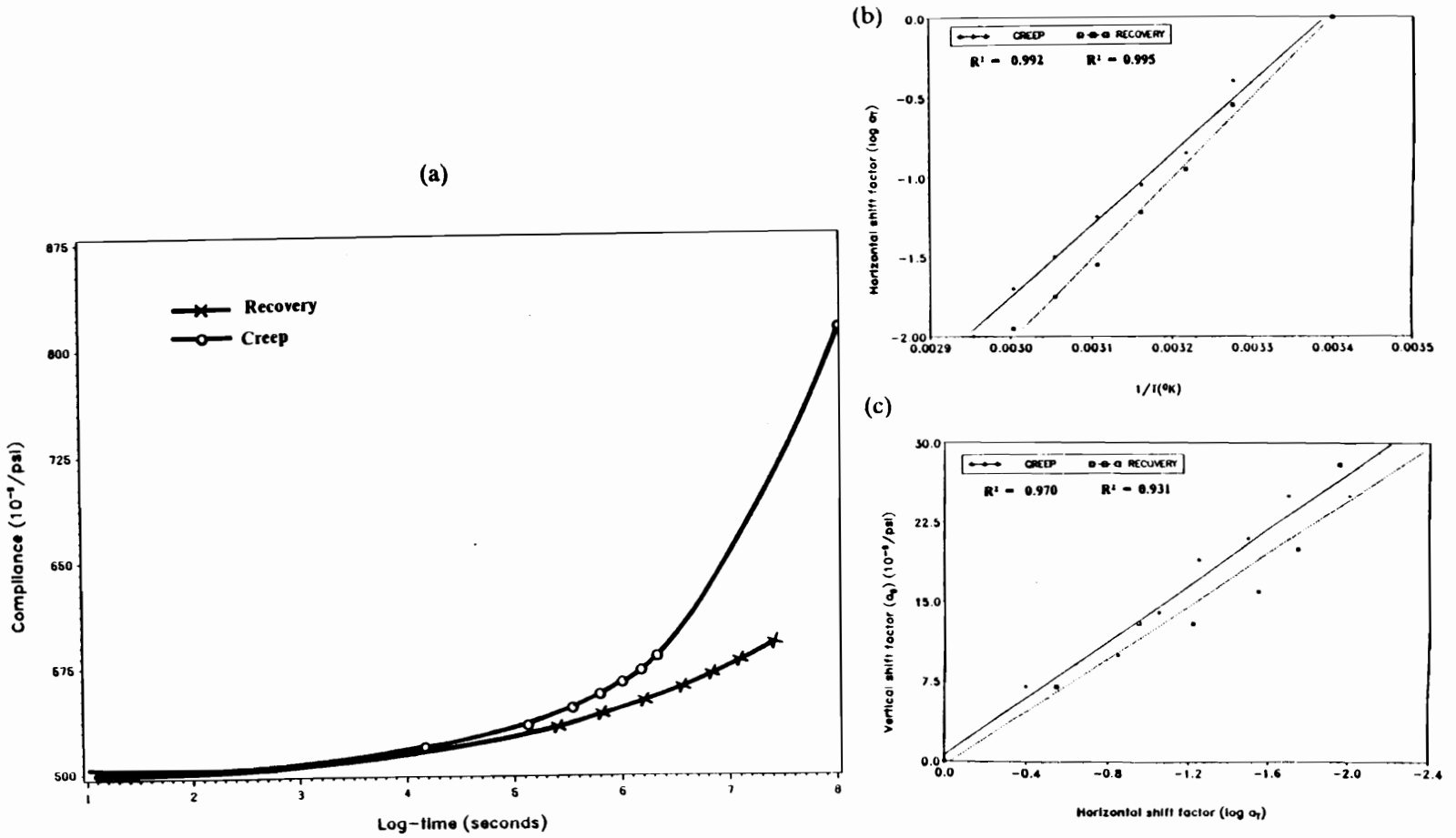

Figure A.14. Master curves and shift factor data for specimen No.10: (a) creep and recovery master curves (b) horizontal shift factor vs. temperature (c) vertical vs. horizontal shift factors

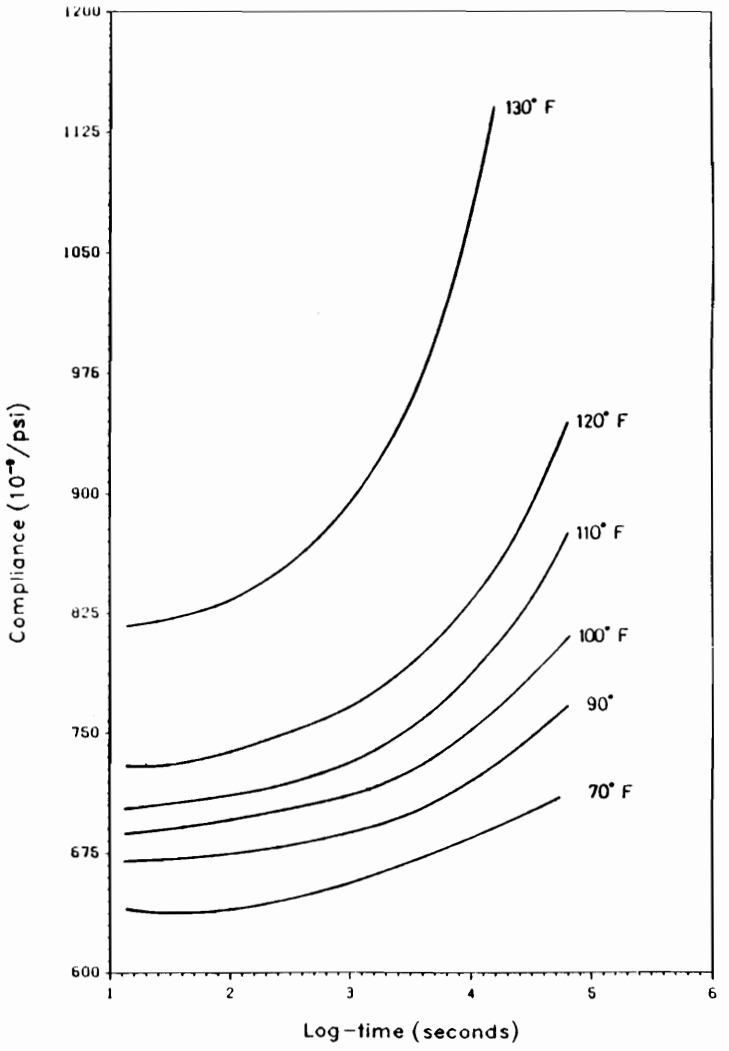

Figure A.15. Short-term accelerated creep data for specimen No.11:

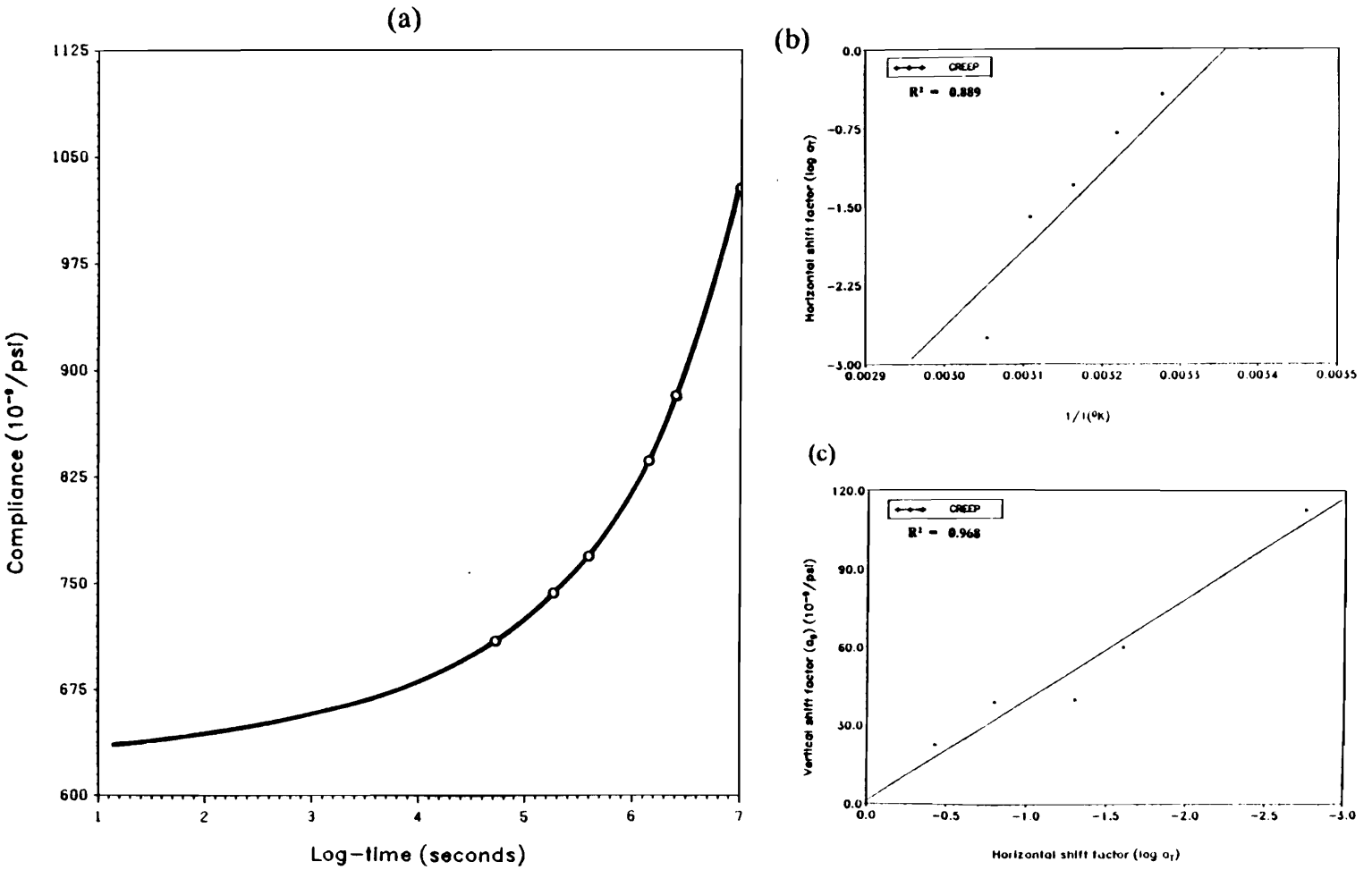

Figure A.16. Master curves and shift factor data for specimen No.11: (a) creep master curve (b) horizontal shift factor vs. temperature (c) vertical vs. horizontal shift factors

Appendix B.

Effect of Variable Thermal Expansion and Shrinkage of Wood on Strain Gage Measurements

In section 4.2 (Chapter 4), it was shown that the long-term creep data were affected by the variable thermal expansion and shrinkage/swelling of wood at the locations were the strain gages were bonded. In this Appendix, computations are carried out to quantify the influence of variability of the thermal expansion and shrinkage/swelling coefficients of the wood on the strain gage measurements.

Effect of Variability of Thermal Expansion Coefficients

Very limited research has been conducted to investigate the influence of the variability of the wood properties on the coefficient of thermal expansion, α, of wood (Wood Handbook, 1987). The α in the longitudinal direction of wood appears to be independent of the specific gravity and species and falls within (1.7 - 2.5) x 10^{-6}/°F

(Wood Handbook, 1987, Gurfinkel, 1981). However, the α in the radial and tangential directions is five to ten times as high as that in the longitudinal direction and is a function of specific gravity. Wood expands when temperature increases. However, increasing temperature causes a loss of moisture content leading to shrinkage. Unless the wood is very dry (3 or 4% or less) the shrinkage due to moisture loss will be greater than the corresponding thermal expansion (Wood Handbook, 1987).

The following computations were carried out to check how the variability of the longitudinal coefficient of thermal expansion, α_L, affects the output of the Wheatstone bridge used in this study. The expansions in the transverse direction were not considered, because the the transverse sensitivity of the strain gages used in this study was only 0.8% of the longitudinal sensitivity.

Since exact values for α_L was not known, it was assumed in the computation that the longitudinal coefficient of thermal expansion of the active specimens, α_{L13}, was 2.5x 10^{-6}/°F and that of the dummy specimens, α_{L24}, was 1.7x10^{-6}/ °F. These values are the maximum and the minimum values of the range of α_L for wood as presented previously.

The Wheatstone bridge output for the bridge circuit used in this study was expressed in Eq. 3.2 (Chapter 3) as,

$$\frac{E_0}{E_i} = \frac{R_1}{R_1 + R_2} - \frac{R_4}{R_3 + R_4} \qquad [B.1]$$

where;

R_1 and R_3 = resistance of active gages

R_2 and R_4 = resistance of dummy gages

E_0 = bridge output voltage

E_i = bridge excitation voltage

If all the gages experience the same temperature variation ΔT, then, the two active gages undergo similar resistance change, ΔR_{13}, due to temperature. The two

dummy gages also experience similar resistance change, ΔR_{24}, but it is lower than the resistance change of active gages because of the assumed α values.

Substituting the resistance changes into Eq. B.1 and assuming equal initial resistance, R, for the gages,

$$\frac{E_0}{E_i} = \frac{\Delta R_{13} + R}{(\Delta R_{13} + R) + (\Delta R_{24} + R)} - \frac{\Delta R_{24} + R}{(\Delta R_{13} + R) + (\Delta R_{24} + R)} \qquad [B.2]$$

Simplifying Eq. B.2 and substituting Eqn. 3.1 expressed as,

$$\frac{\Delta R}{R} = F\,\varepsilon$$

where;

F = gage factor = 2.05

ε = strain in the gage the bridge output can be computed as,

$$\frac{E_0}{E_i} = \frac{F\,(\varepsilon_{13}^T - \varepsilon_{24}^T)}{2 + F\,(\varepsilon_{13}^T + \varepsilon_{24}^T)} \qquad [B.3]$$

In Eq. B.3, . ε_{13}^T and ε_{24}^T are the apparent strains in active and dummy gages, respectively. The apparent strains are due to the difference between thermal expansion of the gage and the wood at the gage locations, and are equal to,

$$\varepsilon_{13}^T = \alpha_{gage} - \alpha_{active} \qquad [B.4]$$

$$\varepsilon_{24}^T = \alpha_{gage} - \alpha_{dummy} \qquad [B.5]$$

where;

α_{gage} = coefficient of thermal expansion of gages ($6x10^{-6}$/degreeF)

α_{active} and α_{dummy}) = thermal expansion coefficients of active and dummy gages, respectively.

Substituting Eq. B.4 and B.5 into Eq. B.3

$$\frac{E_0}{E_i} = \frac{F\,(\alpha_{dummy} - \alpha_{active})}{2 + F\,(2\,\alpha_{gage} - (\alpha_{active} + \alpha_{dummy}))} \qquad [B.6]$$

Substituting α values, F = 2.05, and E_i = 2 volts, into Eq. B.6, the bridge output can be computed as,

$$E_0 = 0.82 \times 10^{-6} \text{ volts/°F} \qquad [B.7]$$

The apparent strain indicated by the strain indicator due to the thermal expansion of wood can be computed by substituting the bridge output to Eq. 3.6 (Chapter 3) expressed as,

$$\varepsilon = \frac{2\,E_0}{F\,(E_i - E_0)} \qquad [B.8]$$

The resultant apparent strain due to 10°F change in temperature, ε^T, is,

ε^T = 4.8 micro-strains

In the next section, the apparent strain due to the variability of shrinkage/swelling coefficients at gage locations is computed and is compared with the apparent strain due to the variable thermal expansion.

Effect of Variability of Shrinkage Coefficients

Wood exhibits anisotropic shrinkage characteristics. Shrinkage is highest in the direction of annual growth rings (tangentially) and about half as much across the rings (radially). Shrinkage along the grain is slight compared to transverse shrinkage. Wood Handbook (1987) states that even in the longitudinal direction where dimensional changes due to moisture change is very slight, shrinkage will still predominate the

corresponding dimensional changes due to thermal expansion unless the wood is very dry initially (3 or 4% or less).

The variation in the shrinkage of different samples of the same wood species subjected to the same environmental conditions results primarily from the following factors (Haygreen and Bowyer, 1982):

Size and shape of the sample: This influences the grain orientation in the sample and uniformity of the moisture content through the thickness.

Density of the sample: Higher the density, higher the shrinkage.

The average longitudinal shrinkage for most wood species varies from 0.1% to 0.2% when drying from green to oven dry conditions. The transverse shrinkage coefficients depend on the wood species and previous studies have shown a coefficient of variation of 15% for the transverse shrinkage of wood (Wood Handbook, 1987). For southern pine, the following shrinkage coefficients are reported in the Wood Handbook (1987).

Shrinkage coefficients for southern pine for drying from green to oven dry conditions

Longitudinal = 0.1 - 0.2%

Radial = 4.8%

Tangential = 7.4%

The shrinkage coefficients for southern pine show that the longitudinal shrinkage per percent change of moisture content varies from 33.3×10^{-6}/ %MC to 66.6×10^{-6}/%MC. These values indicate that a strain gage bonded to a wood specimen would show apparent strains of 33 to 66 micro strains in the longitudinal direction due to only 1% change in the moisture content. However, if all the four specimens used in the bridge had similar shrinkage properties, the net apparent strains due to moisture change would be cancelled by the compensating gages in the bridge.

The shrinkage coefficients stated in the previous paragraph were used in the following computation to check the effect of the variation of the longitudinal shrinkage

of wood specimens on the Wheatstone bridge output. It was assumed that the longitudinal shrinkage coefficient for the two active specimens was 66.6×10^{-6}/%MC and that for the dummy specimens was 33.3×10^{-6}/%MC. The bridge output voltage corresponding to the variable shrinkage in the active and dummy specimens were computed following the same procedure as that used to compute the effect of thermal expansion and the resultant expression was,

$$\frac{E_0}{E_i} = \frac{F(\varepsilon_{13}^{MC} - \varepsilon_{24}^{MC})}{2 + F(\varepsilon_{13}^{MC} + \varepsilon_{24}^{MC})} \qquad [B.9]$$

where;

ε_{13}^{MC} = strain due to shrinkage in the active specimens

ε_{24}^{MC} = strain due to shrinkage in the dummy specimens

For a moisture content change of 1%, these strains are equal to the corresponding shrinkage coefficients already assumed. Substituting the shrinkage parameters into Eq. B.9, the Wheatstone bridge output can be computed as,

$$E_0 = 66.4 \times 10^{-6} \quad \text{volts/\%MC} \qquad [B.10]$$

Substituting voltage into Eq. B.8, the apparent strain due to 1% moisture change, ε^{MC}, is,

$$\varepsilon^{MC} = 32.33 \text{ micro} - \text{strains} \qquad [B.11]$$

In the long-term creep tests moisture variation as much as 3% was observed. The apparent strain for 3% moisture change is 97 micro-strains.

The combined effect of 10°F change in temperature and 3% change in moisture content result in 101 micro-strains. This is equal to a compliance value of 57×10^{-9} (1/psi). This matches very well with the extreme fluctuations of the compliance data (60×10^{-9} 1/psi) observed during the creep tests.

Comparing the effects of the variability of thermal expansion and shrinkage coefficients in the active and dummy specimens it can be seen that the variable shrinkage has a tremendously greater effect on the bridge output than the variable thermal expansion. For example, for the fluctuation of temperature by 10°F and 3% MC observed in the long-term creep test environment, 96% of the total apparent strain is induced by moisture change.

Vita

Sandhya Samarasinghe Gamalath was born in Sri Lanka on August 24th, 1959. She completed her secondary education in Girls' High School in Kandy, Sri Lanka. In 1983, she obtained a Master of Science degree in Mechanical Engineering from Patrice Lumumba Peoples' Friendship University in Moscow, U.S.S.R.

Sandhya worked as an Assistant lecturer for six months in the Mechanical Engineering Department at University of Peradeniya in Sri Lanka and then worked for one year in the Sri Lankan Forest Department. She got married in 1985 and came to U.S.A. to continue studies. She obtained a Master of Science degree in Forest Products at Virginia Tech in 1987 and immediately started working on the Ph.D. degree. Currently she is residing in Christchurch, New Zealand.